NAVAL POSTGRADUATE SCHOOL

MONTEREY, CALIFORNIA

THESIS

THE INFLUENCE OF SHOCK-INDUCED AIR BUBBLE COLLAPSE RESULTING FROM UNDERWATER EXPLOSIVE EVENTS

by

Steven M. Arbogast

June 2012

Thesis Co-Advisors: Young W. Kwon
Jarema M. Didoszak

Approved for public release; distribution is unlimited

THIS PAGE INTENTIONALLY LEFT BLANK

REPORT DOCUMENTATION PAGE			Form Approved OMB No. 0704-0188
Public reporting burden for this collection of information is estimated to average 1 hour per response, including the time for reviewing instruction, searching existing data sources, gathering and maintaining the data needed, and completing and reviewing the collection of information. Send comments regarding this burden estimate or any other aspect of this collection of information, including suggestions for reducing this burden, to Washington headquarters Services, Directorate for Information Operations and Reports, 1215 Jefferson Davis Highway, Suite 1204, Arlington, VA 22202-4302, and to the Office of Management and Budget, Paperwork Reduction Project (0704-0188) Washington DC 20503.			
1. AGENCY USE ONLY *(Leave blank)*	**2. REPORT DATE** June 2012	**3. REPORT TYPE AND DATES COVERED** Master's Thesis	
4. TITLE AND SUBTITLE The Influence of Shock-Induced Air Bubble Collapse resulting from Underwater Explosive Events		**5. FUNDING NUMBERS**	
6. AUTHOR(S) Steven M. Arbogast			
7. PERFORMING ORGANIZATION NAME(S) AND ADDRESS(ES) Naval Postgraduate School Monterey, CA 93943-5000		**8. PERFORMING ORGANIZATION REPORT NUMBER**	
9. SPONSORING /MONITORING AGENCY NAME(S) AND ADDRESS(ES) N/A		**10. SPONSORING/MONITORING AGENCY REPORT NUMBER**	
11. SUPPLEMENTARY NOTES The views expressed in this thesis are those of the author and do not reflect the official policy or position of the Department of Defense or the U.S. Government. IRB Protocol number _____N/A_____.			
12a. DISTRIBUTION / AVAILABILITY STATEMENT Approved for public release; distribution is unlimited		**12b. DISTRIBUTION CODE** A	

13. ABSTRACT (maximum 200 words)

During an underwater explosion (UNDEX) event, a cavitation zone is created which alters the shockwave propagation parameters through this region. A cavitation zone is generally comprised of air bubbles whose material properties closely resemble water vapor. Multiple scenarios were created using these properties to simulate the presence of bubble regions during an UNDEX event. Initial simulations involved large rectangular bubble regions which reduced the pressure from the initial shockwave, providing a buffering effect. To better simulate homogeneous air bubbles, additional studies were conducted using circular shapes of varying diameters. For small diameters, the pressure greatly increased in the immediate vicinity of the bubble. These bubbles were studied further using a refined Eulerian mesh. For large diameters, a second pressure peak was encountered, but the pressure magnitude remained roughly the same. Since large homogeneous bubbles are not typically prevalent in nature, a small region of several smaller bubbles was evaluated. This data showed that multiple small bubbles result in an overall lower pressure when compared to a single air bubble of similar area. The pressure increase incurred from the initial shockwave interaction with these air bubbles may be minimized by increasing the distance from the bubble center.

14. SUBJECT TERMS UNDEX, underwater explosion, shockwave, shock-induced bubble collapse, numerical analysis, DYSMAS modeling & simulation, fluid dynamics			**15. NUMBER OF PAGES** 118
			16. PRICE CODE
17. SECURITY CLASSIFICATION OF REPORT Unclassified	**18. SECURITY CLASSIFICATION OF THIS PAGE** Unclassified	**19. SECURITY CLASSIFICATION OF ABSTRACT** Unclassified	**20. LIMITATION OF ABSTRACT** UU

NSN 7540-01-280-5500

Standard Form 298 (Rev. 2-89)
Prescribed by ANSI Std. 239-18

THIS PAGE INTENTIONALLY LEFT BLANK

Approved for public release; distribution is unlimited

THE INFLUENCE OF SHOCK-INDUCED AIR BUBBLE COLLAPSE RESULTING FROM UNDERWATER EXPLOSIVE EVENTS

Steven M. Arbogast
Lieutenant, United States Navy
B.S., United States Naval Academy, 2007

Submitted in partial fulfillment of the
requirements for the degree of

MASTER OF SCIENCE IN MECHANICAL ENGINEERING

from the

NAVAL POSTGRADUATE SCHOOL
June 2012

Author: Steven M. Arbogast

Approved by: Young W. Kwon
Thesis Co-Advisor

Jarema M. Didoszak
Thesis Co-Advisor

Knox Millsaps
Chair, Department of Mechanical and Aerospace Engineering

THIS PAGE INTENTIONALLY LEFT BLANK

ABSTRACT

During an underwater explosion (UNDEX) event, a cavitation zone is created which alters the shockwave propagation parameters through this region. A cavitation zone is generally comprised of air bubbles whose material properties closely resemble water vapor. Multiple scenarios were created using these properties to simulate the presence of bubble regions during an UNDEX event. Initial simulations involved large rectangular bubble regions which reduced the pressure from the initial shockwave, providing a buffering effect. To better simulate homogeneous air bubbles, additional studies were conducted using circular shapes of varying diameters. For small diameters, the pressure greatly increased in the immediate vicinity of the bubble. These bubbles were studied further using a refined Eulerian mesh. For large diameters, a second pressure peak was encountered, but the pressure magnitude remained roughly the same. Since large homogeneous bubbles are not typically prevalent in nature, a small region of several smaller bubbles was evaluated. This data showed that multiple small bubbles result in an overall lower pressure when compared to a single air bubble of similar area. The pressure increase incurred from the initial shockwave interaction with these air bubbles may be minimized by increasing the distance from the bubble center.

THIS PAGE INTENTIONALLY LEFT BLANK

TABLE OF CONTENTS

THIS PAGE INTENTIONALLY LEFT BLANK

LIST OF FIGURES

THIS PAGE INTENTIONALLY LEFT BLANK

LIST OF TABLES

THIS PAGE INTENTIONALLY LEFT BLANK

LIST OF ACRONYMS AND ABBREVIATIONS

UNDEX	Underwater Explosion
TNT	Trinitrotoulene
DYSMAS	Dynamic System Mechanics Advanced Simulation
HBX	Hexahydro-1,3,5 Trinitro-8-Triazine
DoD	Department of Defense
EOS	Equation of State
TORPEX	Torpedo Explosive
HE	High Explosive
CJ	Chapman Jouget

THIS PAGE INTENTIONALLY LEFT BLANK

ACKNOWLEDGMENTS

I would like to thank Professor Young Kwon of the Naval Postgraduate School Mechanical Engineering Department. His explanation of finite element modeling and structural mechanics enhanced my technical background with information pertinent to my thesis. Furthermore, his direction over the course of this thesis was instrumental in the selection of additional areas of study.

I would like to thank Professor Jarema Didoszak of the Naval Postgraduate School Mechanical Engineering Department. He was instrumental in explaining underwater explosion theory and the ship shock trial process. His expertise in regard to the DYSMAS suite and associated programs proved invaluable to the successful completion of this thesis.

Lastly, I would like to thank my wife Stephanie. Her love and support helped me through the late nights at school while I worked on my thesis. We will always remember the exciting days of planning a wedding and completing a thesis at the same time.

THIS PAGE INTENTIONALLY LEFT BLANK

I. INTRODUCTION

A. BACKGROUND

The United States Navy conducts shock hardening tests on new construction and operational surface ships in order to validate ship survivability [1]. The bulk of these shock hardening tests are conducted during ship shock trials to resolve any material or design deficiencies and evaluate the structural response of the ship. Since shock trials involve a fully manned surface ship operating under normal conditions and exposed to a large subsurface detonation, the risk to human and marine life is high. The extraordinary amount of manpower and resources required to successfully conduct shock trials is also of concern. The estimated cost of the shock trials for USS JOHN PAUL JONES (DDG 53) was 30 million dollars and for USS WINSTON S. CHURCHILL (DDG 81) was 20 million dollars [2]. The current political and economic conditions in the United States government make the Department of Defense (DoD) budget more restrictive.

Technological advancements in recent years provided the supercomputers and supporting systems used in computer modeling and simulation, one possible alternative to full ship shock trials. The Dynamic System Mechanics Advanced Simulation (DYSMAS) suite is one such system that is utilized to model various underwater explosion events and is currently being assessed for accuracy in comparison to real-world ship shock trials. Some advantages of the DYSMAS suite are:

- Small economic investment
- Short time for preparation, experimentation, and data collection
- Fully variable parameters

The latter advantage is most pertinent to this study. Shock trials on the USS WINSTON S. CHURCHILL (DDG 81) were conducted using a specified explosive at only three locations: port-side amidships, port-side bow, and starboard-side amidships.

Mounted sensors consisted of accelerometers, velocity meters, and strain gauges mounted on the ship. Environmental conditions modeled were those recorded on the day of the trials [2].

The DYSMAS suite enables the user to control key parameters such as the charge placement, charge weight, and environmental conditions. With fully variable parameters, areas other than the ship response can be examined. One area that is commonly overlooked is the influence of ambiguities in the water column during an Underwater Explosion (UNDEX) event. Examples of these ambiguous entities include: air bubbles, fish, and trash. Most of these coalesce near the water surface which may impede a shockwave and affect the pressure propagation. Without a doubt these ambiguities are present during the real world shock trials, but are not readily included in the computer modeling process. Their inclusion may have significance on the shockwave propagation.

B. SCOPE OF RESEARCH

Previous research indicated that cavitation zones may provide a buffering effect to marine structures which are subjected to UNDEX events [3]. A cavitation zone is comprised of millions of bubbles of varying shapes and sizes. This study investigated the cavitation zone from the point of view of an air bubble.

Since an air bubble is neither completely air nor completely water, but a mixture of the two, the properties of water vapor were selected as suitable Equation of State (EOS). The simulations were conducted using a two dimensional Eulerian mesh whose dimensions remained constant. A simulation devoid of air bubbles was evaluated to be used as a control for comparison of follow-on simulations.

Rectangular air bubble regions were initially evaluated to mimic a ship hull surrounded by a bubble layer. In a real world application, this bubble layer would be made up of countless individual bubbles delivered by a hull-mounted pressurized air system. The computer modeling software permitted an approximation of this rectangular air bubble region as one homogenous region with the properties of an air bubble. The

properties on an air bubble were similar to those of water vapor and served as the basis for future simulations. These simulations resulted in the investigation of circular air bubble regions.

The circular regions were generally small in size and designed to mimic individual bubbles in the water column. Their size was carefully selected in order to best approximate a realistic size of a naturally occurring air bubble. The software modeled them as a homogeneous region using the water vapor properties. Since the results involving the circular regions proved more realistic, follow-on simulations involved regions of various diameters to inhibit maximum pressure deviations from the control simulation.

As a return to prior simulations involving rectangular air bubbles, a scenario was constructed involving multiple individual air bubbles in close proximity to each other. This was designed to evaluate a real world scenario where a ship hull is surrounded not by one large homogeneous air bubble, but millions of smaller bubbles in close proximity.

Throughout this study it was found that small circular air bubbles dramatically increased the pressure within a small radius. Meanwhile large circular and rectangular air bubbles tended to act more as a buffer zone by either delaying the shockwave arrival or disrupting the shockwave propagation. It was apparent that as the distance from the air bubble region was increased, the effect of the pressure increase dropped off substantially thus creating the desired buffering effect.

THIS PAGE INTENTIONALLY LEFT BLANK

II. UNDERWATER SHOCK EXPLOSION THEORY

A. COMPONENTS OF AN UNDERWATER EXPLOSION

An explosion is a chemical reaction which involves the rapid expansion of gases and a large release of energy. For UNDEX events, this energy release manifests itself in the form a shockwave which is capable of causing extensive destruction on underwater structures. Figure 1 shows a typical UNDEX event. While this study is concerned with deep-water events, Figure 1 provides a detailed description of an UNDEX event in a shallow water environment. The main difference between deep-water and shallow water events is the propagation of bottom reflected shockwaves; deep-water events have bottom reflected shockwaves, however, they are negligible when compared to the direct shockwaves. Note the location and size of the bulk cavitation zone. Also, both direct and indirect (reflected) shockwaves pass through this region. How a shockwave is impacted by passing through this region is of interest and is examined in this study.

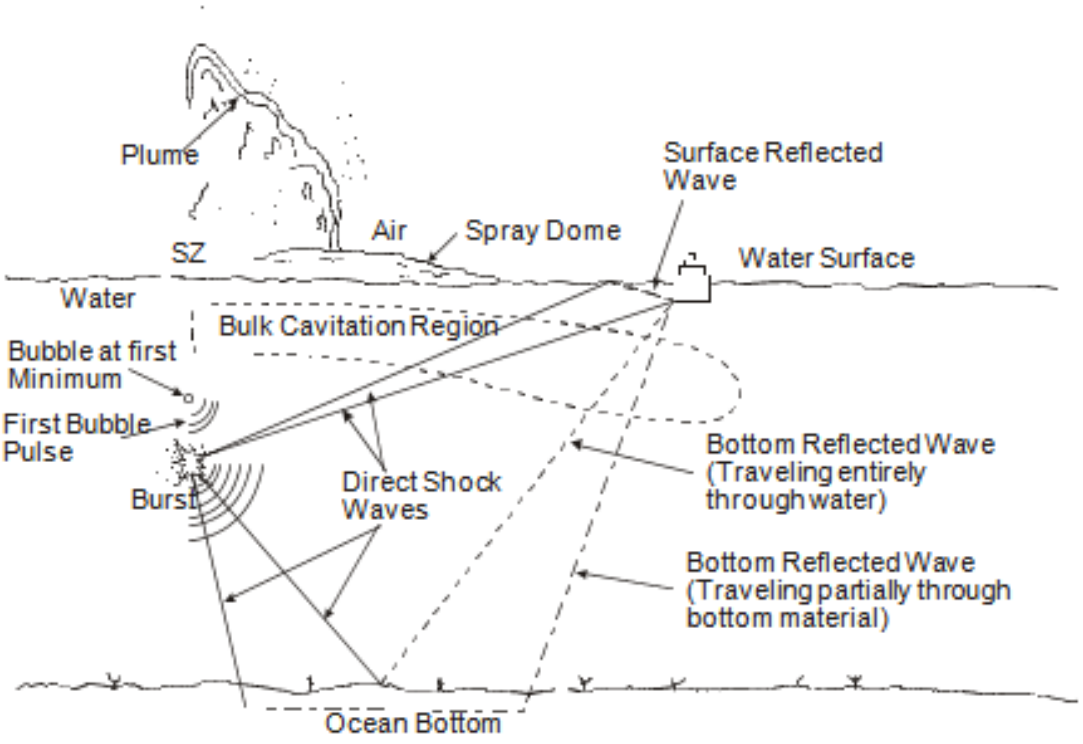

Figure 1. Schematic of a typical UNDEX event (From [4])

1. Explosive Materials

Common explosive materials used in naval applications include Trinitrotoluene (TNT), Torpedo Explosive (TORPEX), and Hexahydro-1,3,5 Trinitro-8-Triazine (HBX-1). TNT is prevalent in military and mining applications as a bulk explosive. It is inherently stable which is desirable to prevent accidental detonation. The primary ingredient of TNT is toluene. It is also commonly used to measure the energy released during an explosion, this is called the TNT equivalent.

TORPEX was developed during World War II for use in underwater ordnance applications such as mines, torpedo warheads, and depth bombs since it was 141% more powerful than TNT. TORPEX-1 consisted of 45% RDX, 37% TNT, and 18% Aluminum power (1% wax added) [5]. A critical disadvantage of TORPEX was its increased sensitivity in comparison to TNT. This was exemplified in the Port Chicago, CA accident in 1944, after which production ceased.

The HBX family of explosives was created to replace TORPEX and is commonly used in modern day UNDEX events. A common mixture is HBX-1 which consists of 66.08% Composition B, 4.66% Composition D-2, 17.10% Aluminum, 11.66% Additional TNT, 0.50% Calcium Chloride, and 0.47% Calcium Silicate [6]. HBX is 98-100% more powerful, albeit substantially less sensitive, than TORPEX [5].

2. Gas Sphere

Upon detonation of the high explosive charge, the remaining gases and particulates become trapped in a high pressure gas sphere. This sphere has an extremely high pressure compared to the surrounding water. As a result, it expands until its internal pressure equals the surrounding hydrostatic pressure. Having exhausted a significant amount of energy during expansion, the sphere begins to contract into itself. The final portion of this contraction results in a bubble pulse causing an increase in pressure. This pressure increase is substantially less in magnitude than the pressure expended at detonation. The process of expansion and contraction continues for several periods, until the energy is nearly exhausted. While this process occurs, the sphere migrates towards the water surface due to Archimedes' principle.

Figure 2 provides a good visualization of the expansion and contraction process of the gas sphere and the associated pressure-time record throughout the UNDEX event.

The top portion shows pressure versus time. At the time of detonation, there is an initial pressure peak which coincides with the initial shockwave arrival. The abrupt decrease in pressure is a result of the passing of the shockwave. The additional pressure increases are minor in comparison to the initial peak and occur due to the full contraction of the gas sphere. As time progresses, the pressure increases from the bubble pulses become less significant until the pressure reaches ambient conditions.

The lower portion shows the movement of the gas sphere from the time of detonation until it nears the water surface. This vertical movement is known as bubble migration and occurs due to the principles of buoyancy. For each period of expansion and contraction, the maximum bubble radius decreases slightly. Ultimately, the gas sphere vents at the surface of the water and dissolves into a region of miniscule bubbles.

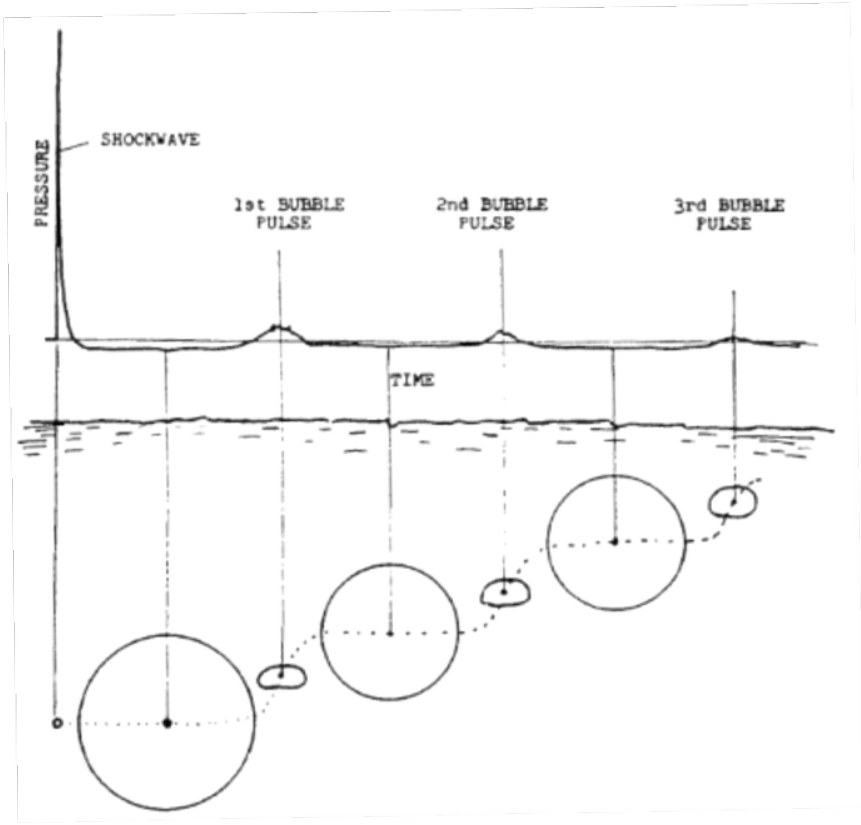

Figure 2. Gas Sphere Characteristics. (From [7])

3. Shock Wave

For spherical charges, a high pressure shockwave is created which propagates radially outward. The high pressure in comparison to ambient water pressure causes outward movement of the water column. A 300 pound charge of TNT, for example, generates a shockwave with a nominal pressure of $2x10^6$ psi ($13.79x10^{10}$ dyne/cm^2) [8]. While an extreme increase in pressure ensues, the duration of this peak only lasts a couple milliseconds. The shockwave is characterized in the top portion of Figure 2. The initial increase occurs near instantaneously and the decrease occurs rapidly in a near-exponential manner. Regardless of the short peak-time, this increase in pressure is substantial and of grave concern to marine structures.

B. BULK CAVITATION

Bulk cavitation is a phenomenon that occurs during an UNDEX event. When the initial shockwave reaches the air-water interface, a large portion of the shockwave is reflected which creates a low pressure region where the bulk cavitation forms [9]. To the naked eye bulk cavitation appears as a region of air bubbles.

1. Subsurface Effects

Due to the shockwave reflection, the bulk cavitation forms near the water surface. Figure 3 shows a bulk cavitation zone that was created during a test near the air-water interface [10]. The zone appears as the black region bordering the air-water interface in the center of the image. This region is comprised of millions of air bubbles which are constantly collapsing and expanding due to variation in hydrostatic pressure. The formation and collapse of these air bubbles is a transient occurrence lasting a few milliseconds. Also of interest is the gas sphere located just below the cavitation zone. Having just detonated, it is still in the expansion phase.

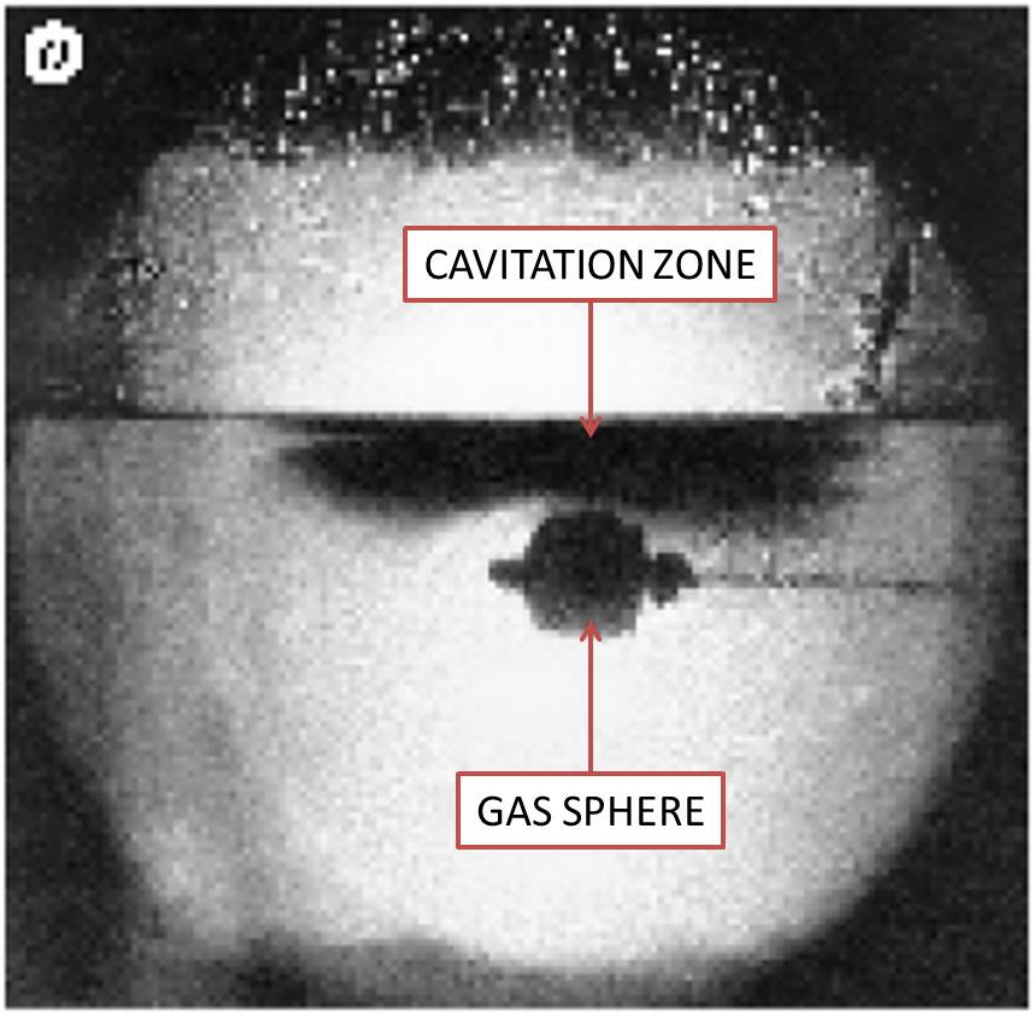

Figure 3. Bulk Cavitation Zone created during an UNDEX event. (From [10])

2. Surface Effects

From the surface, the bulk cavitation zone appears more dramatic, though this is dependent on charge location and weight. Charges placed nearer to the water surface tend to have a larger cavitation zone surface area. A variation in charge weight will also vary the cavitation zone size i.e., a heavier charge will create a larger zone.

Figure 4 shows the surface effects surrounding an UNDEX event conducted on a U.S. Navy destroyer. The white region is the bulk cavitation zone which dwarfs the nearby destroyer. Again this region dissipates rapidly and is overcome by the plume breaching the water surface for near surface explosions.

Figure 4. Surface Effects of Bulk Cavitation during an UNDEX event. U.S. Navy Photo.

III. COMPUTER MODELING SYSTEMS

A. DYSMAS CODE

The Dynamic System Mechanics Advanced Simulation (DYSMAS) code is the result of an ongoing joint project between the German Ministry of Defense and the Indian Head Naval Surface Warfare Center. DYSMAS is a hydrocode used to simulate underwater explosion events and their effects on marine structures. It is widely used in naval applications and achieved validation following extensive testing on the former German guided missile destroyer, ex-LÜTJENS (D198).

The key components of the DYSMAS code are: the Eulerian fluid solver (Gemini), the Lagrangrian structural solver (ParaDyn), and the fluid-structure interaction module (Standard Coupler Interface) [11]. To evaluate the effects of air bubble collapse in this study, Gemini was the primary component utilized.

B. GEMINI

The Gemini code is an Eulerian solver used to solve the fluid portions of model. This code has been extensively validated for UNDEX events including shock propagation, bubble formation and jetting, and fluid-structure interaction [11]. The key components of the Gemini code are:

- GemGrid – generates a non-uniform grid
- PreGemini – generates restart file and rezones the flow field
- Gemini – solves Euler equations for multi-material flow
- GemHis – generates history plot files
- GemField – creates contour plot files

C. MODELING STAGES

In order to successfully evaluate an UNDEX event, it must pass through three different stages: pre-processing, execution (main program), and post-processing. The data-flow path is shown in Figure 5.

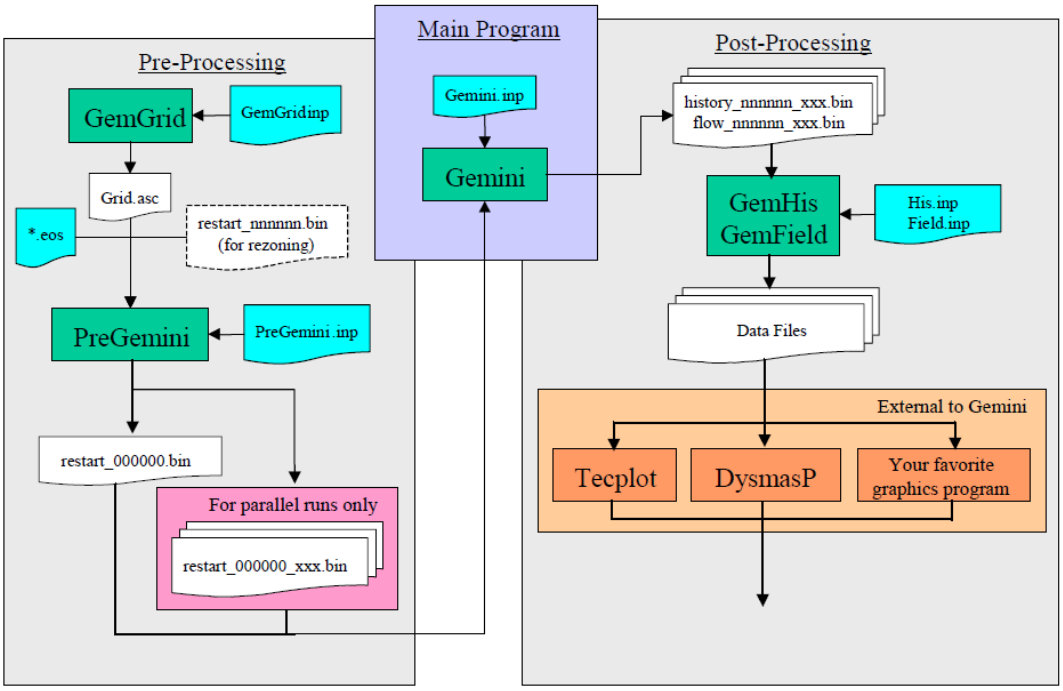

Figure 5. Key Gemini Components and Data-Flow Path. (From [11])

1. Pre-Processing

During pre-processing, GemGrid and PreGemini are the primary codes utilized. GemGrid is used to specify the overall grid size in the X, Y, and Z directions. Initial runs were contained elements that were uniform in size in order to reduce computational time. Later runs involved refined mesh elements around a region of interest in order to provide more accurate results. Refinement of the mesh was accomplished through GemGrid.

PreGemini compiles numerous parameters and generates several files required to operate Gemini. Critical parameters include: the grid coordinate system (generated by GemGrid), material equations of state, and rezoned flow fields. By rezoning certain areas of the flow field, one can add regions of varying material properties to the ambient fluid. This procedure enabled the addition of air bubble regions to the ambient fluid which was water. A sample of the PreGemini file is located in the Appendix.

2. Execution (Main Program)

The majority of the calculations of each simulation are completed using the Gemini code which is a finite-difference solver. Based upon the user-specified parameters in GemGrid and PreGemini, Gemini solves the Euler equations using the Hamming computing cluster at the Naval Postgraduate School.

The Gemini code allows user inputs include: setting start/end conditions and defining cell history locations. The cell history feature was heavily utilized for data collection at user-specified locations within the mesh.

3. Post-Processing

Following execution of the simulation, the GemHis and GemField programs provide visual representations of the simulation. Visualization of the simulations was made possible through the DYSMAS/P 2010 interactive graphic system.

GemField creates a frame-by-frame representation of the UNDEX event. The timing between frames is specified within the Gemini input file. Selection of a suitable time-step is critical. The shockwave propagation can be readily observed throughout the duration of the event, providing an appropriate time-step was selected. If the time-step is too large, minute propagation details are lost in the visualization since the UNDEX event lasts several microseconds. This visualization is critical when studying the phenomena associated with shock-induced air bubble collapse.

GemHis is used to generate a time history of user-selected parameters based upon the Gemini input file. Output parameters include: pressure, velocity, and total energy.

THIS PAGE INTENTIONALLY LEFT BLANK

IV. STANDARD SETUP PARAMETERS

While there were multiple simulations conducted during this research, certain parameters remained the same for all simulations. This provided relative ease of comparison of data across the simulations.

A. REFINED MESH MEASUREMENTS

Initial simulations did not require a refined mesh and consisted wholly of cells with dimensions of 2cm x 2cm.

When more precise calculations were required, the following refined mesh measurements were utilized. The refined mesh was consisted of two dimensions, X and Z. Table 1 shows the grid dimensions utilized for these simulations. The unrefined cell size was 2cm x 2cm. In the refined region the cell size was reduced to 0.1cm to permit more exact calculations. Prior to and following this refined region, there were transition regions to adjust the cell size from 2cm to 0.1cm. These regions are annotated in Table 1 as blocks 2 and 4. The total number of cells, in the refined mesh, was 947,964.

Table 1. Refined Mesh Parameters (X and Z-Directions)

X Grid Lines					
Block	Cells	a1	a2	Ratio	Width (cm)
1	121	2	2	1	242
2	12	2	0.096539	0.759161	8
3	40	0.1	0.1	1	4
4	12	0.1	1.977088	1.311658	8
5	406	2	2	1	812
Total	591				1074
Z Grid Lines					
Block	Cells	a1	a2	Ratio	Width (cm)
1	896	2	2	1	1792
2	12	2	0.096539	0.759161	8
3	40	0.1	0.1	1	4
4	12	0.1	1.977088	1.311658	8
5	144	2	2	1	288
6	500	2	2	1	1000
Total	1604				3100

B. EQUATIONS OF STATE

In order to specify the material properties used in each simulation, several equations of state were required to be input via PreGemini in the form of material files. These files state the desired properties of air, water, and explosive for each simulation. Tables 2 through 6 are the equations of state used in this study.

Table 2. Equation of State for Air

Material	Air		
EOS Type	Gamma-Law		
Equation	$p = (\gamma - 1)\rho e$		
Material Property			Units
Reference Density	ρ_{ref}	0.0013	g/cm^3
Reference Specific Energy	e_{ref}	1.9230769E+09	erg/g
Reference Speed of Sound	c_{ref}	3.28E+04	cm/s
Minimum Density	ρ_{min}	1.0d-06	g/cm^3
Minimum Specific Energy	e_{min}	1.0d-4	erg/g
Gamma	γ	1.4	N/A

Table 3. Equation of State for Water (Tillotson Model)

Material	Water		
EOS Type	Tillotson		
Equation	$p = p_o + \omega\rho(e - e_o) + A\mu + B\mu^2 + C\mu^3$ where $\mu = \frac{\rho}{\rho_o} - 1$		
Material Property			Units
Reference Density	ρ_{ref}	1	g/cm^3
Reference Specific Energy	e_{ref}	3.54E+09	erg/g
Reference Speed of Sound	c_{ref}	147600	cm/s
Minimum Density	ρ_{min}	9.999E-03	g/cm^3
Minimum Specific Energy	e_{min}	-9.999E+10	erg/g
Minimum Pressure	p_{min}	50000	$dyne/cm^2$
Omega	ω	2.80E-01	N/A
Constant	A	2.20E+10	N/A
Constant	B	9.54E+10	N/A
Constant	C	1.457E+11	N/A

Table 4. Equation of State for Water Vapor

Material	Water Vapor		
EOS Type	Gamma-Law		
Equation	$p = (\gamma - 1)\rho e$		
Material Property			Units
Reference Density	ρ_{ref}	0.00082	g/cm^3
Reference Specific Energy	e_{ref}	3.04878E+09	erg/g
Reference Speed of Sound	c_{ref}	4.03E+04	cm/s
Minimum Density	ρ_{min}	1.0d-06	g/cm^3
Minimum Specific Energy	e_{min}	1.0d-4	erg/g
Gamma	γ	1.33	N/A

Table 5. Equation of State for HBX-1 (Solid)

Material	HBX-1 (Solid)		
EOS Type	Tait for Unburned High Explosive (HE)		
Equation	$p = p_o + B\left(\left(\frac{\rho}{\rho_o}\right)^{\gamma} - 1\right)$ *where* $B = \frac{F(p_{CJ} - p_o)}{(\frac{\rho_{CJ}}{\rho_o})^{\gamma} - 1}$		
Material Property			Units
Reference Density	ρ_{ref}	1.72	g/cm^3
Reference Specific Energy	e_{ref}	6.52E+10	erg/g
Reference Speed of Sound	c_{ref}	4.06E+5	cm/s
Minimum Density	ρ_{min}	1.0d-06	g/cm^3
Minimum Specific Energy	e_{min}	10000.0	erg/g
Gamma	γ	1	N/A
Ambient Pressure	p_o	1.0E+6	$dyne/cm^2$
Unburned Explosive Density	ρ_o	1.72	g/cm^3
CJ Density	ρ_{CJ}	2.25567	g/cm^3
CJ Specific Energy	e_{CJ}	7.455692E+10	erg/g
CJ Pressure	p_{CJ}	1.355396E+11	$dyne/cm^2$
Detonation Velocity	D	5.75045E+05	cm/s
Factor	F	0.95	N/A

Table 6. Equation of State for HBX-1 (Gaseous Product)

Material	HBX-1 (Gaseous Product)		
EOS Type	JWL		
Equation	$p = A\left(1 - \frac{\omega\rho}{R_1\rho_o}\right)e^{-R_1\frac{\rho_o}{\rho}} + B\left(1 - \frac{\omega\rho}{R_2\rho_o}\right)e^{-R_2\frac{\rho_o}{\rho}} + \omega\rho e$		
Material Property			Units
Reference Density	ρ_{ref}	1.72	g/cm^3
Reference Specific Energy	e_{ref}	6.52E+10	erg/g
Reference Speed of Sound	c_{ref}	4.06E+5	cm/s
Minimum Density	ρ_{min}	1.0d-06	g/cm^3
Minimum Specific Energy	e_{min}	10000.0	erg/g
Omega	ω	0.25	N/A
Constant	A	5.183E+12	N/A
Constant	B	4.390E+09	N/A
Constant	R_1	5.183	N/A
Constant	R_2	3.5E-01	N/A

C. EXPLOSIVE CHARGE

Throughout this study the charge type, size, and location remained constant. Therefore, the shockwave propagation characteristics remain constant and were easily comparable. The charge contained 27.515kg (60.619lb) of HBX-1 and was spherical in shape. It was located 1000cm (32.808ft) beneath the surface of the water on the Z-axis.

V. TWO DIMENSIONAL SIMULATION WITHOUT AIR BUBBLE REGION

A. JUSTIFICATION

The UNDEX event modeling was conducted in two dimensions in order to reduce computational time. This initial simulation involved a fluid column with no air bubble region. It was designed to act as a control group against which follow-on simulations would be compared. Additionally, analytical calculations were conducted in order to compare the accuracy of the computer simulation. Units were consistently in the centimeter-gram-second (CGS) system.

B. COMPUTER SIMULATION

1. Grid Setup

Figure 6 shows the grid setup for this simulation. While the grid appears rectangular in shape, it was calculated using cylindrical coordinates. This is a feature of DYSMAS that permits conversion to a three dimensional coordinate system with relative ease. For purposes of these calculations, the difference between Cartesian and cylindrical modes is negligible. The mesh for this simulation contained cells of uniform size; each was 2cm x 2cm. The x-axis (radial direction) consisted of 537 cells equaling 1074cm. The z-axis (axis of rotation) consisted of 1550 cells equaling 3100cm. The Euler and cell origins are annotated in Figure 6. The HBX-1 charge was placed 1000cm below the air-water interface. Region A was the location of three data collection points. The locations consisted of an upper cell (126,903), middle cell (126,901), and lower cell (126,899). These cells were in-line vertically and evenly spaced apart by 2cm. The run was evaluated for 10ms.

Boundary conditions were fixed at the left and bottom edges. At the right and top edges the boundary was free. This simulated an accurate environment where the UNDEX effects would reflect off the ocean floor or continue to propagate across the water column.

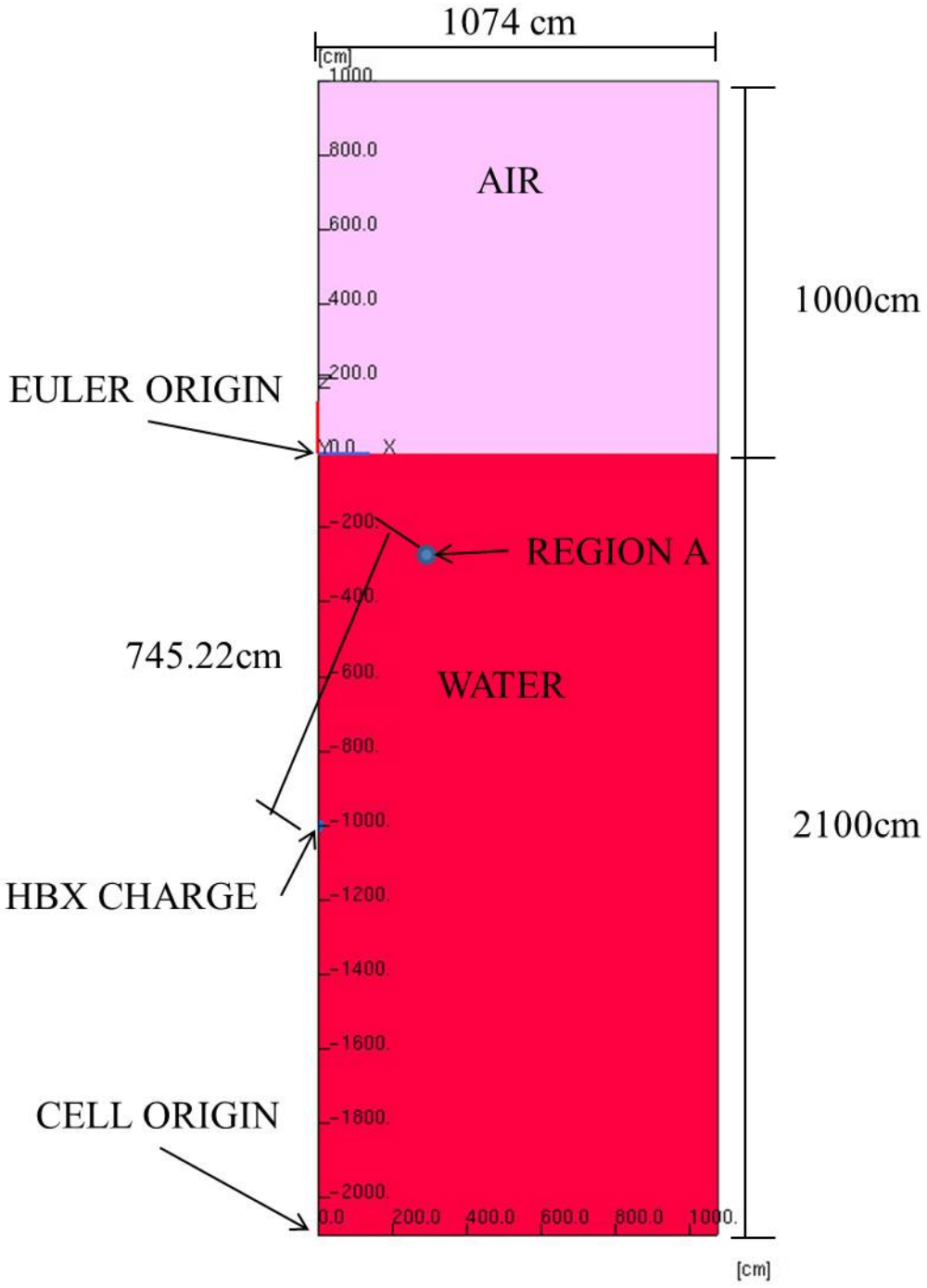

Figure 6. Setup without Air Bubble

2. Animated Results

Since no air bubbles were included in this simulation, the shockwave propagated outward uninhibited. Figure 7 shows this propagation at three different times. Note the initial high pressure surrounding the exploded charge and how rapidly the pressure decreases as the shockwave forms and propagates outward. As the simulation progressed beyond 6ms, the shockwave rapidly diminished and had negligible effect.

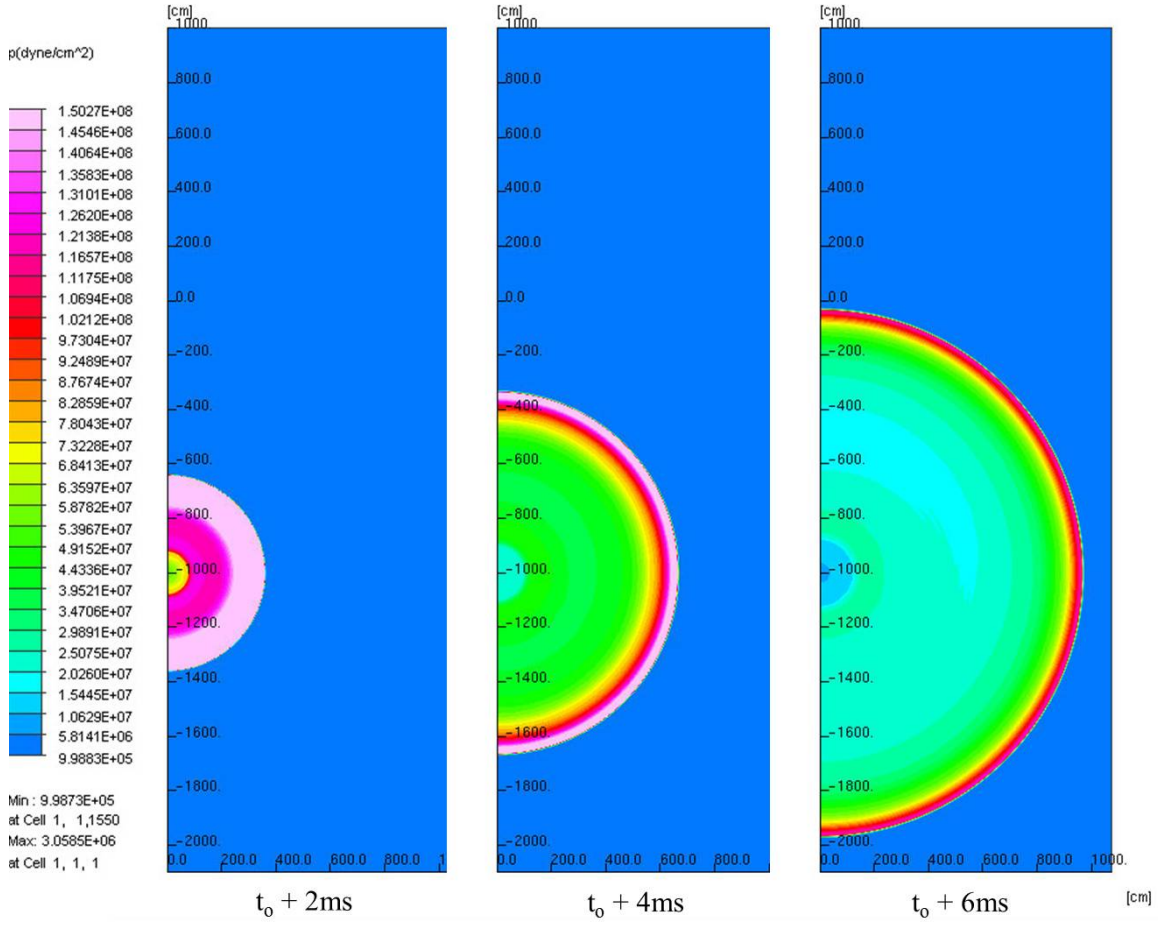

Figure 7. Formation of Shockwave due to an UNDEX Event

3. Pressure-Time History Results

Figure 8 shows the pressure history at the three data collection locations within Region A. The pressure reaches a near instantaneous maximum at approximately 4.5ms when the shockwave passes. Immediately thereafter it decreases exponentially as the

shockwave continues past. This decrease continues until approximately 8.25ms at which point there is a sudden decrease to ambient pressure conditions. This drop in pressure occurs due to the surface cutoff which is when the shockwave interacts with the air-water interface and a portion is reflected. After this time, the pressure in Region A is negligible.

When comparing the pressure plots near Region A, one can see that they are nearly convergent on each other. Of importance is the maximum peak pressure. To calculate the pressure at this point an average of all three data locations was conducted. When averaged they equate to a nominal pressure of 159.95×10^6dyne/cm^2 (2319.88psi).

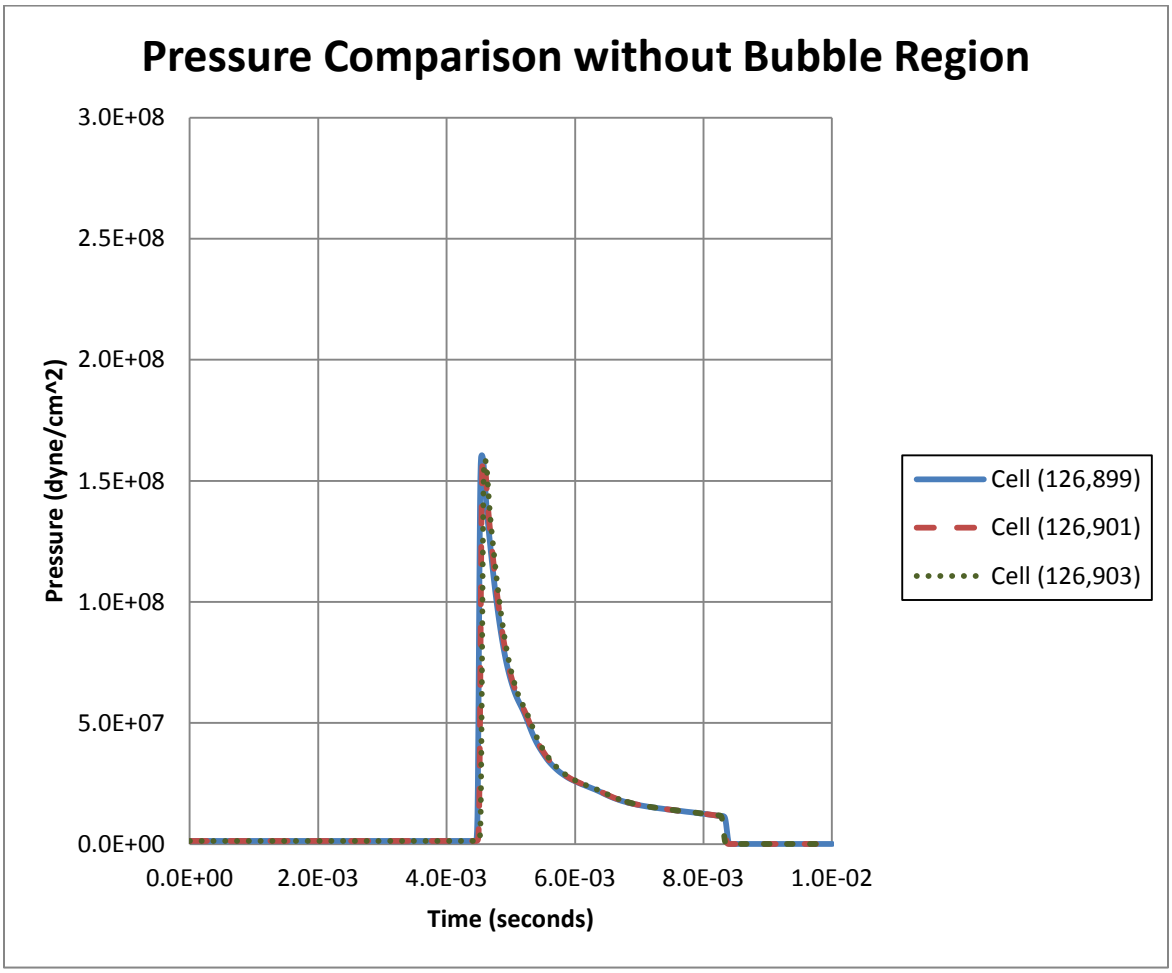

Figure 8. Pressure-Time History of Region A

C. ANALYTICAL CALCULATIONS

In order to confirm the validity of the computer simulation, analytical calculations were conducted. Equation 1.1 is a shockwave equation used to determine pressure at a specified distance from the charge [12]. The specified distance is commonly known as the standoff distance (R) and is input into Equation 1.1 in feet. W is the charge weight entered in pounds. In keeping with standard charge parameters, the charge weight was 60lb of HBX-1. K_1 and A_1 are constant shock wave parameters and are unitless. For HBX-1, K_1 is 22347.6 and A_1 is 1.144. The pressure output (P_{max}) associated with this is psi.

$$P_{\max} = K_1 \left(\frac{W^{1/3}}{R} \right)^{A_1} (psi) \tag{1.1}$$

The standoff distance was determined using geometry. The measurements are shown in Figure 9. Since the charge was located 1000cm beneath the water surface and 251.5cm from the Z-axis, the standoff distance was determined to be 745.22cm (24.45ft). This distance coincided with the area of interest, Region A.

After entering these variables into Equation 1.1, the pressure at Point A was determined to be 190.25 x 10^6dyne/cm^2 (2759.36psi) which was greater than the pressure perceived by the computer simulation.

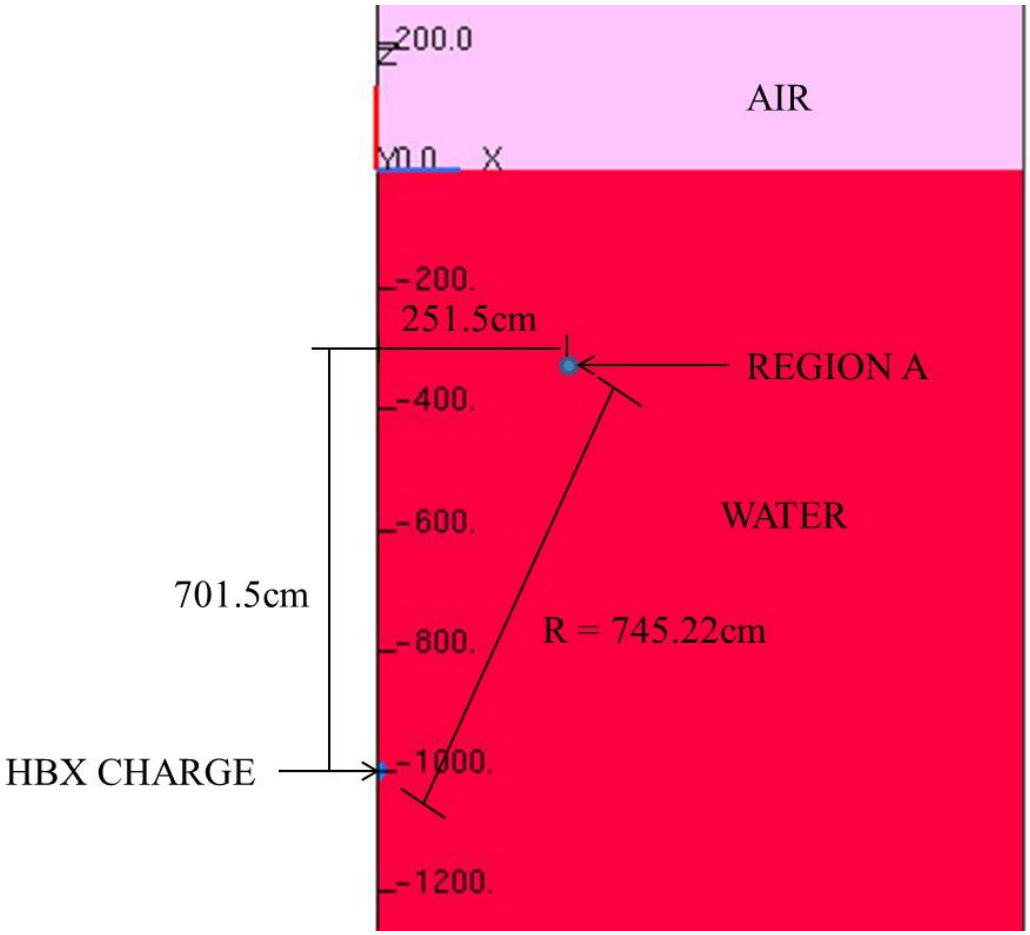

Figure 9. Standoff Distance Measurements for Analytical Calculations

D. DISCUSSION OF RESULTS

After completion of the computer simulation and analytical calculations, a comparison of the pressures by each process was conducted. The analytical calculations produced a higher pressure value, 190.25×10^6 dyne/cm^2, than the computer simulation. The computer simulation determined a pressure of 159.95×10^6 dyne/cm^2 at the location of Region A. The difference between these two methodologies is acceptable.

VI. TWO DIMENSIONAL SIMULATION INVOLVING MULTIPLE RECTANGULAR AIR BUBBLE REGIONS

A. JUSTIFICATION

The first simulation involving the addition of air bubbles consisted of six regions of rectangular shape. The shape of these regions developed from the concept that a ship hull may be surrounded by a region of air bubbles in order to buffer the ship from an UNDEX event. This region could be created by a future derivative of the Prairie/Masker air system. The Prairie/Masker air system is a noise suppression system currently employed on several U.S. Navy vessels including Ticonderoga class guided missile cruisers and Arleigh Burke class guided missile destroyers [13]. It is designed to conceal machinery noise for ships operating in regions with possible undersea warfare threats. Figure 10 is a schematic of the Prairie/Masker air system on U.S. Navy frigate. Note the dual air emitter belts mounted on the hull near amidships.

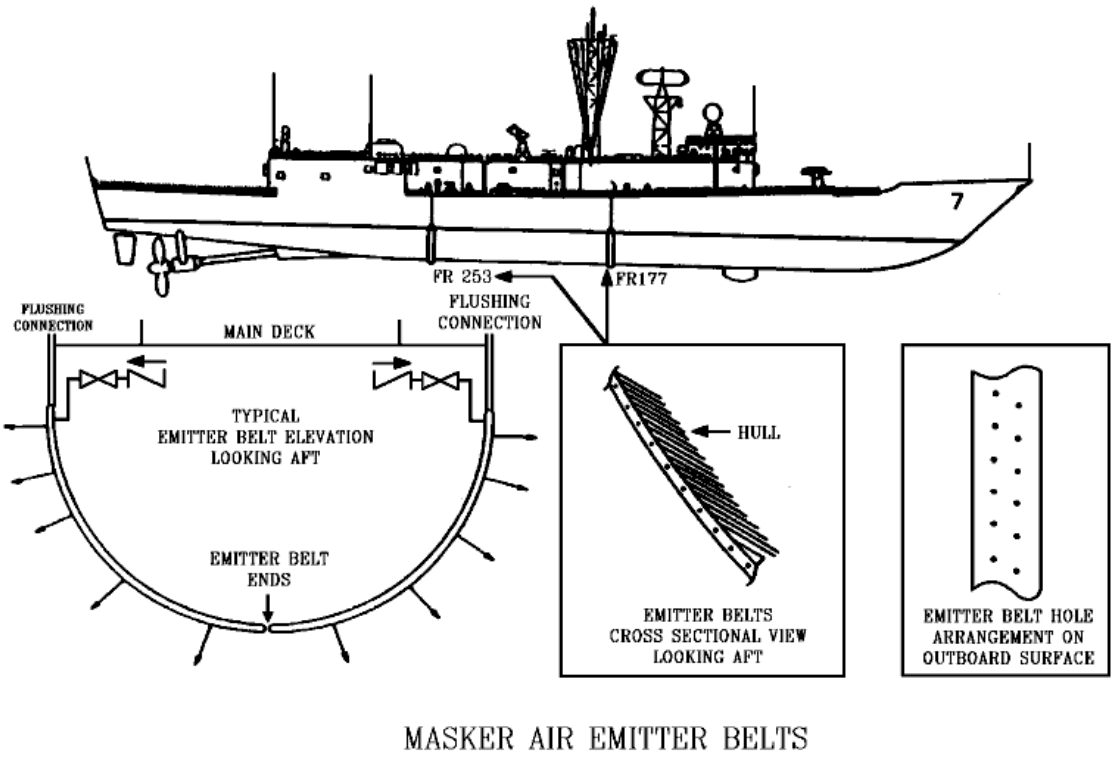

Figure 10. Prairie/Masker Air System Configuration for an Oliver Hazard Perry Class Guided Missile Frigate. (From [13])

Initial simulations involved the rectangular regions near the surface of the water in an effort to simulate a surface vessel hull surrounded by air bubbles. However, at this location, it was difficult to distinguish the reflected shockwave due to the air-water interface from the reflected shockwave due to the air bubble regions. So, the regions were moved down the water column to separate the two phenomena and better examine any buffering effect provided by the air bubbles.

B. AIR BUBBLE REGION PROPERTIES

Since the properties of an air bubble contain a mixture of water and air, a new equation of state was required to create these regions in Gemini. The equation of state was based upon the properties of water vapor and is shown in detail in Table 4.

One may initially believe that water vapor should be denser than air due to addition of water to dry air, yet this is in fact not true. Dry air is primarily composed of the diatomic molecules O_2 and N_2. O_2 has an atomic mass of 32 atomic units while N_2 has an atomic mass of 28 atomic units. Water is comprised of H_2O of which two molecules are hydrogen totaling an atomic mass of 18 atomic units, less than oxygen or nitrogen. When water vapor and dry air are at similar temperatures, the less dense water molecules displace the heavier oxygen and nitrogen molecules creating a less dense water vapor mixture [14]. Table 7 shows a comparison of select properties of air, water, and water vapor.

Table 7. Comparison of Material Properties of Air, Water, and Water Vapor

	Air	Water	Water Vapor
EOS Type	Gamma-Law	Tillotson	Gamma-Law
Density (g/cm^3)	0.0013	1	0.00082
Energy (erg/g)	1.92308×10^9	3.542×10^9	3.04878×10^9
Speed of Sound (cm/s)	3.28×10^4	14.76×10^4	4.03×10^4

This phenomenon can best be described when a person exhales and it is cold outside. A person's breath is composed of a mixture of exhaled gases which includes water vapor from our moist lungs. When the water vapor is exhaled and interacts with

the cold air, it transforms from a gas state into a solid/liquid for which is visible to the human eye [15]. The less dense water vapor (your breath) displaces the heavier air molecules and rises due to the principles of buoyancy.

While air bubble regions may vary in size and shape, on the molecular level they are best approximated by the properties of water vapor. For this reason, these properties were selected for use in the equation of state.

C. GRID SETUP

The grid dimensions were unchanged from the previous simulation. This simulation involved the addition of a row of six separate rectangular bubble regions. Each region was 4cm in height and 50cm in length. There was a spacing of 50cm between each region. Figure 11 depicts a zoomed-in view of the grid setup for the six bubble regions in relation to the HBX-1 charge and the air-water interface. Data collection remained at Region A and was collected using the same three points from the previous simulation.

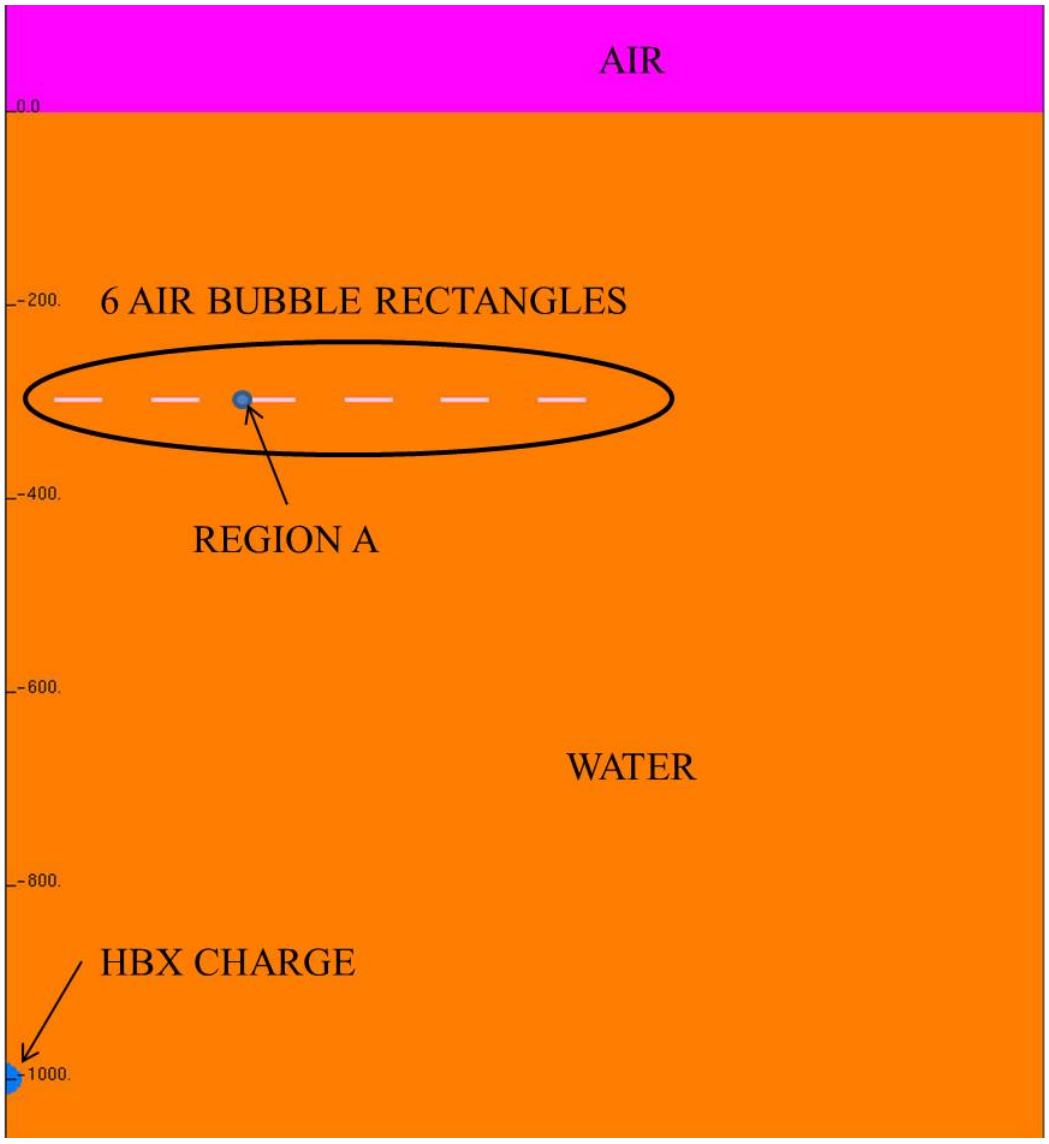

Figure 11. Grid Setup for Six Rectangular (4cm x 50cm) Air Bubble Regions

Figure 12 shows a close up view of Region A and the three data collection points. The different colors represent different materials used in the simulation. The grid spacing remained uniform with each cell measuring 2cm x 2cm. The data collection points were selected in order to provide a good spectrum of data in that vicinity. The lower cell (126,899) recorded the total pressure from the shockwave prior to interacting with the air bubble region. The middle cell (126,901) recorded the pressure within the air bubble region. The upper cell (126,903) recorded the pressure near the backside of the air bubble region and evaluated any buffering effect provided by the air bubbles.

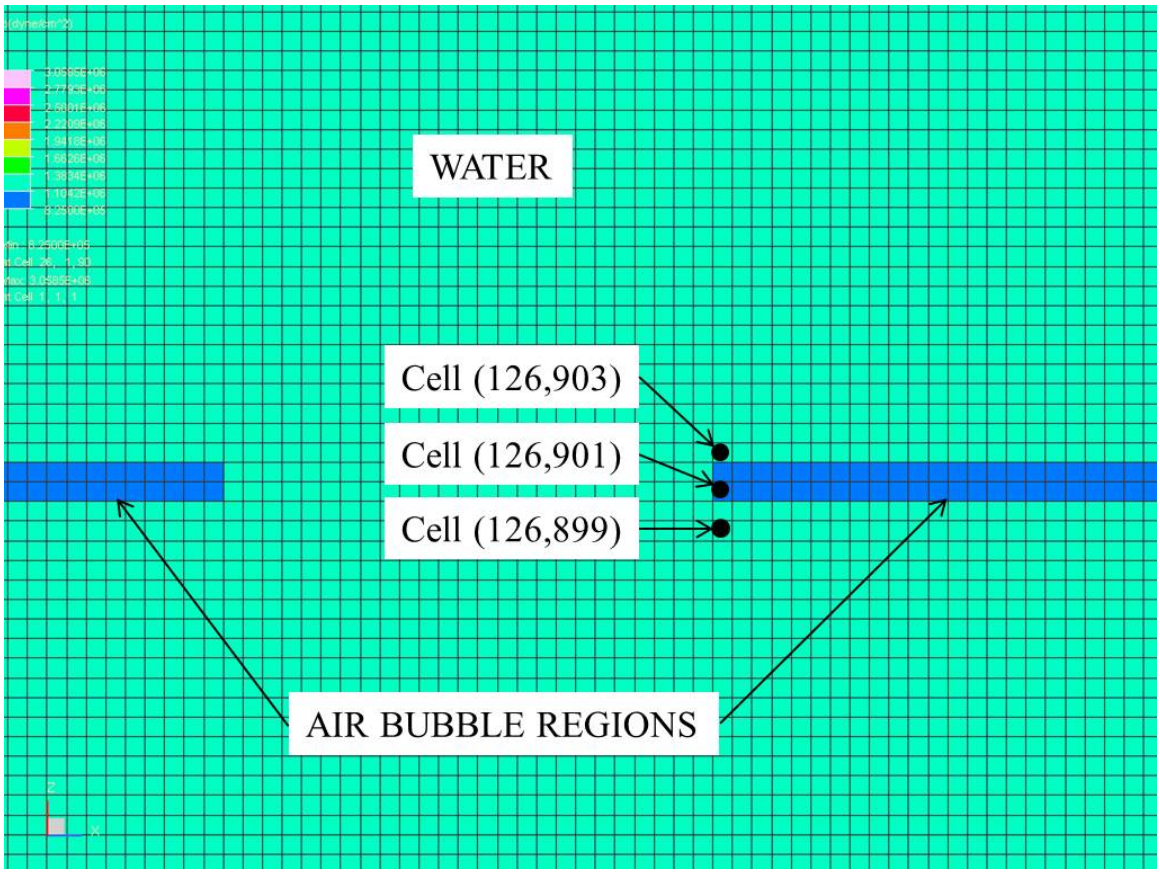

Figure 12. Data Collection Points in Region A for Six Rectangular (4cm x 50cm) Air Bubble Regions

D. ANIMATED RESULTS

With the addition of the rectangular air bubble regions, the shockwave propagation behaved quite differently from the previous simulation with no air bubbles. Figure 13 shows a representation of this simulation from 4ms until 5ms after the initial time of detonation (t_o). At t_o+4ms, the shockwave has nearly reached its maximum size prior to interaction with the air bubbles. At t_o+4.5ms, a portion of the shockwave has collided with several air bubble regions. The shock front behind these regions diminishes substantially, but portions of the shockwave continue to propagate through the separation areas between the rectangular air bubble regions. At t_o+5ms, the shockwave continued to propagate around the air bubbles and the shock front continued to break down. Some high pressure areas from the initial shockwave remained. These portions passed through the water regions in between each air bubble.

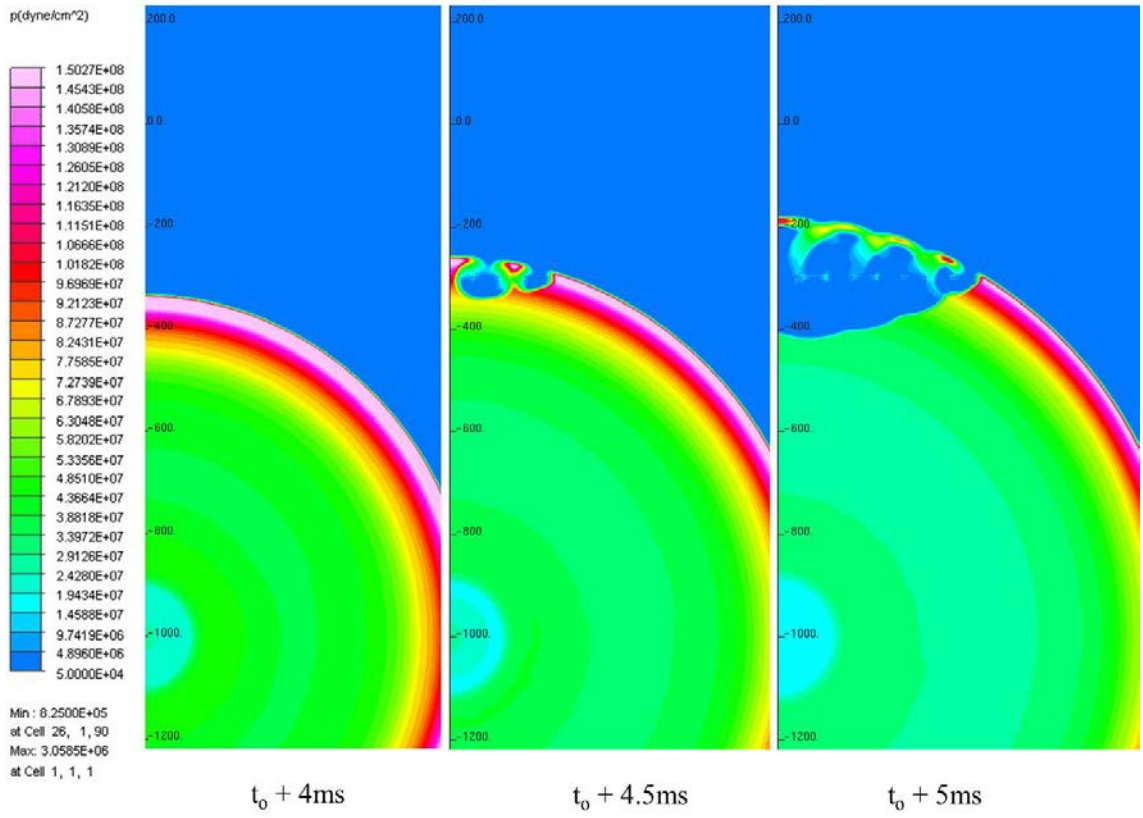

Figure 13. Interaction of Shockwave with Six Rectangular (4cm x 50cm) Air Bubble Regions from 4ms to 5ms following Detonation

Figure 14 shows an animated representation of this simulation from 5.5ms until 6.5ms. At t_o+5.5ms, the shock front has passed the area of concern and dissipates into the surrounding environment. At t_o+6ms, several of the air bubble regions exhibit an emission of high pressure despite the shockwave having passed by completely. This second pulse enacts a substantial amount of pressure on the surrounding environment which is similar to the initial shockwave pressure perceived by this region. This second pulse is due to the delayed collapse of the air bubble regions following the shockwave passing. At t_o+6.5ms, the pressure from the second pulse diminished quickly. While it failed to attain a defined shape and propagate further, it affected the immediate area surrounding the air bubble region with a sizeable pressure increase. This second loading could prove detrimental to a marine structure by disabling it or possibly destroying it.

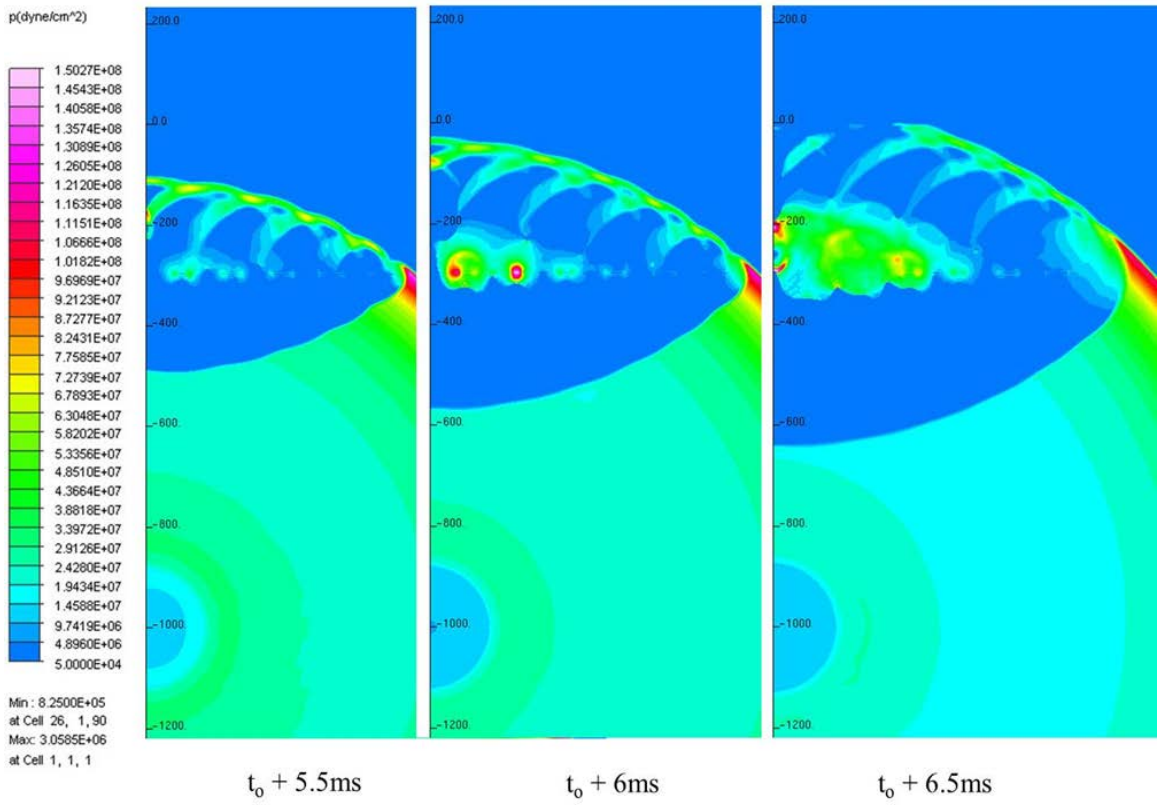

Figure 14. Interaction of Shockwave with Six Rectangular (4cm x 50cm) Air Bubble Regions from 5.5ms to 6.5ms following Detonation

E. PRESSURE-TIME HISTORY RESULTS

Figure 15 shows the pressure comparison across the three data collection points in Region A. The lower cell (126,899) experiences an immediate pressure increase of approximately 131.61×10^6 dyne/cm^2 (1908.78psi). The middle cell (126,901) is largely buffered from the shockwave due to its location within the air bubble region and experiences a nominal pressure increase. The upper cell (126, 903) does experience a pressure increase due to the initial shockwave, though not as large as the pressure at the lower cell. This is due to the reduction of energy and pressure of the initial shockwave when it interacts with the air bubble regions. This phenomenon occurs when the shockwave propagates around the air bubble region due to the impedance mismatch between the properties of the water and the air bubble region, whose properties mirror those of water vapor.

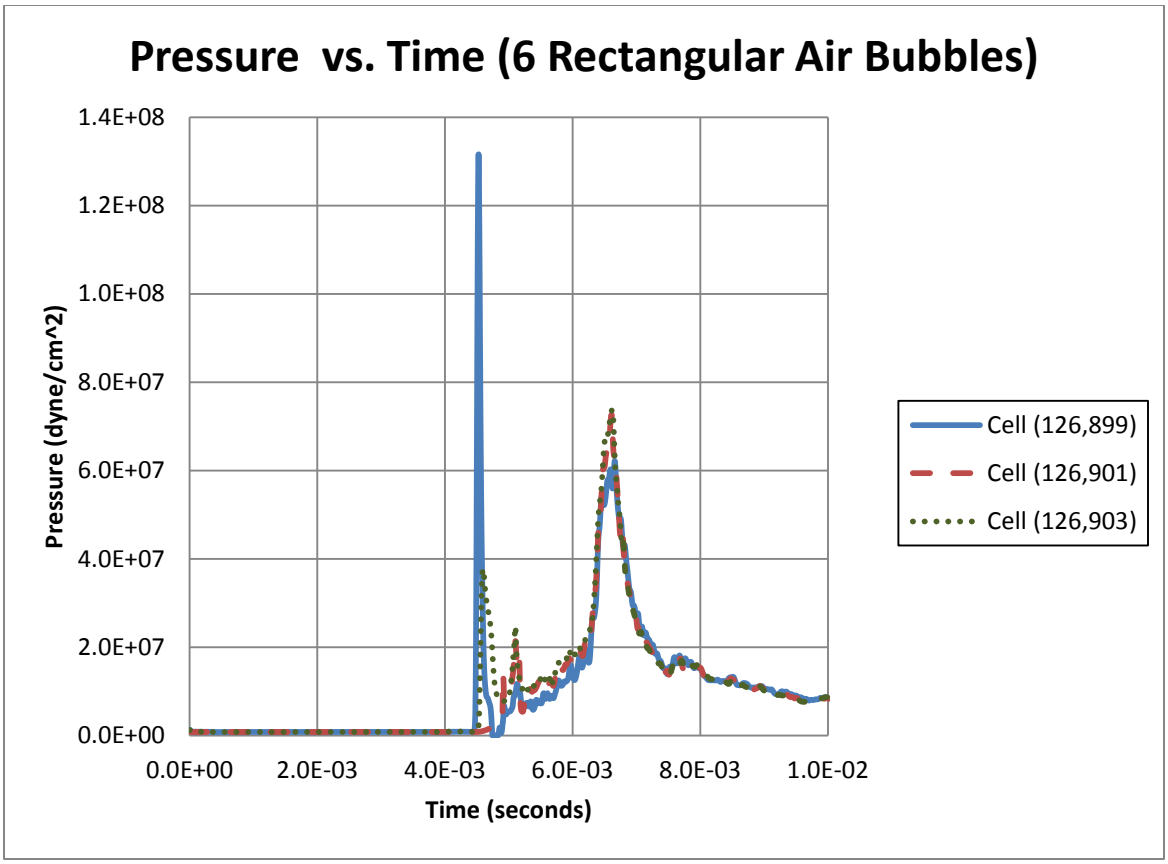

Figure 15. Pressure-Time Comparison of Region A with Six Rectangular (4cm x 50cm) Air Bubble Regions

A major difference that occurred in this simulation vice the previous simulation without any air bubble regions is the occurrence of a second pressure peak. This occurs at approximately 6.6ms after the detonation. A reason for this occurrence is the collapse and expansion of the air bubble region due to the high pressure shockwave.

Table 8 lists the pressures and their respective times at the two pressure peaks. With the exception of the lower cell, the second peak is substantially larger in magnitude in comparison to the first peak. The middle cell experiences a 240% increase in pressure while the upper cell experiences a 95% increase in pressure.

Table 8. Comparison of First and Second Pressure Peaks Resulting from an UNDEX Event Involving Six Rectangular Air Bubble Regions

	First Peak		Second Peak	
	Pressure (dyne/cm^2)	Time (ms)	Pressure (dyne/cm^2)	Time (ms)
Lower Cell	1.3161E+08	4.525	6.2206E+07	6.658
Middle Cell	2.1363E+07	5.105	7.2600E+07	6.613
Upper Cell	3.7766E+07	4.593	7.3749E+07	6.613

While these pressure increases are substantial, they are relatively low when compared to the simulation without air bubbles. Figures 16 through 18 compare the pressures at each data collection point collected during the simulation with no air bubbles and the simulation with six rectangular air bubbles.

Figure 16 compares the pressures recorded at the lower cell. This data location remained unchanged from the simulation without an air bubble permitting an easy comparison of the data. The first pressure peak occurred near-instantaneously and was followed by a rapid decrease in pressure. This occurred due to the reflection of the shockwave from the air bubble region. The pressures essentially cancel each other out. However, the pressure continues to rise steadily until the second pressure peak which occurs when the air bubble region collapses. This second pressure peak exceeds the pressure perceived by the lower cell at the same time during the simualtion without air bubbles. Following this second peak, the pressure decreases exponentially. Overall, the pressure perceived by the lower cell is less than the pressure encountered during the simulation without air bubbles.

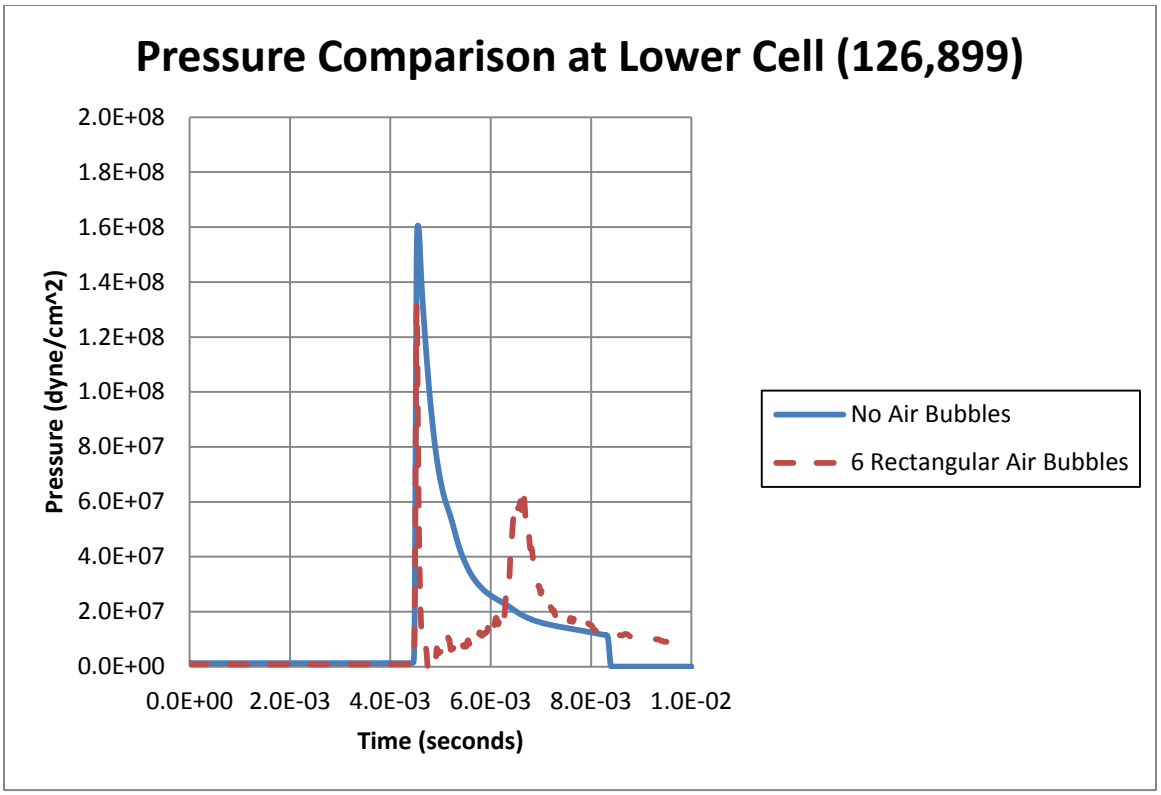

Figure 16. Pressure-Time History Comparison of the Lower Cell for Regions with and without Rectangular Air Bubbles

Figure 17 compares the pressures recorded at the middle cell which is within the air bubble region. The middle cell is largely buffered from the initial shockwave, but does experience a steady increase in pressure following the initial impact with the shockwave. The second pressure peak is higher than the pressure experienced by the lower cell. This is due to the closer proximity of the cell to the center of the air bubble collapse and expansion.

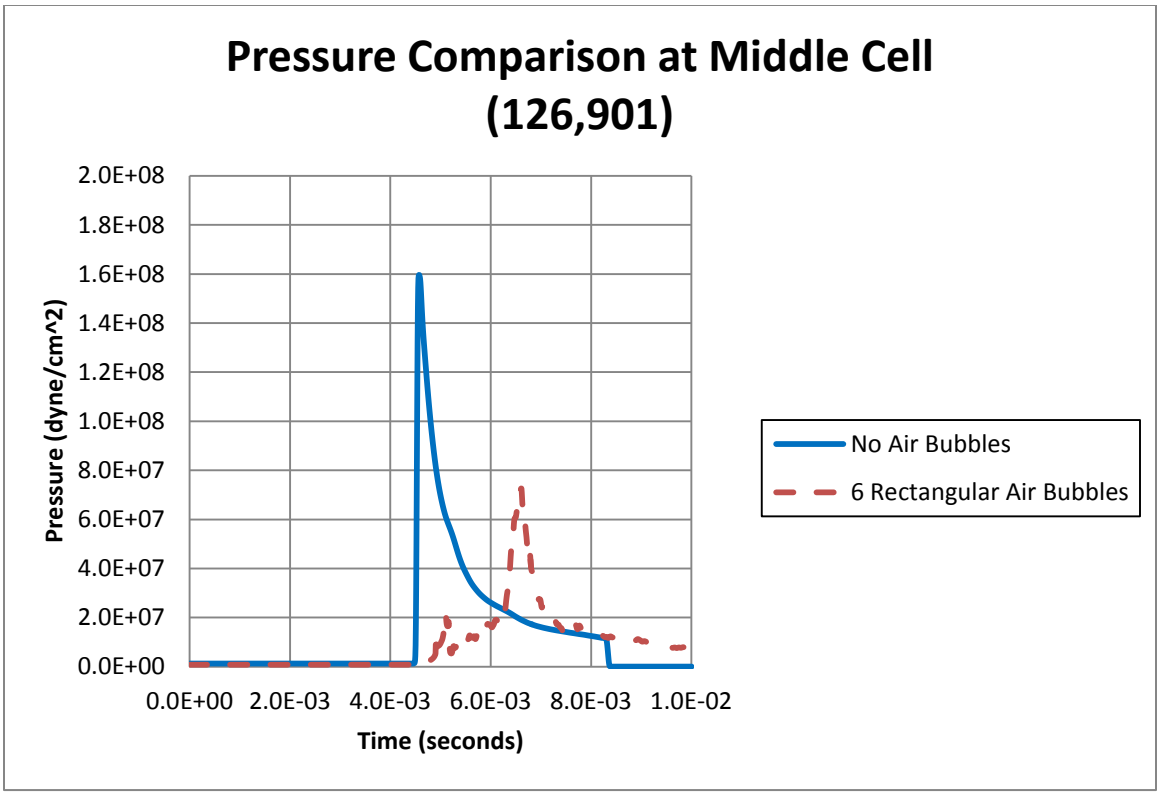

Figure 17. Pressure-Time History Comparison of the Middle Cell for Regions with and without Rectangular Air Bubbles

Figure 18 compares pressures at the last location to be examined, which is the upper cell. Since the upper cell is located at the border of the air bubble region and water, it experiences a slight pressure increase during the initial peak. This rise in pressure occurs when the shockwave wraps around the air bubble region and interacts with the backside of the region. The peak pressure is substantially less had the air bubble region not been there, so buffering did occur. The second pressure peak occurs at a similar time and with a similar magnitude as the peak encountered at the middle cell.

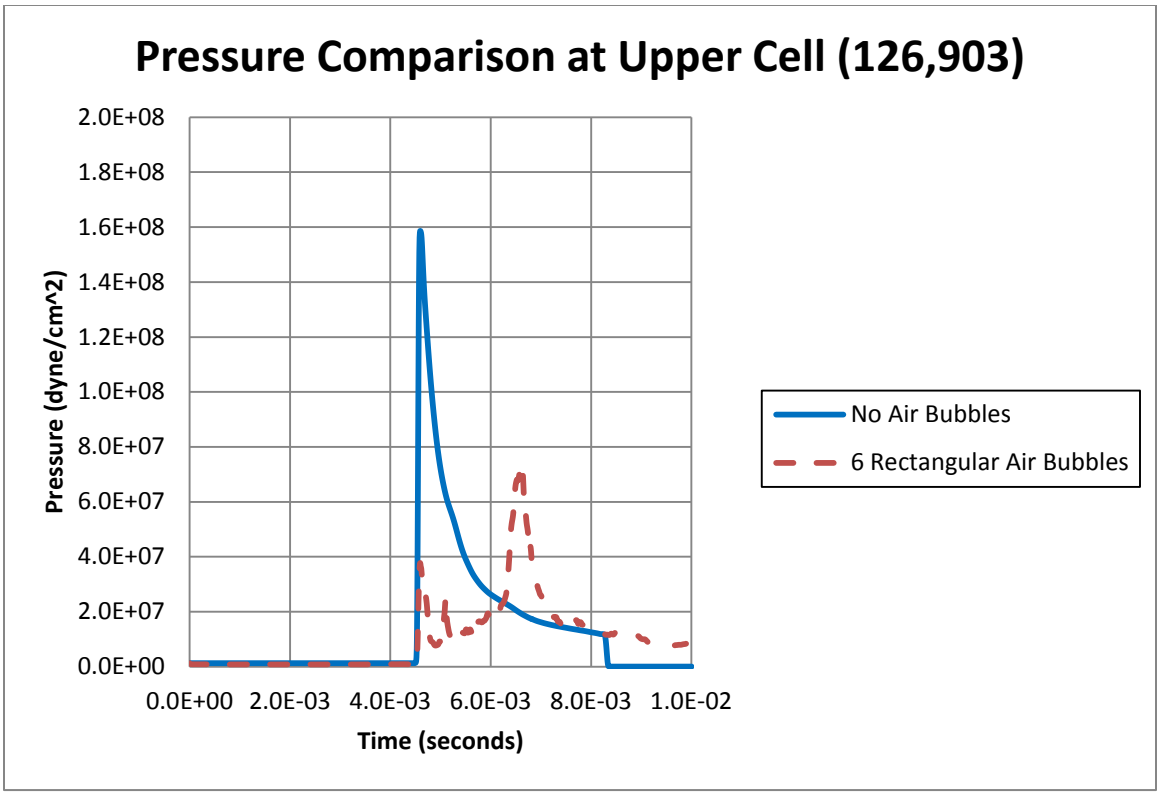

Figure 18. Pressure-Time History Comparison of the Upper Cell for Regions with and without Rectangular Air Bubbles

F. DISCUSSION OF RESULTS

When comparing the pressure-time histories, it is apparent that the rectangular air bubble regions provide a buffering effect in response to the first peak pressure. However, the shockwave compresses the bubbles initially which expand shortly thereafter. This expansion of energy is released in the form of a second pressure peak which is greater than the pressure previously encountered without the air bubble regions. Indeed the second pressure peak exceeds the initially perceived pressure at these data locations, but this is irrelevant when comparing the maximum pressure attained at each location throughout the event. When comparing maximum pressure over the entire timeframe, the pressures attained by the simulation with the rectangular air bubble regions do not exceed the maximum pressures encountered during the simulation without air bubbles. Hence, the six rectangular air bubble regions provided a buffering effect.

VII. TWO DIMENSIONAL SIMULATIONS INVOLVING CIRCULAR AIR BUBBLE REGIONS OF VARYING DIAMETERS

A. OVERVIEW

While the rectangular air bubble regions provided evidence of a buffering effect from a shockwave, their shape and size was not wholly realistic in terms of naturally occurring bubble regions. Since an air bubble does not have a defined shape or size, it was approximated as a circle in this study. By modeling the air bubble region as a circle, it closer resembles a naturally occurring bubble. Simulations were conducted on bubbles of varying diameters.

B. 4CM DIAMETER CIRCULAR AIR BUBBLE REGION

1. Justification

A diameter of 4cm was selected to serve as a transition from the 4cm x 50cm rectangular regions. The air bubble region aligned well with the previous setup and no major modifications were required of the grid or data collection locations.

2. Grid Setup

The grid was constructed in the same manner as shown in Figure 6 with the exception that a 4cm diameter circular air bubble region was added to Region A. Figure 19 shows the data collection locations in relation to the circle air bubble. These locations were unchanged to accommodate easy comparison of the results to prior simulations.

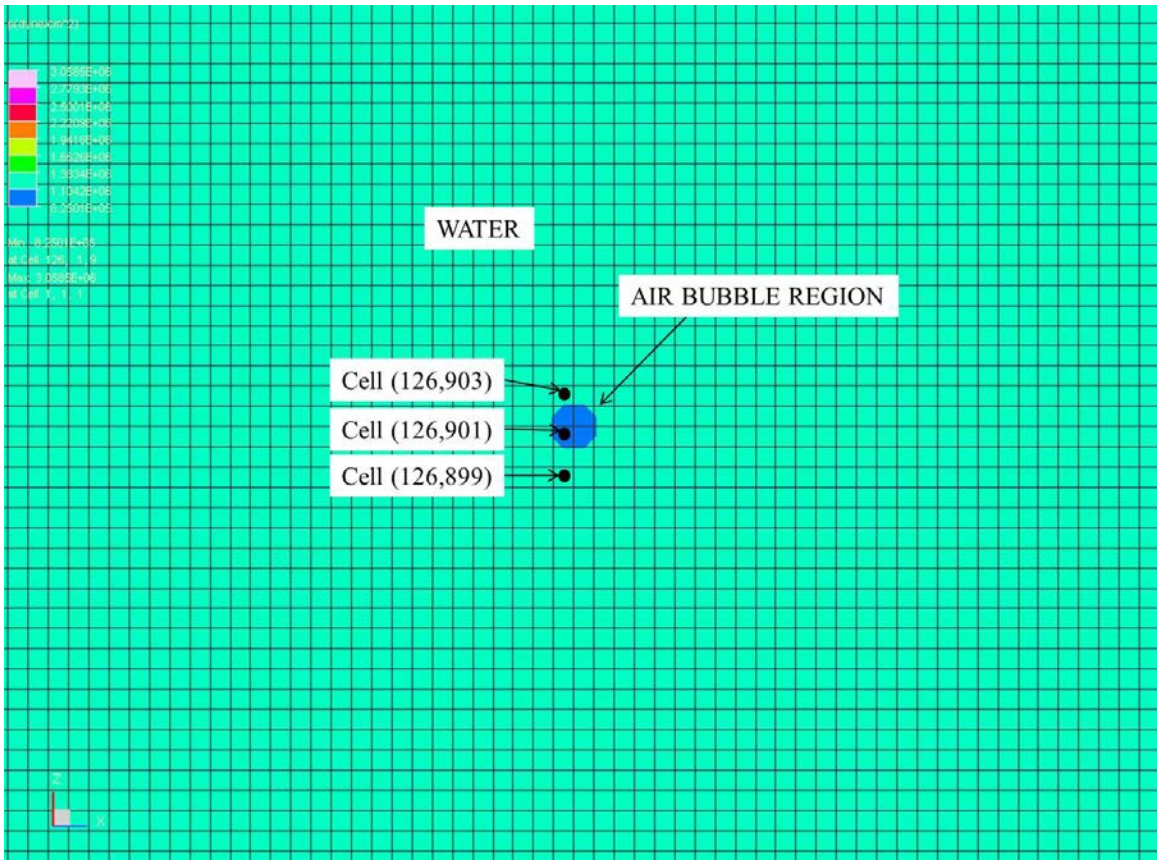

Figure 19. Data Locations for a 4cm Diameter Circular Air Bubble Region

3. Animated Results

After completion of the simulation, the results revealed a substantial reflection by the circular air bubble region. Visualization of the results is presented in Figures 20 and 21.

Figure 20 shows the shockwave progression from 4.5ms to 6ms after detonation. Between 4.5ms and 5ms, the shockwave causes the air bubble to collapse and subsequently expand leading to second pressure peak. At t_o+5ms, the reflected shockwave propagates outward from the location of the circular air bubble. This reflected shockwave has a magnitude equivalent to the initial shockwave which propagated around and beyond the circular air bubble. Because of this disruption, the initial shock front diminished slightly following its interaction with the air bubble. However, the reflected shockwave is following directly behind with a similar pressure

magnitude. At t_o+5.5ms, a cavitation region developed in the lower left portion of the reflected shockwave. This occurs due to the reflection of the initial shockwave from the air bubble region. At t_o+6ms, the reflected shock front closely follows the initial shock front. There are some minor color differences between the two shock fronts, indicating a pressure difference. The reflected shock front has a nominal pressure of 8.9769E+07dyne/cm^2 while the initial shock front has nominal pressure of 9.9632E+07dyne/cm^2. This difference in magnitude between the two fronts occurs because the reflected shockwave pressure decreases more rapidly than the initial shockwave.

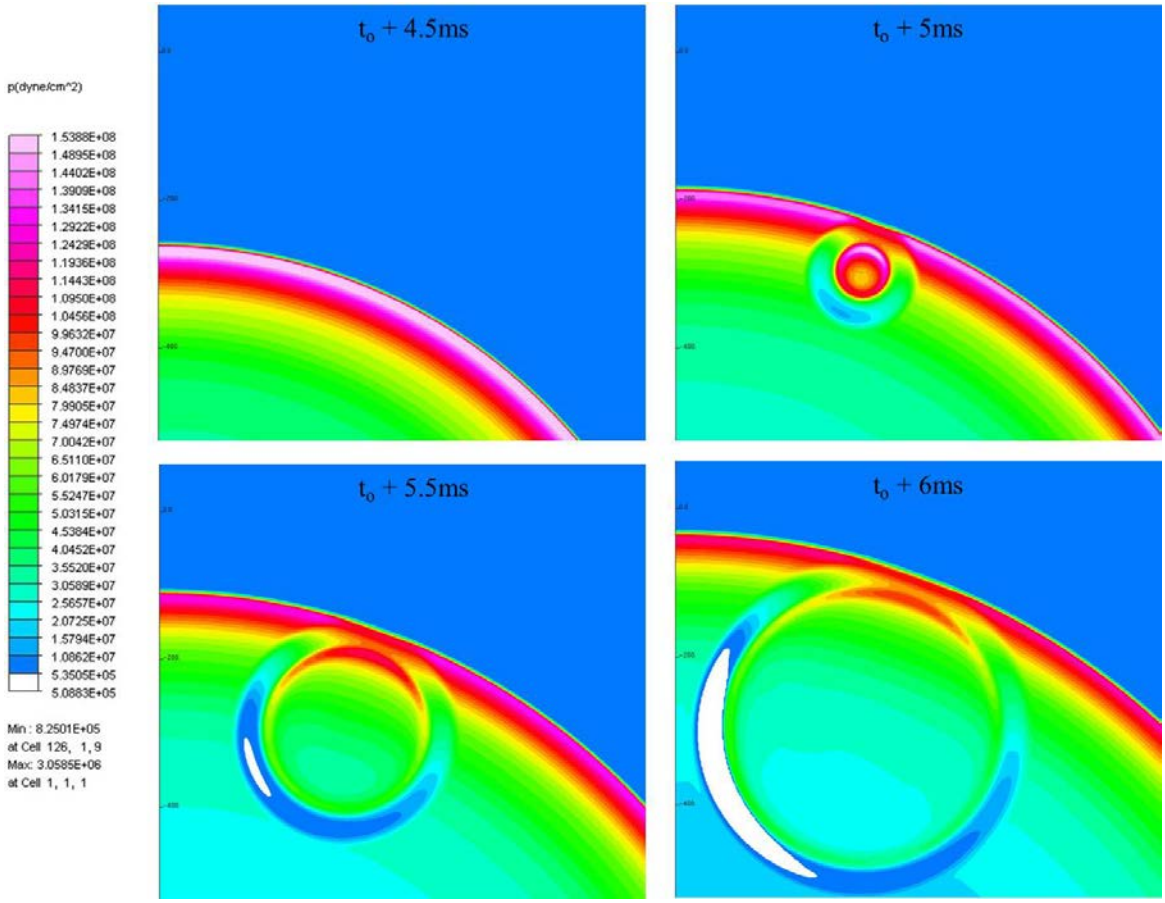

Figure 20. Interaction of Shockwave with a 4cm Diameter Air Bubble Region from 4.5ms to 6ms following Detonation

Figure 21 shows the shockwave progression from t_o+6.5ms until t_o+8ms. In this series of images, the reflected shockwave is nearly diminished in terms of pressure while

the initial shockwave continued to propagate outward with a sizeable pressure front. The initial shockwave reached the surface of the water and is reflected back into the water. This reflection creates a cavitation zone which is visible near the air-water interface. As the time history progresses, the cavitation zone propagates downward into the water column at which point the simulation is terminated.

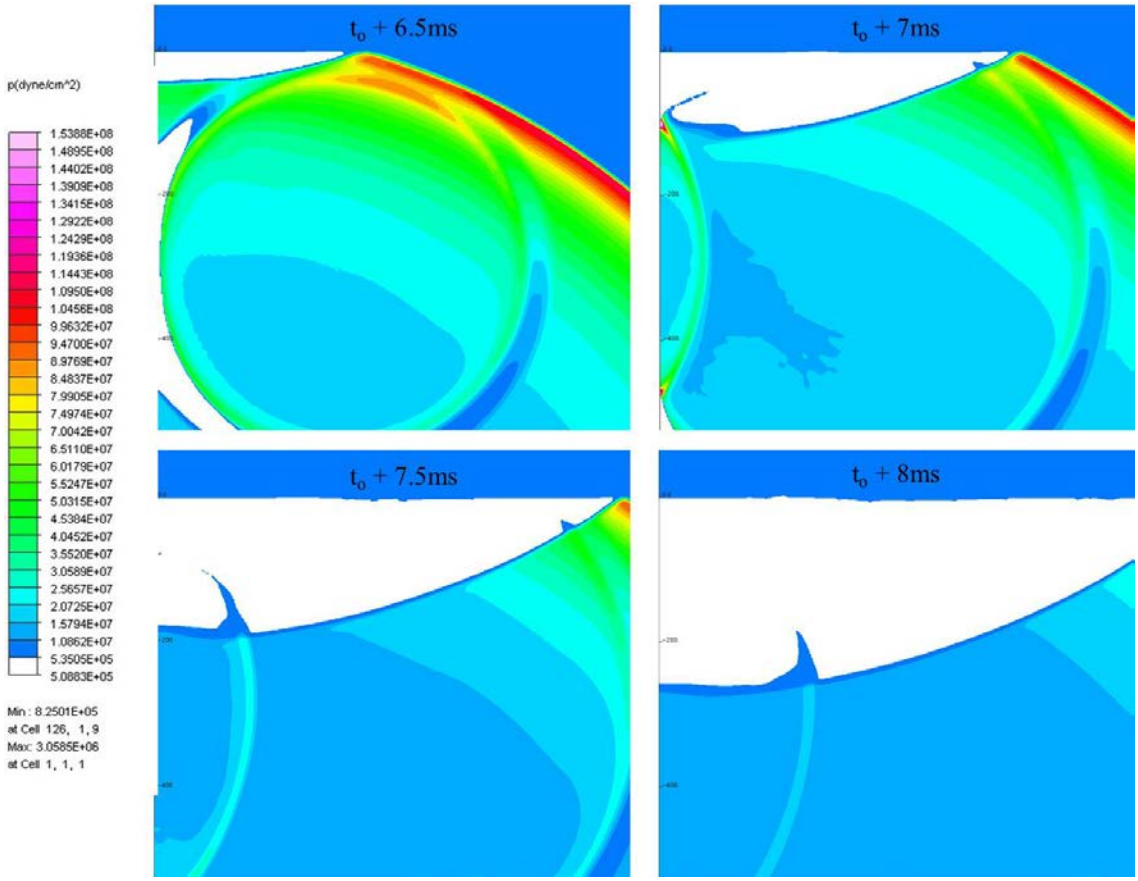

Figure 21. Interaction of Shockwave with a 4cm Diameter Air Bubble Region from 6.5ms to 8ms following Detonation

Table 9 lists the pressures recorded at the data locations surrounding the air bubble. These locations are annotated in Figure 19. All locations experience maximum pressures greater than the pressures encountered during the initial simulation with no air bubble. For comparison, the maximum pressure at the middle cell (126,901) during the initial simulation was 1.5964×10^8 dyne/cm^2. While the first peak pressure experienced by

the lower cell is less than the maximum pressure attained during the initial simulation, a second pressure peak is observed only by this cell. This second pressure peak is 60% larger in magnitude than the first pressure peak.

Table 9. Pressure Comparison of a 4cm Diameter Air Bubble subjected to an UNDEX Event

	First Peak		Second Peak	
	Pressure (dyne/cm^2)	Time (ms)	Pressure (dyne/cm^2)	Time (ms)
Lower Cell	1.3298E+08	4.525	2.1295E+08	4.832
Middle Cell	2.9306E+08	4.798	N/A	N/A
Upper Cell	2.9260E+08	4.798	N/A	N/A
Middle Cell (No Air Bubble)	1.5964E+08	4.571	N/A	N/A

4. Pressure-Time History Results

Figure 22 is the pressure-time history plot for the simulation involving the 4cm diameter air bubble region. The first pressure peak of the lower cell (126,899) is clearly separated from the main grouping of pressure peaks occurring at 4.8ms. Upon closer inspection, it is apparent that the pressure rise of the upper cell (126,903) occurs prior to the rise of the middle cell (126,901). The cause of this faster rise originates from the sound propagation properties of water and water vapor. As noted in Table 7, the speed of sound in water is over three and a half times faster than the speed of sound in water vapor. Since pressure waves propagate with similar properties to that of sound, the pressure wave reaches the upper cell prior to reaching the middle cell.

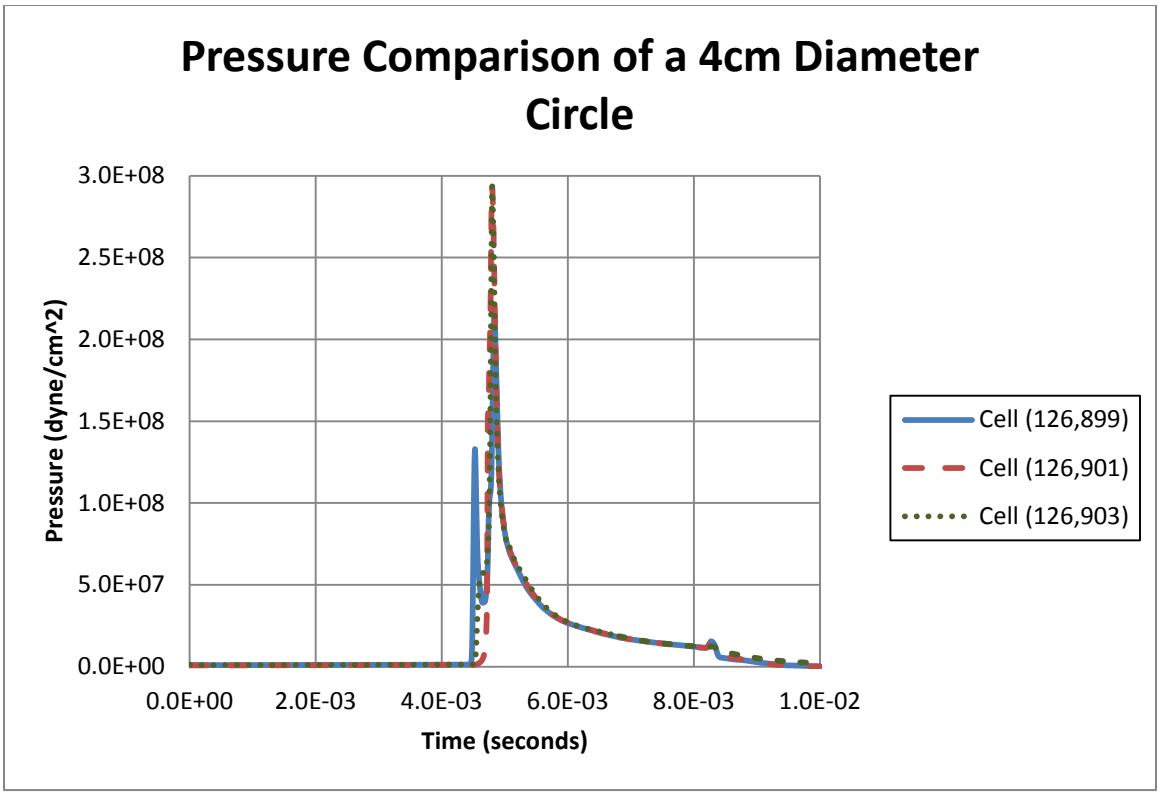

Figure 22. Pressure-Time Comparison of Region A with a 4cm Diameter Circular Air Bubble Region

5. Discussion of Results

After comparison of the data with previous simulations, it is apparent that the interaction of a 4cm air bubble with a shockwave amplifies the initial pressure of the shock front. Since the pressure increase is substantially greater than the pressure observed without any air bubbles, the associated stresses observed by marine structures in the vicinity of this air bubble could lead to failure of the structure.

The second pressure peak, experienced in previous simulations with rectangular air bubble regions, was essentially non-existent in this simulation. This second peak did not appear due to the smaller size of the air bubble region.

This simulation shows that the introduction of a small circular air bubble region during an UNDEX event increases the pressures in the immediate vicinity which could prove detrimental to a nearby marine structure.

C. 2CM DIAMETER CIRCULAR AIR BUBBLE REGION

1. Justification

Following simulation of the 4cm diameter circle, other sizes of circle air bubble regions were considered in order to compare and contrast the results at both ends of the spectrum. A 2cm diameter region was evaluated to represent the small end of the range.

2. Grid Setup

The grid dimensions and layout remained the same as noted in Figure 6 with the exception that a 2cm diameter air bubble was added in Region A. The grid was uniformly spaced and the data locations remained unchanged from previous simulations. Figure 23 shows the data collection locations in relation to the air bubble region. Their locations provided good pressure readings before, during, and after the pressure wave passed.

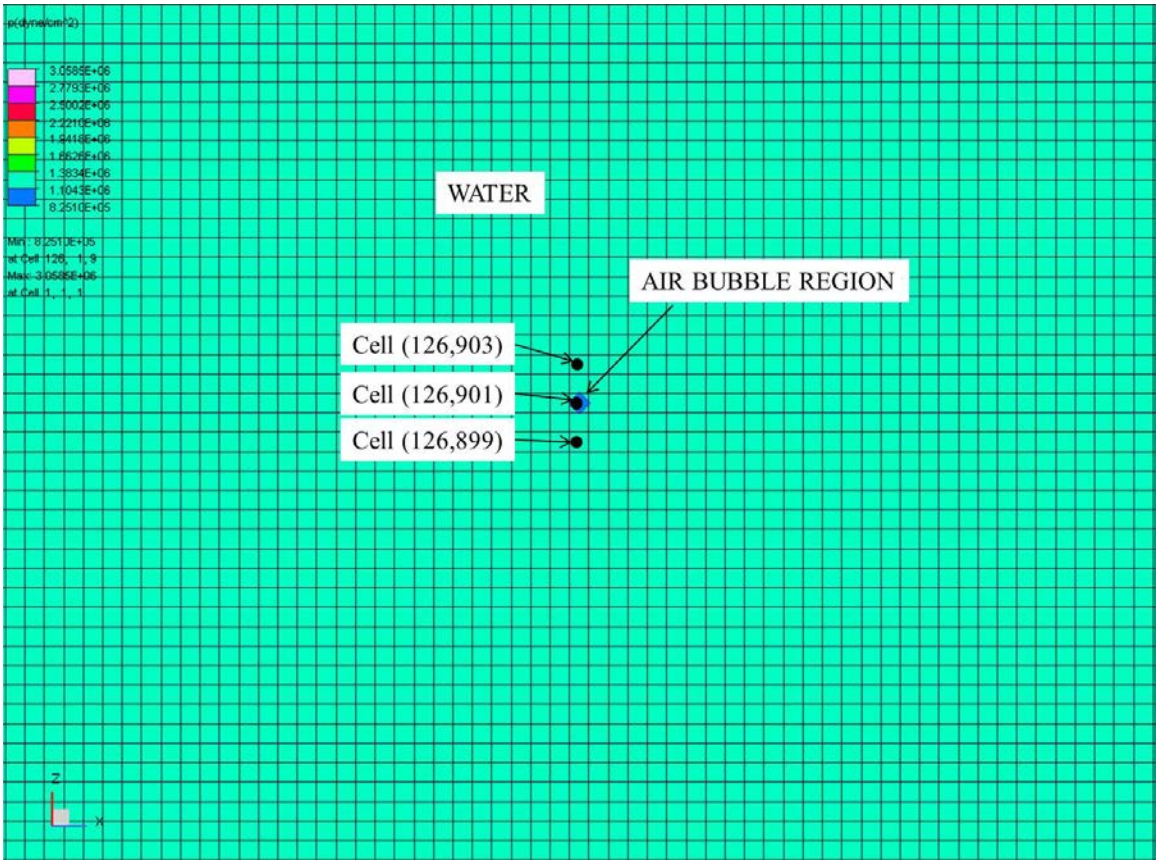

Figure 23. Data Locations for a 2cm Diameter Circular Air Bubble Region

3. Animated Results

Figure 24 shows the recorded animation from t_o+4.5ms to t_o+ 6ms. During this time, the shockwave reaches and interacts with the air bubble. Due to the small size of the air bubble, the shockwave passes largely unhindered and the shock front maintains its initial shape and magnitude. A minor reflection is visible at t_o+5ms which propagates outward. The reflected shock front quickly reflects into the initial shock front which appears undiminished by t_o+6ms.

No cavitation areas are formed between t_o+4.5ms and t_o+6ms. This is different from the simulation involving a 4cm diameter air bubble. By reducing the air bubble size, the likelihood of formation of these areas is reduced.

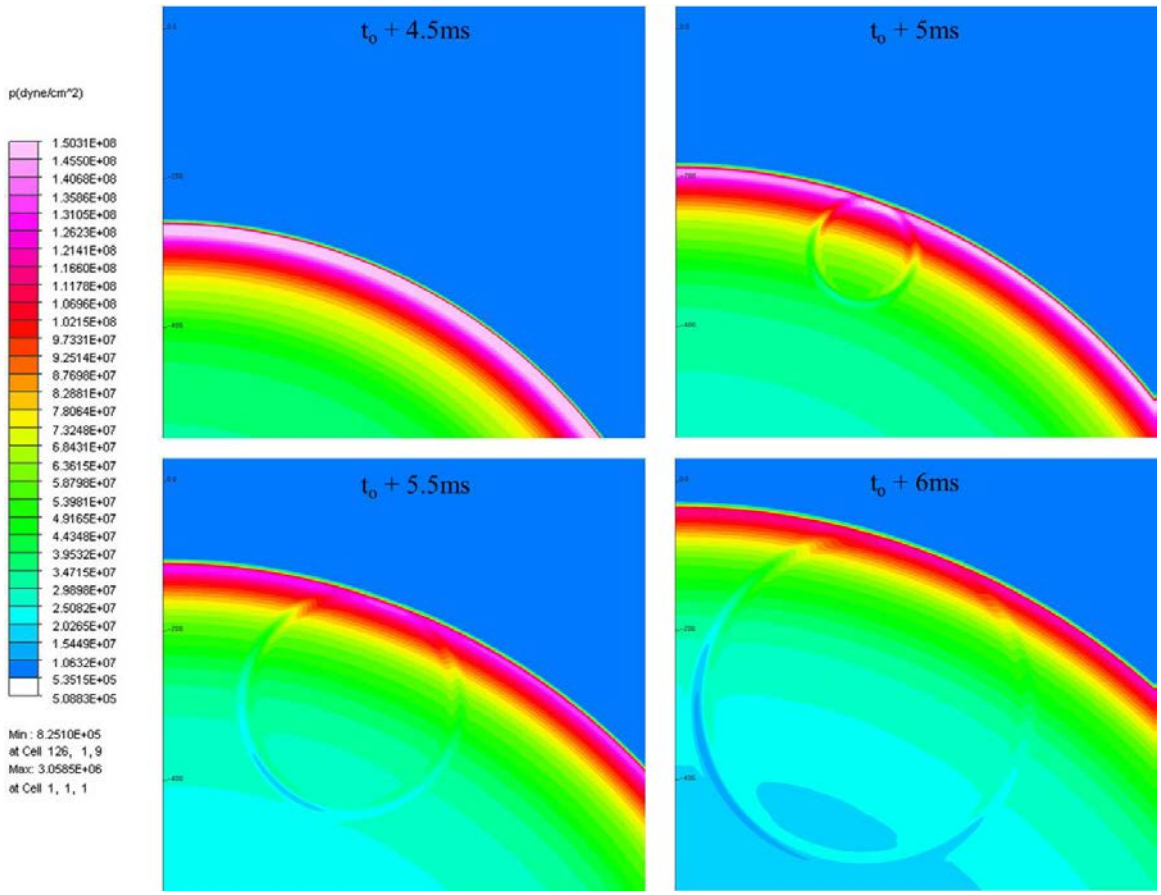

Figure 24. Interaction of Shockwave with a 2cm Diameter Air Bubble Region from 4.5ms to 6ms following Detonation

Figure 25 shows an animated history of the simulation from t_o+6.5ms to t_o+8ms. The shock front appears wholly undeterred by the air bubble interaction. The cavitation zone (represented by the white region) forms below the water surface and propagates outward.

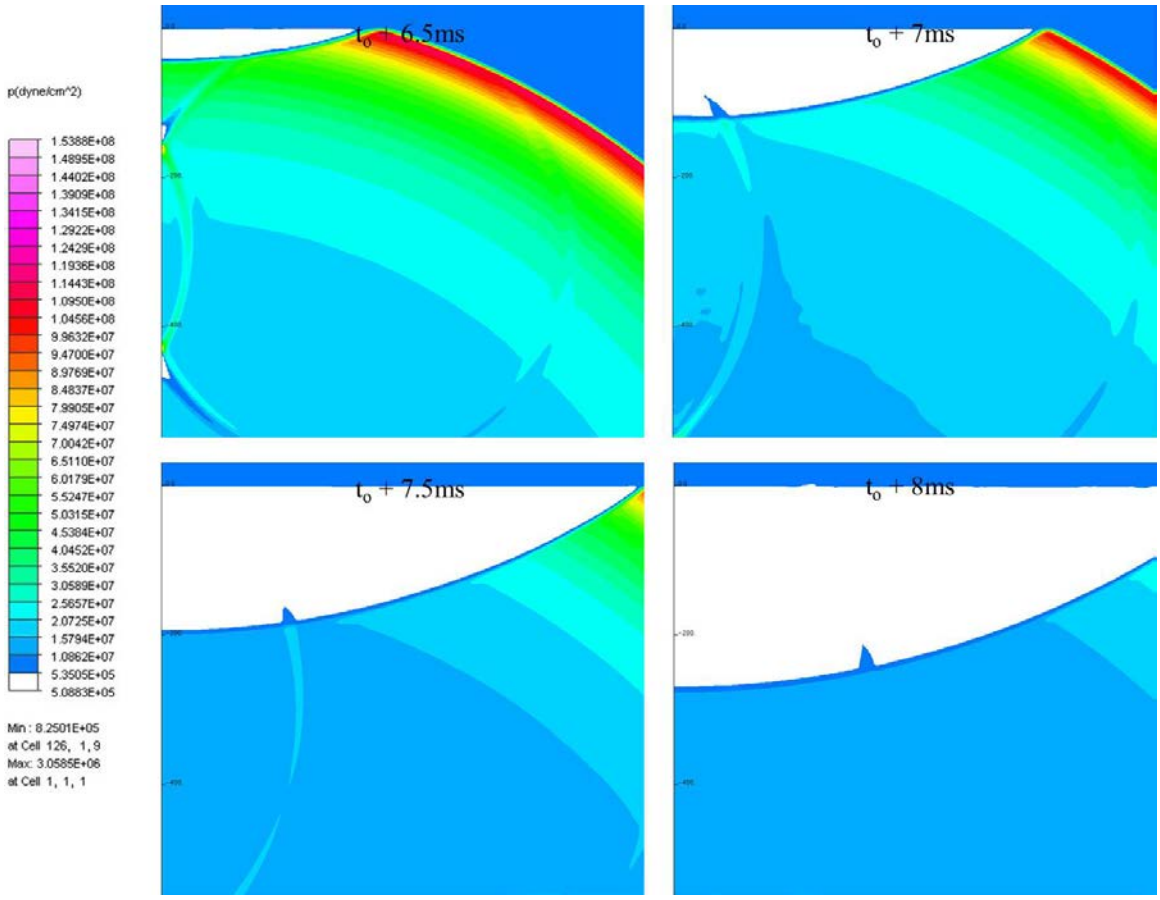

Figure 25. Interaction of Shockwave with a 2cm Diameter Air Bubble Region from 6.5ms to 8ms following Detonation

4. Pressure-Time History Results

When comparing the pressure-time history in Figure 26, it is important to note the general shape of the curve. The shape appears similar to the pressure-time history of the simulation with no air bubble in Figure 8. With the exception of the lower cell (126,899),

the other cells experience an instantaneous increase in pressure due to the shockwave arrival. This sharp increase is followed by a constant exponential decrease in pressure. The steady decrease continues until t_o+8ms, at which time the surface cutoff occurs.

Upon closer examination of Cell (126,899), it is apparent there are two pressure increases although they occur near-simultaneously and appear as one continuous pressure increase. The pressure at this cell increases prior to the other cell locations, as expected. The pressure rises at the middle and upper cells at approximately the same time due to the small diameter of the air bubble. If this were a larger air bubble a slight difference between these two pressure increases would be apparent.

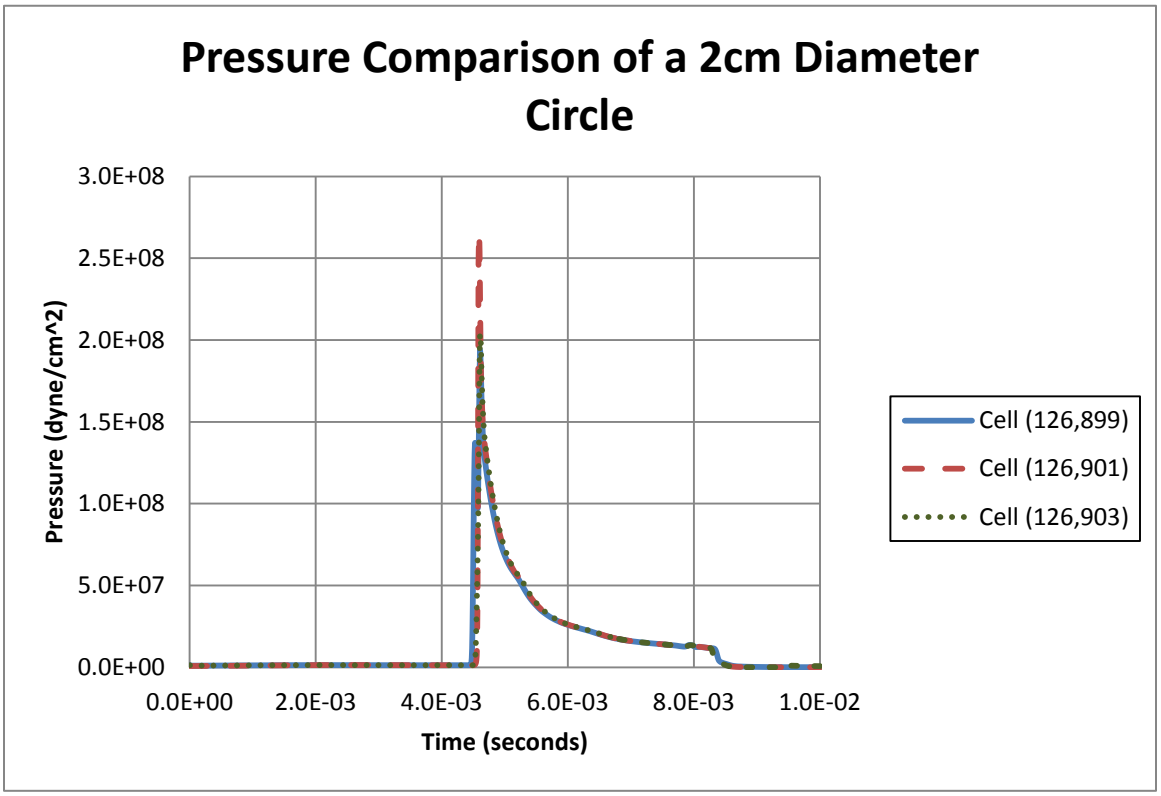

Figure 26. Pressure-Time Comparison of Region A with a 2cm Diameter Circular Air Bubble Region

5. Discussion of Results

For this simulation involving a decrease in the air bubble radius, it is visually apparent that the effect this region has on the shockwave is less than the impact of the

4cm diameter air bubble. However, when comparing the pressure-time history analysis, the amount of pressure perceived by the data collection locations is much greater than the pressures encountered by the same locations during the simulation with no air bubble. For comparison, the pressures are tabulated in Table 10. All locations experience a maximum pressure greater than the pressure experienced in a region devoid of air bubbles. The conclusion can be made that the presence of a small air bubble significantly magnifies the initial pressure generated during an UNDEX event.

Table 10. Pressure Comparison of a 2cm Diameter Air Bubble subjected to an UNDEX Event

	First Peak		Second Peak	
	Pressure (dyne/cm^2)	Time (ms)	Pressure (dyne/cm^2)	Time (ms)
Lower Cell	1.3689E+08	4.525	1.9296E+08	4.605
Middle Cell	2.6525E+08	4.593	N/A	N/A
Upper Cell	2.0356E+08	4.605	N/A	N/A
Middle Cell (No Air Bubble)	1.5964E+08	4.571	N/A	N/A

D. 20CM DIAMETER CIRCULAR AIR BUBBLE REGION

1. Justification

Having already determined the results from small air bubble regions previously, a simulation involving an air bubble at the opposite end of the spectrum was desired. In order to accommodate this, a 20cm diameter air bubble was created and evaluated to compare with the previous results.

2. Grid Setup

For this simulation, the overall dimensions and layout were maintained as noted in Figure 6, however, a 20cm diameter air bubble was added in Region A. The grid was uniformly spaced with cells of 2cm x 2cm. Due the increase in diameter of air bubble, the data locations required Hopkinson scaling to remain equidistant from the air bubble.

The parameters were based upon the previous simulation involving the 4cm diameter air bubble. Figure 27 shows the data collection locations in relation to the air bubble region.

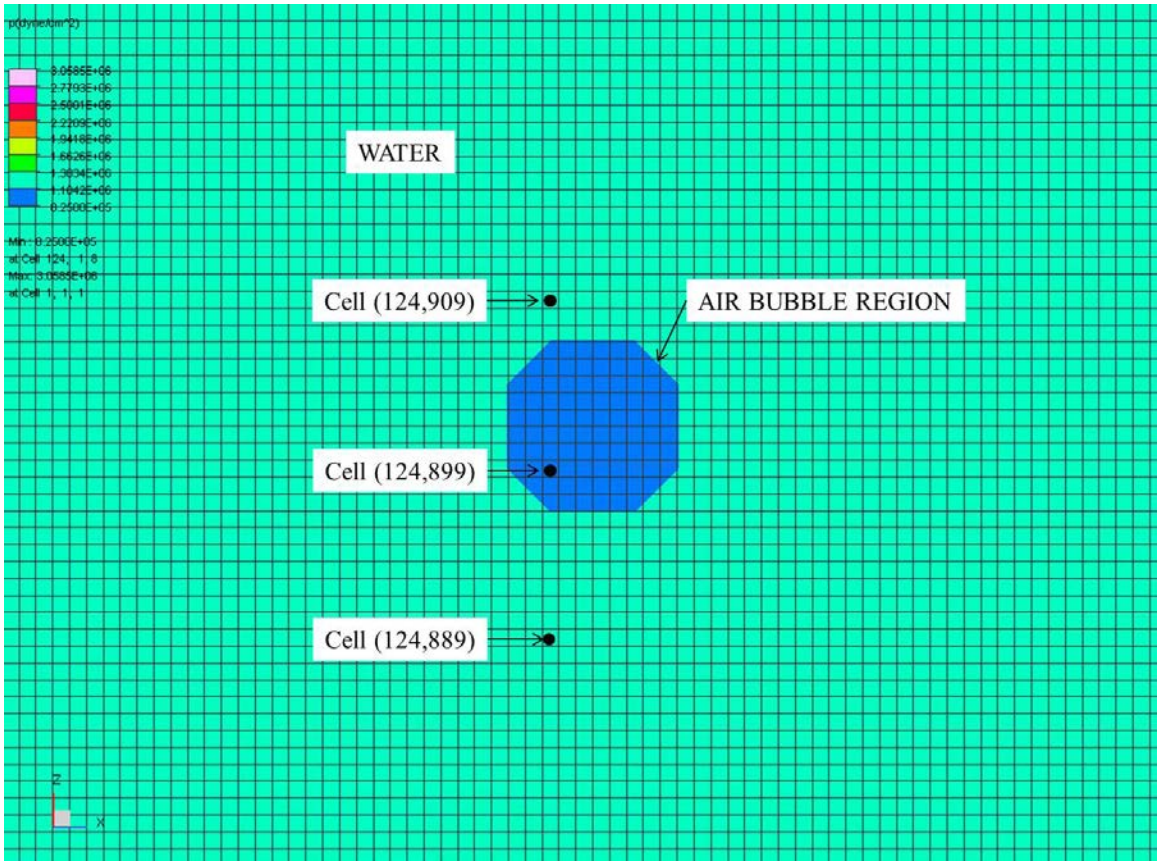

Figure 27. Data Locations for a 2cm Diameter Circular Air Bubble Region

3. Animated Results

Figures 28 and 29 are visual representations of the UNDEX event. These images were selected to best portray the event following the initial detonation time (t_o). At t_o+4.5ms, the shockwave makes contact with the air bubble and the shock front becomes indented. From t_o+5ms through t_o+6ms, the shockwave reflects off the air bubble and a cavitation zone is created. This air bubble induced cavitation zone forms in the lower left region in the direction of the detonated charge and becomes comparable in size to the surface cavitation zone which forms shortly thereafter at t_o+6.5ms.

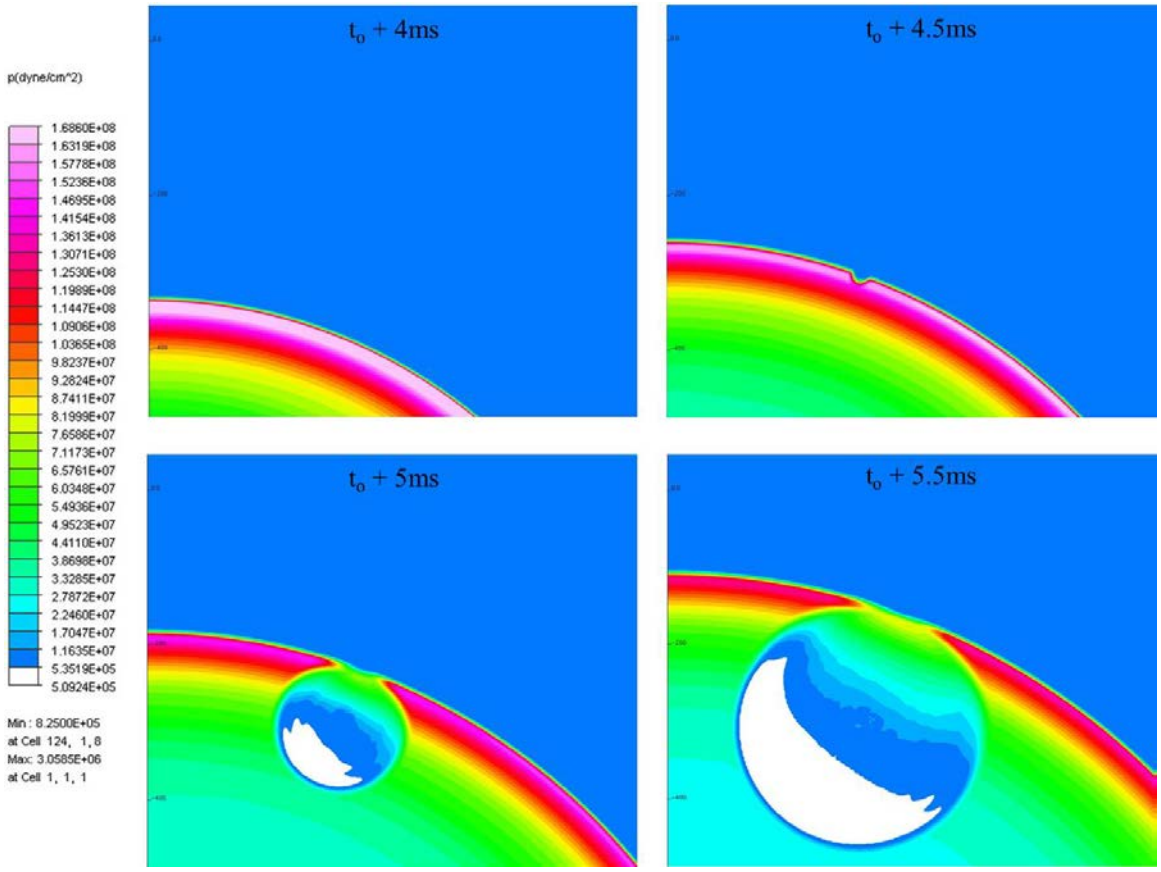

Figure 28. Interaction of Shockwave with a 20cm Diameter Air Bubble Region from 4ms to 5.5ms following Detonation

Figure 29 shows the later stages of this simulation. At t_o+6.5ms, the surface and air induced cavitation zones are formed and propagating outward. Also at this time, pressure starts to rise at the location of the air bubble. This is the start of the expansion phase following the air bubble's collapse due the shockwave. At t_o+7ms, the air bubble continues to expand and the pressure increases greatly. However, by t_o+7.5ms, the pressure from this expansion is largely diminished and produces little effect beyond the immediate vicinity of the original air bubble.

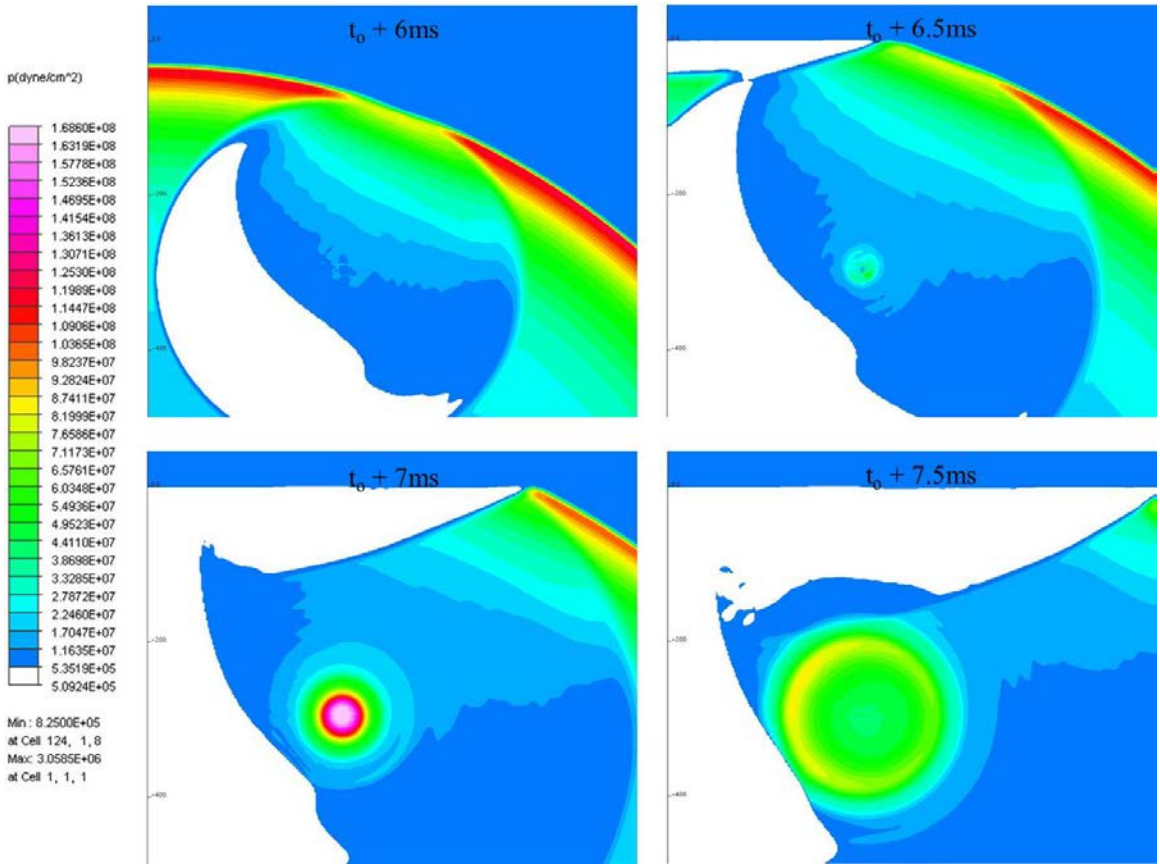

Figure 29. Interaction of Shockwave with a 20cm Diameter Air Bubble Region from 6ms to 7.5ms following Detonation

4. Pressure-Time History Results

While the animated results are excellent for gaining a visual understanding of this phenomenon, the pressure-time history provides quantifiable information at the prescribed data collection locations noted in Figure 27. There are two defined pressure peaks perceived by the lower cell. The sharp decrease in pressure following the first pressure peak is due to the reflection of the shockwave from the air bubble. After this, the pressures of all cells remain relatively low, but begin to rise slowly. At approximately t_o+7ms, the second pressure peak occurs. This second pressure peak occurs at a substantially later time and at a lower pressure than second pressure peaks studied in earlier simulations. This is due to the increased size of the air bubble region.

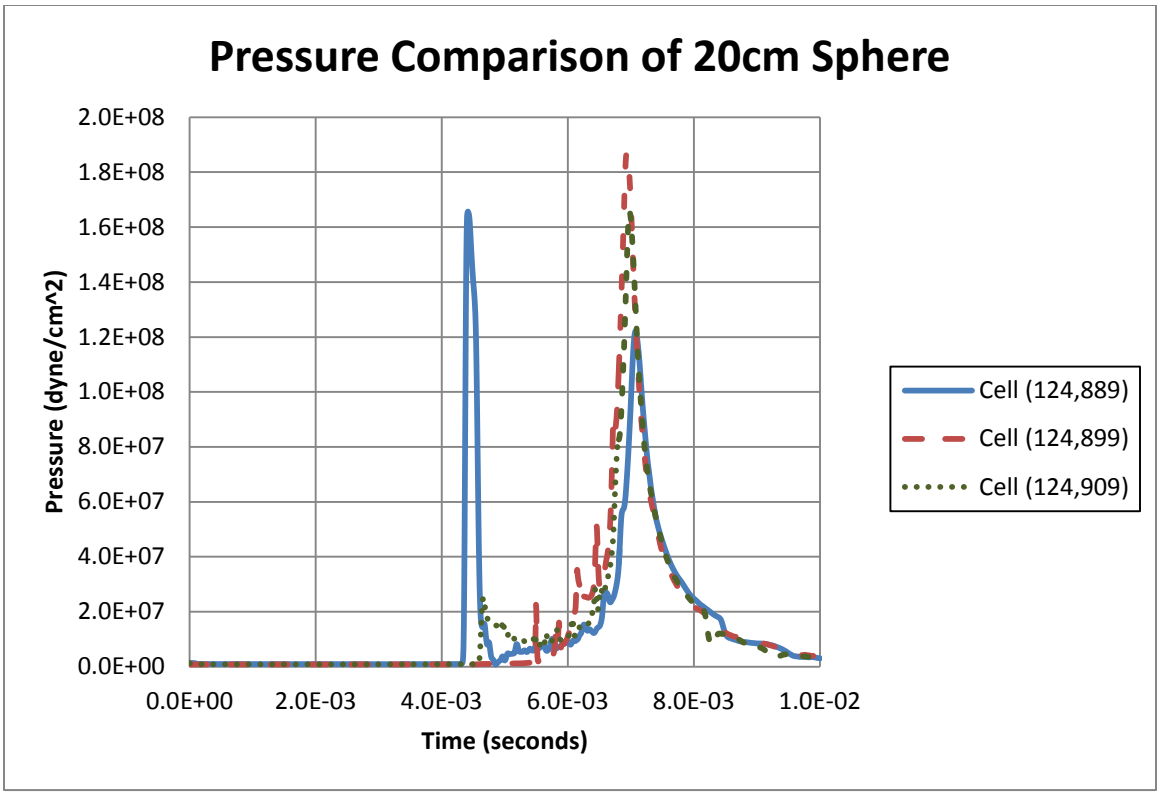

Figure 30. Pressure-Time Comparison of Region A with a 20cm Diameter Circular Air Bubble Region

5. Discussion of Results

When comparing the pressures associated with this simulation, it is apparent that the large air bubble region does little to increase the pressure. Table 11 compares the pressures at the three data locations used in this simulation against the pressure from the simulation without an air bubble. There is a buffering effect that occurs for the lower cell following the first pressure peak. The pressures at the lower and upper cells largely remain similar to the initial simulation, whose pressure was 1.5964E+08dyne/cm^2. When comparing the middle cell for both simulations, the 20cm diameter air bubble generated a higher pressure than perceived initially.

Table 11. Pressure Comparison of a 20cm Diameter Air Bubble subjected to an UNDEX Event

	First Peak		Second Peak	
	Pressure (dyne/cm^2)	Time (ms)	Pressure (dyne/cm^2)	Time (ms)
Lower Cell	1.6560E+08	4.412	1.2211E+08	7.072
Middle Cell	1.8734E+08	6.934	N/A	N/A
Upper Cell	1.6566E+08	6.980	N/A	N/A
Middle Cell (No Air Bubble)	1.5964E+08	4.571	N/A	N/A

E. COMPARISON OF ALL CIRCULAR AIR BUBBLE REGIONS

1. Overview

The following pressure-time history analyses directly compare the results of each circle diameter with the initial simulation with no air bubble. The data collection locations remained the same for all simulations with the exception of the 20cm diameter air bubble which required scaling in relation to the center point of Region A.

2. Pressure-Time History Comparison and Analysis

The first data comparison is of the pressure-time history collected at the lower data location, shown in Figure 31. This location experienced the brunt force of the shockwave due to its location directly in the path between the charge and the air bubble (if present) in Region A. All scenarios experienced a near-instantaneous increase in pressure when the shockwave arrived. The addition of small air bubble regions (2cm and 4cm) increased the pressure encountered at this location. The pressure for these two air bubble regions decrease in a similar manner as the region with no air bubble. Only the 20cm diameter air bubble region experienced a second pressure peak. However, this pressure peak was less in magnitude than the first pressure peak.

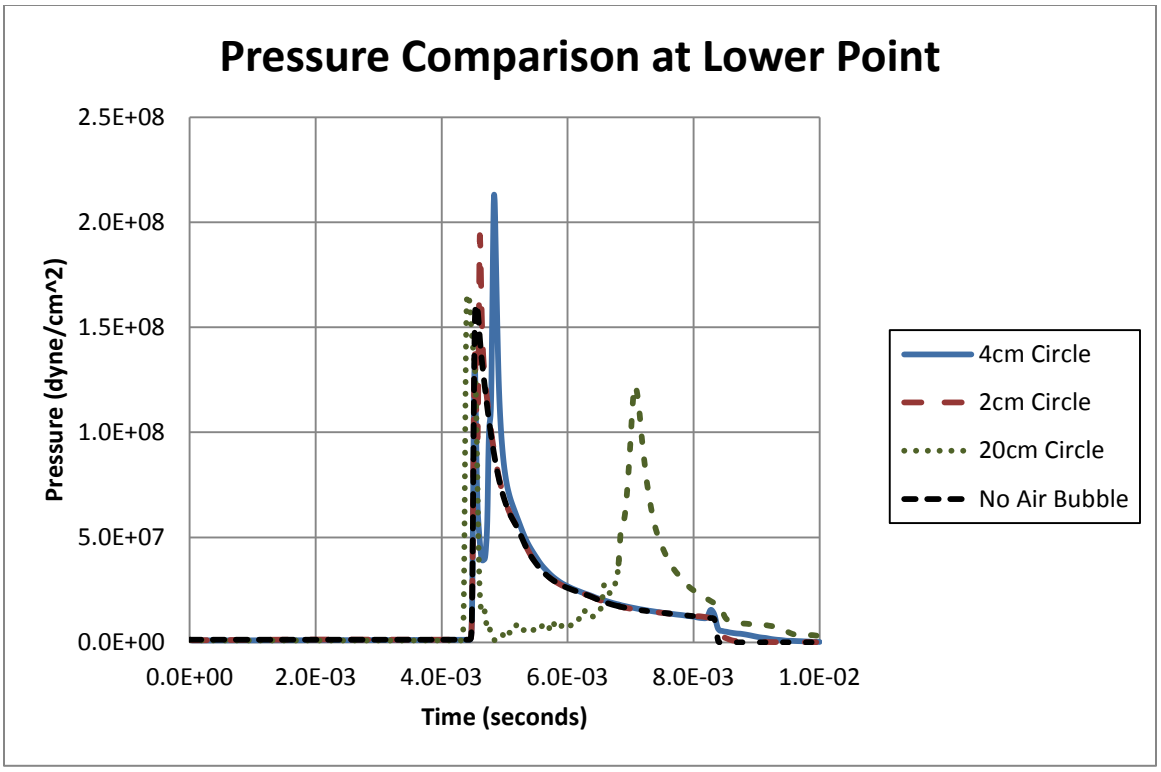

Figure 31. Pressure-Time Comparison at the Lower Data Location for all Circle Diameters

The second area to be compared was the data collected at the middle location which remained within the air bubble region for simulations where it was added. In Figure 32, the initial pressure increase is apparent. Coincidentally, the pressure is greatly increased for the 2cm and 4cm diameter air bubbles. This is due to the collapse and expansion of the air bubble region which causes a release of energy in the form an additional shockwave. For the 4cm diameter air bubble, the increase in pressure is nearly 100% which is substantial. Following the pressure peak, these two simulations decrease similar to the simulation with no air bubble. Meanwhile, the 20cm diameter air bubble does not experience a pressure increase until much later. This increase is not as substantial as the smaller air bubble regions. It is due to the large initial size of the air bubble which requires more energy to be compressed. The size of the air bubble greatly affects the maximum pressure(s) perceived.

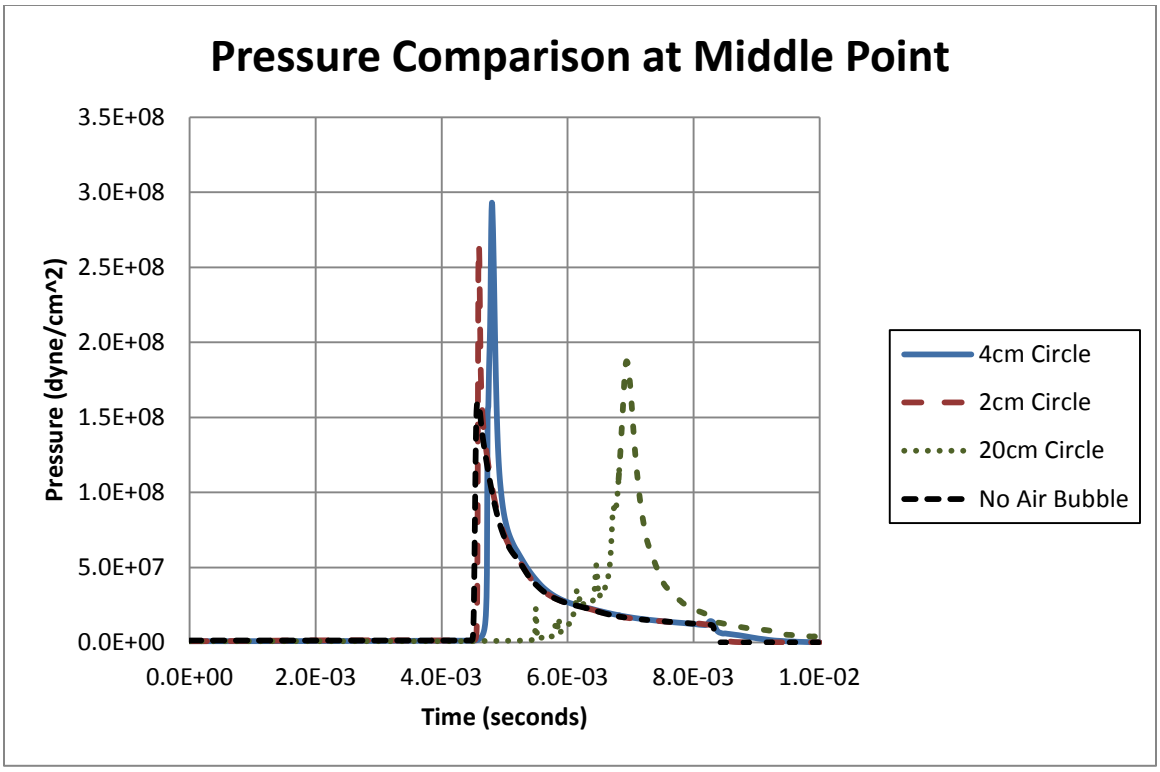

Figure 32. Pressure-Time Comparison at the Middle Data Location for all Circle Diameters

The final area to be compared was the upper cell location which is a probable location for a marine structure. Figure 33 compares the pressures at this location. As seen previously, the pressure increased dramatically when the shockwave arrived. The pressure increase of the 4cm diameter air bubble was the greatest, again a near 100% increase in magnitude. The 2cm diameter air bubble experienced an increase in pressure though not as pronounced as previously. Both these simulations decreased in the same manner as the example with no air bubble. The 20cm diameter cell did not undergo a pressure increase until much later. This is again due to the time and energy required to compress the initial air bubble. The peak pressure of this scenario was nominally equal to the simulation without an air bubble. Therefore, the addition of a 20cm air bubble affects the pressure in neither a positive nor negative manner.

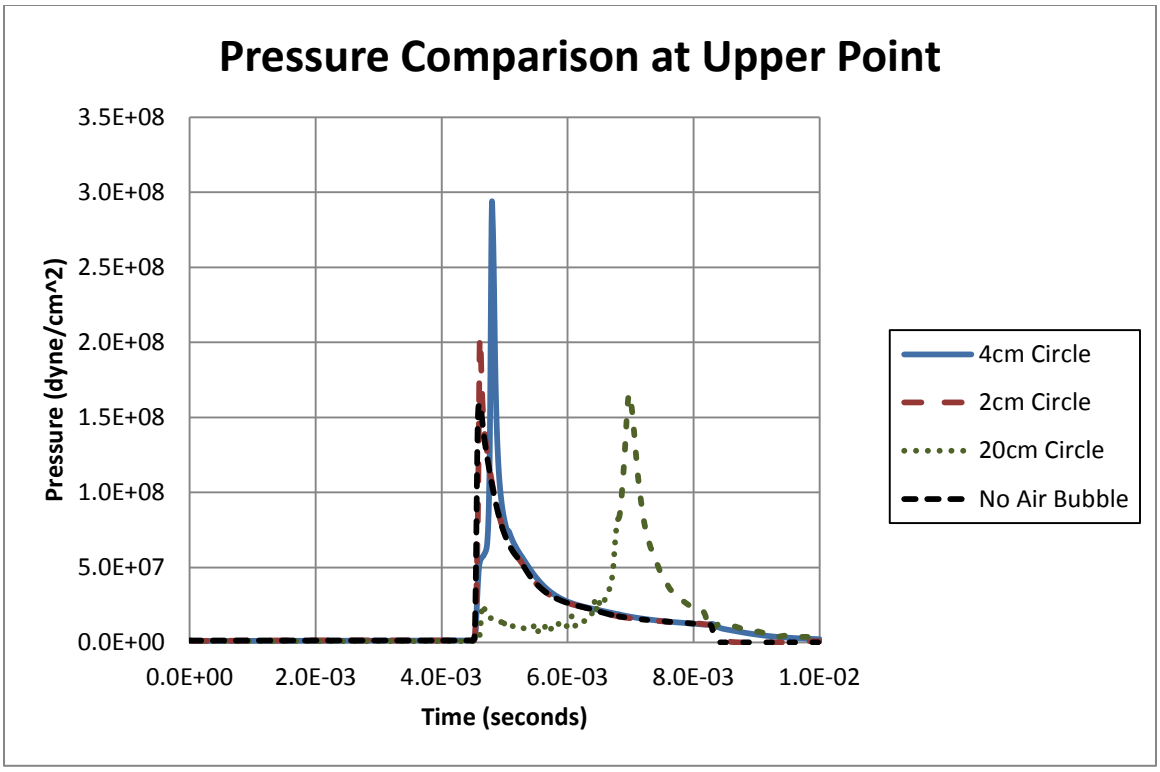

Figure 33. Pressure-Time Comparison at the Upper Data Location for all Circle Diameters

3. Discussion of Analysis

After review of these results, it is apparent that the size of the air bubble region greatly influences the pressure output. A smaller air bubble magnifies the pressure significantly while a larger air bubble magnifies it to a lesser extent. This occurred largely at the middle cell. This pressure could further damage a marine structure in the vicinity of an UNDEX event.

Also, the air bubble size influences the time for a shockwave to propagate as noted with the 20cm diameter scenario where the pressure peak did not occur until a later time when compared to the smaller bubble diameters. However, it does not necessarily buffer the region downstream from the shockwave effects. At the very least, the shockwave propagates through the air bubble region delivering the same amount of pressure to the other side.

THIS PAGE INTENTIONALLY LEFT BLANK

VIII. TWO DIMENSIONAL SIMULATIONS INVOLVING A SMALL AIR BUBBLE REGION USING A REFINED MESH

A. REFINED MESH WITHOUT AIR BUBBLE REGION

1. Justification

During the mesh refinement, it was discovered that the pressure output by the shock-induced air bubbles was substantially greater than the unrefined mesh simulations run previously. In order to eliminate the possibility of computer miscalculations and provide a reliable comparison for future results, a simulation was created without an air bubble added.

2. Grid Setup

The overall dimensions were the same as shown in Figure 6. The mesh was refined in accordance with the measurements in Table 1. No air bubble was present in Region A.

3. Animated Results

The animated results are not shown due to their similarity to the images shown in Figure 7. A minor change exists between this simulation and follow-on refined mesh simulations in regards to the time step. The time step for this simulation was set at 0.5ms whereas in the follow-on simulations involving a refined mesh the time step was set at 0.1ms. This difference is considered minor.

4. Pressure-Time History Results

The pressure-time history results are not presented since all cells had a similar pressure profile as shown in Figure 8. It is important to note that the main difference between the refined and unrefined pressure readings was the maximum pressure recorded. An abbreviated comparison of the pressure recordings is shown in Table 12. The maximum pressures at the remaining data locations were similar in magnitude to these pressures and occurred at similar times.

Table 12. Pressure Comparison of a Region without Air Bubbles in a Refined Mesh subjected to an UNDEX Event

	First Peak		Second Peak	
	Pressure (dyne/cm^2)	Time (ms)	Pressure (dyne/cm^2)	Time (ms)
HORIZONTAL COLUMN				
Cell (143,929)	1.5004E+08	4.585	N/A	N/A
Cell (153,929)	1.5024E+08	4.595	N/A	N/A
Cell (163,929)	1.5001E+08	4.591	N/A	N/A
VERTICAL COLUMN				
Cell (153,919)	1.5040E+08	4.586	N/A	N/A
Cell (153,929)	1.5024E+08	4.595	N/A	N/A
Cell (153,939)	1.5001E+08	4.599	N/A	N/A
DIAGONAL COLUMN				
Cell (143,919)*	1.5040E+08	4.582	N/A	N/A
Cell (153,929)	1.5024E+08	4.595	N/A	N/A
Cell (163,939)	1.4986E+08	4.598	N/A	N/A
Cell (183,959)	1.4869E+08	4.648	N/A	N/A
Middle Cell (No Air Bubble, Unrefined)**	1.5964E+08	4.571	N/A	N/A

*Equivalent cell for this location is the Middle Cell (No Air Bubble, Unrefined)
**Equivalent cell for this location is Cell (143,919)

5. Discussion of Results

For regions without an air bubble, the difference between a refined and unrefined mesh is slight. The pressure difference is approximately 0.0924E+08dyne/cm^2. The reason for this difference is due to the increased density of cells within Region A. Having a higher concentration of cells in this region improves the calculation within it based upon the principles of finite element analysis. Thus the pressures determined at data collection locations within this refined mesh are considered more accurate than those pressures determined using an unrefined or coarse mesh.

B. REFINED 4CM DIAMETER CIRCULAR AIR BUBBLE REGION

1. Justification

Since the 4cm diameter produced the largest pressure increase, it was desired to further investigate this particular size of bubble. In order to better understand this scenario, a refined mesh was designed to improve accuracy of calculation and obtain a better representation of this phenomenon. This refined mesh encompassed the air bubble with 0.1cm x 0.1cm square cells. Also, the time-step for the animated portions was reduced to 0.1ms to allow better visualization of the experiment. This was a shift from previous animations which had a 0.5ms time step.

2. Grid Setup

The refined mesh was constructed based upon the design parameters outlined in Table 1. The adjustment in cell size can be seen in Figure 34. As the area of interest is approached, where the air bubble is located, the cells decrease in size from 2cm x 2cm to 0.1cm x 0.1cm.

For this simulation, 25 data points were recorded. A benefit of having this amount of cells was that the shockwave effects could be studied at greater distances from the air bubble, this was not possible previously since the data locations were in the immediate vicinity of the air bubble. Here the cells were positioned in three columns of nine: one horizontal, one vertical, and one diagonal. These columns intersected at the center of the air bubble which was selected to be cell (153,929). A close up depiction of this layout is shown in Figure 35, less the far outlying cells which are shown in Figure 34. These outer cells proved advantageous in discovering the pressure effects at a short distance from the air bubble center.

The location of the air bubble remained in Region A as noted previously in Figure 6. The major difference in terms of the grid for this simulation was the refinement of the mesh in the region surrounding the air bubble.

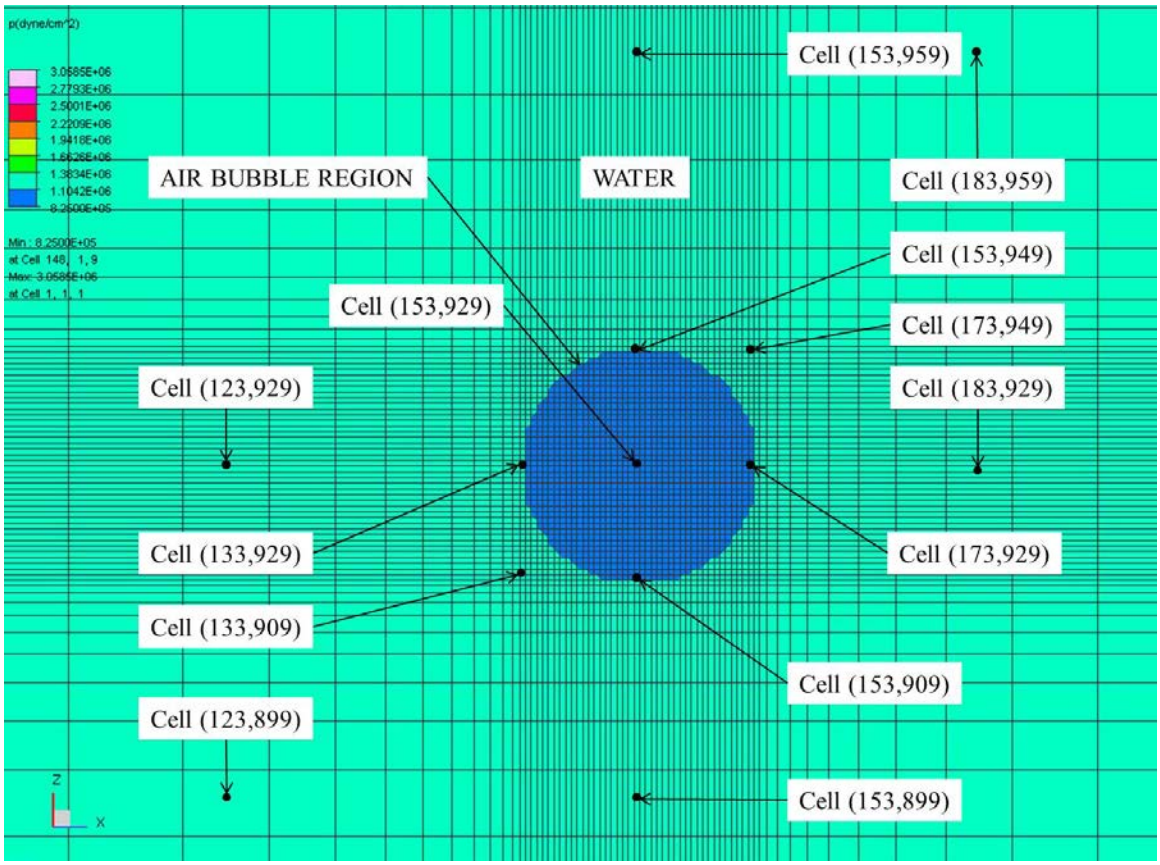

Figure 34. Outer Data Locations for a 4cm Diameter Circular Air Bubble Region in a Refined Mesh

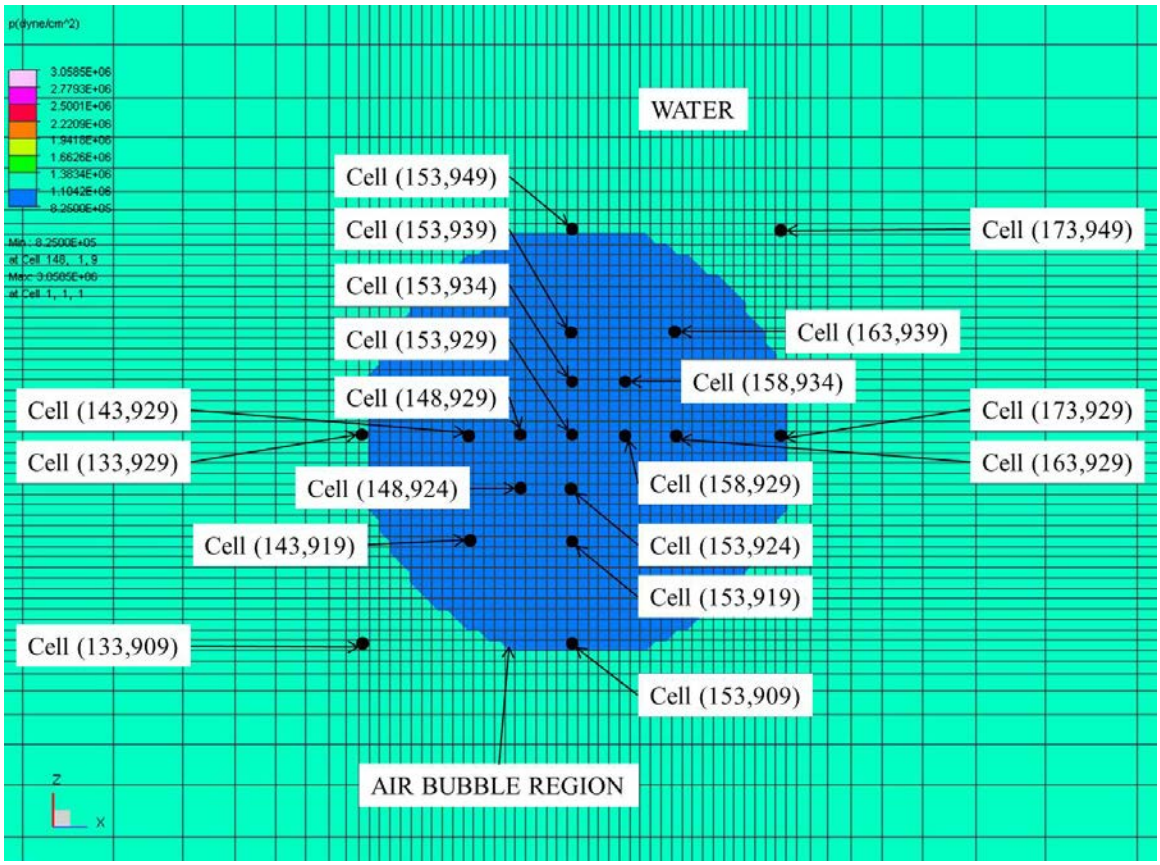

Figure 35. Inner Data Locations for a 4cm Diameter Circular Air Bubble Region in a Refined Mesh

3. Animated Results

With the time step reduced to 0.1ms, minute details that were previously overlooked were better examined. The simulation lasted 10ms after the time of detonation (t_o). Figure 36 covers the initial interaction with the shockwave until the start of expansion of the air bubble. At t_o+4.5ms, the shockwave reaches the air bubble and the indentation is barely visible. By t_o+4.6ms, the shockwave wraps around the air bubble and continues to propagate outward creating a weakened shock front following the wrapping of the air bubble. The shock front recovers somewhat at t_o+4.7ms and the pressure around the air bubble is substantially lower than the surrounding area. This low pressure area occurs due to two factors: (1) compression of the air bubble by the initial shockwave and (2) reflection of the shockwave from the air bubble due to difference in material properties of these two regions. Next the air bubble reaches its maximum

compressible size and begins to expand. This can be seen at t_o+4.8ms where the pressure of this expanding air bubble exceeds the surrounding shock front. This high pressure region is indicated by the light pink circle. Of note is the observation that the initial shock front has fully wrapped around the air bubble and reformed, though not as well defined or powerful as initially. This also occurs at t_o+4.8ms.

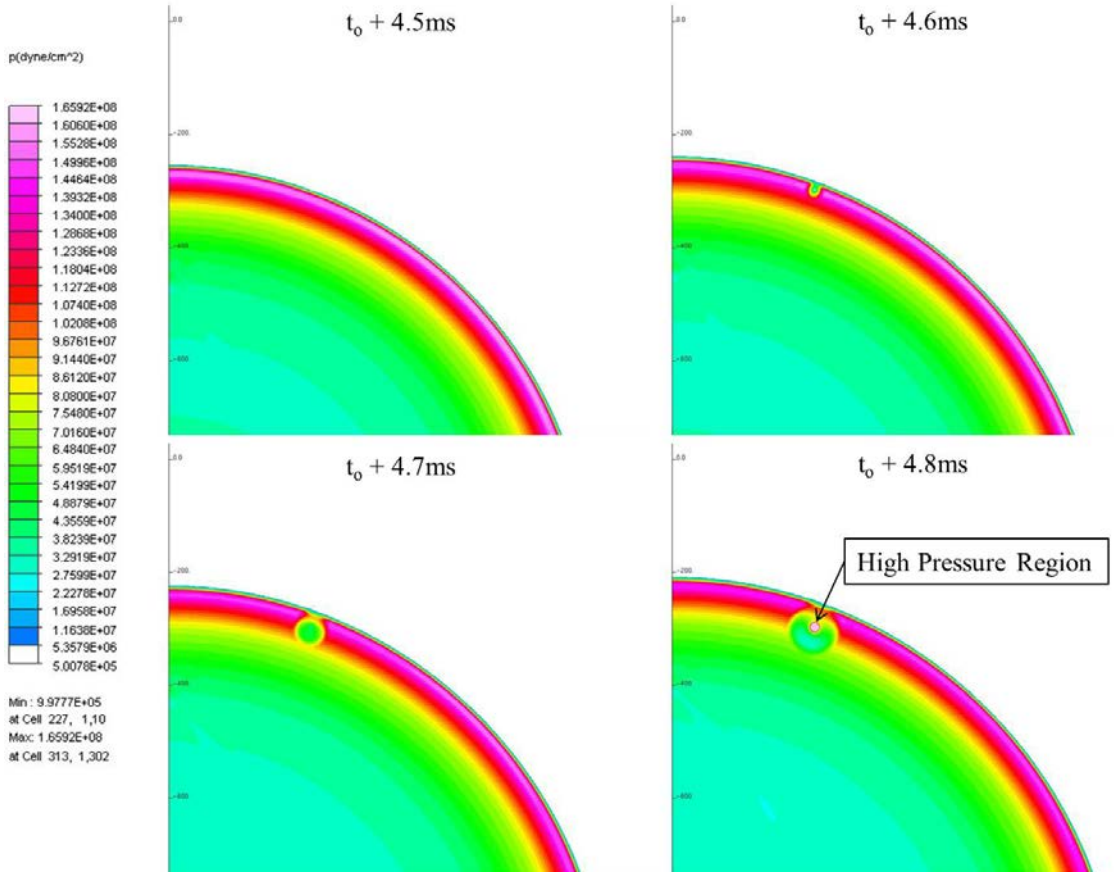

Figure 36. Interaction of Shockwave with a 4cm Diameter Air Bubble Region in a Refined Mesh from 4.5ms to 4.8ms following Detonation

The next set of images shows the relatively short life cycle of the expanding air bubble region. In Figure 37, the air bubble continues to expand though it is apparent that much of the high pressure decreases rapidly. At t_o+4.9ms and t_o+5.0ms, the pressure reaches its maximum and begins to decline. It is apparent that the pressure increases just as quickly as it decreases. From t_o+5.0ms through t_o+5.2ms, a low pressure region takes shape at the lower left portion of the air bubble pressure wave.

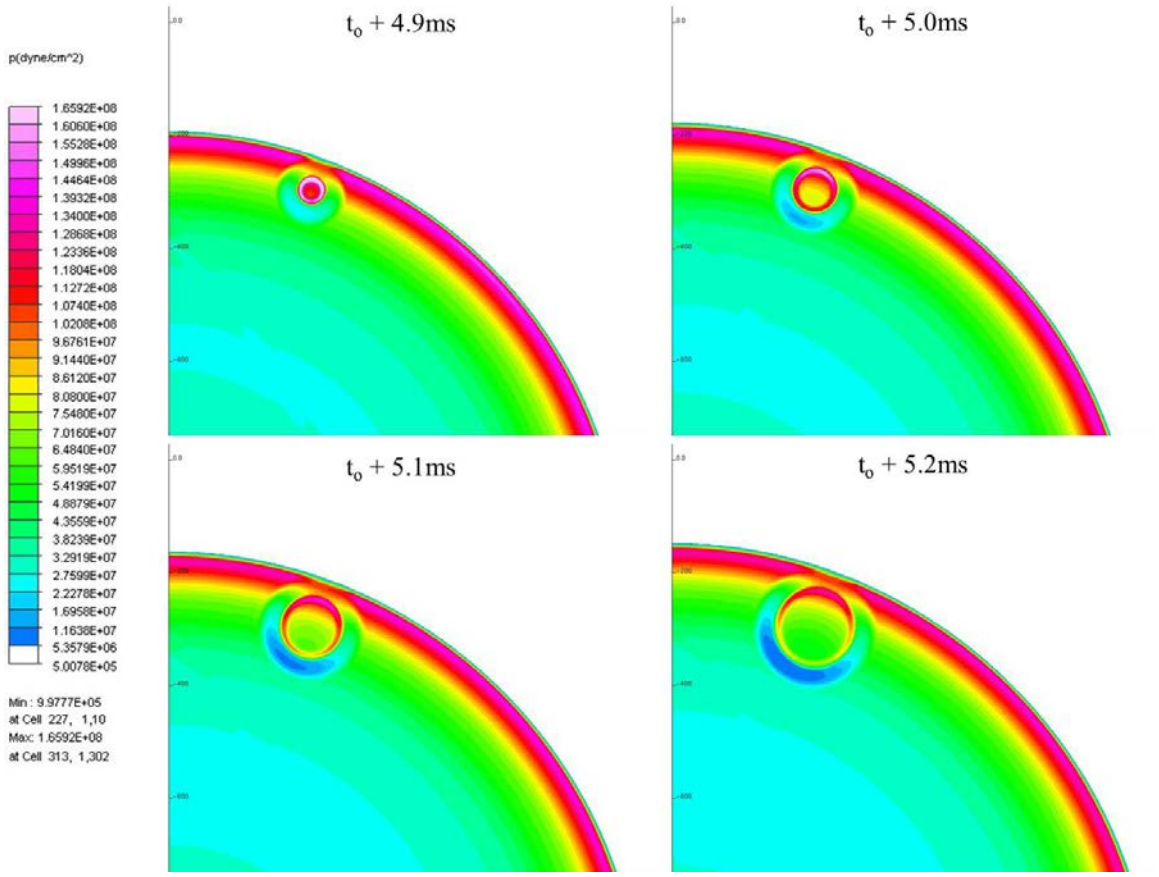

Figure 37. Interaction of Shockwave with a 4cm Diameter Air Bubble Region in a Refined Mesh from 4.9ms to 5.2ms following Detonation

Figure 38 shows the propagation of the shockwave and the formation of a cavitation zone. The cavitation zone first forms at t_o+5.3ms and continues to expand as the air bubble shock wave expands. At t_o+5.4ms, the shockwave generated by the air bubble appears to closely follow the initial shock front in the region that was previously diminished by the interaction with the air bubble. However, this follow-on shockwave does not appear to have as high a pressure as the initial shockwave preceding it. Also, the thickness of this air bubble shockwave is not nearly as pronounced as the initial shockwave. From t_o+5.5ms until t_o+5.6ms, the cavitation region continues to expand.

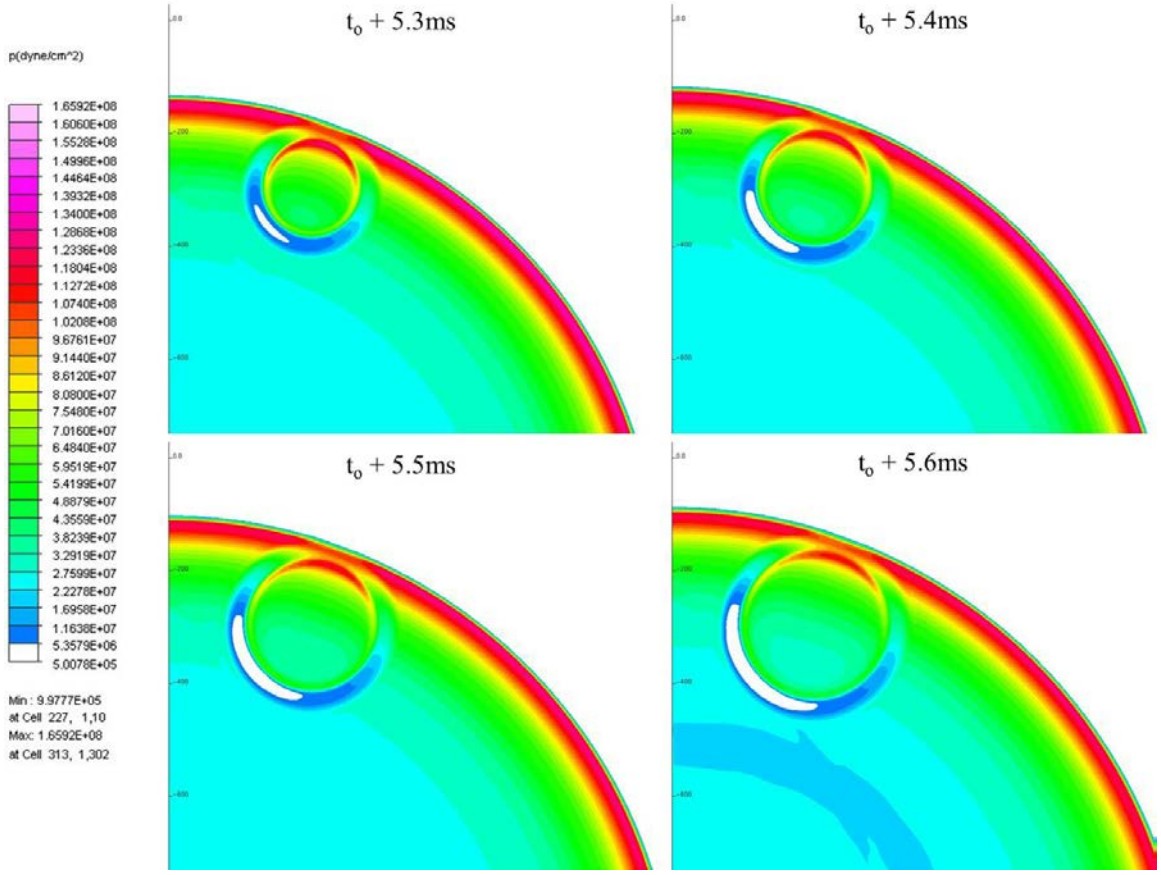

Figure 38. Interaction of Shockwave with a 4cm Diameter Air Bubble Region in a Refined Mesh from 5.3ms to 5.6ms following Detonation

Figure 39 is a collection of images that shows the continued propagation of the shockwaves. Of note is the decrease in the reflected shockwave in comparison to the initial shockwave. The reflected shockwave becomes thinner and the overall pressure decreases at a faster rate than the initial shockwave. Coincidentally, the nearby portion of the initial shockwave maintains a lower pressure than neighboring portions of that initial shockwave. Assuming these decreases in pressure continue, it is likely that an air bubble may act as a buffer zone at greater distances based upon these observations. This would be a benefit of an air bubble addition in that it would create the desired buffering effect.

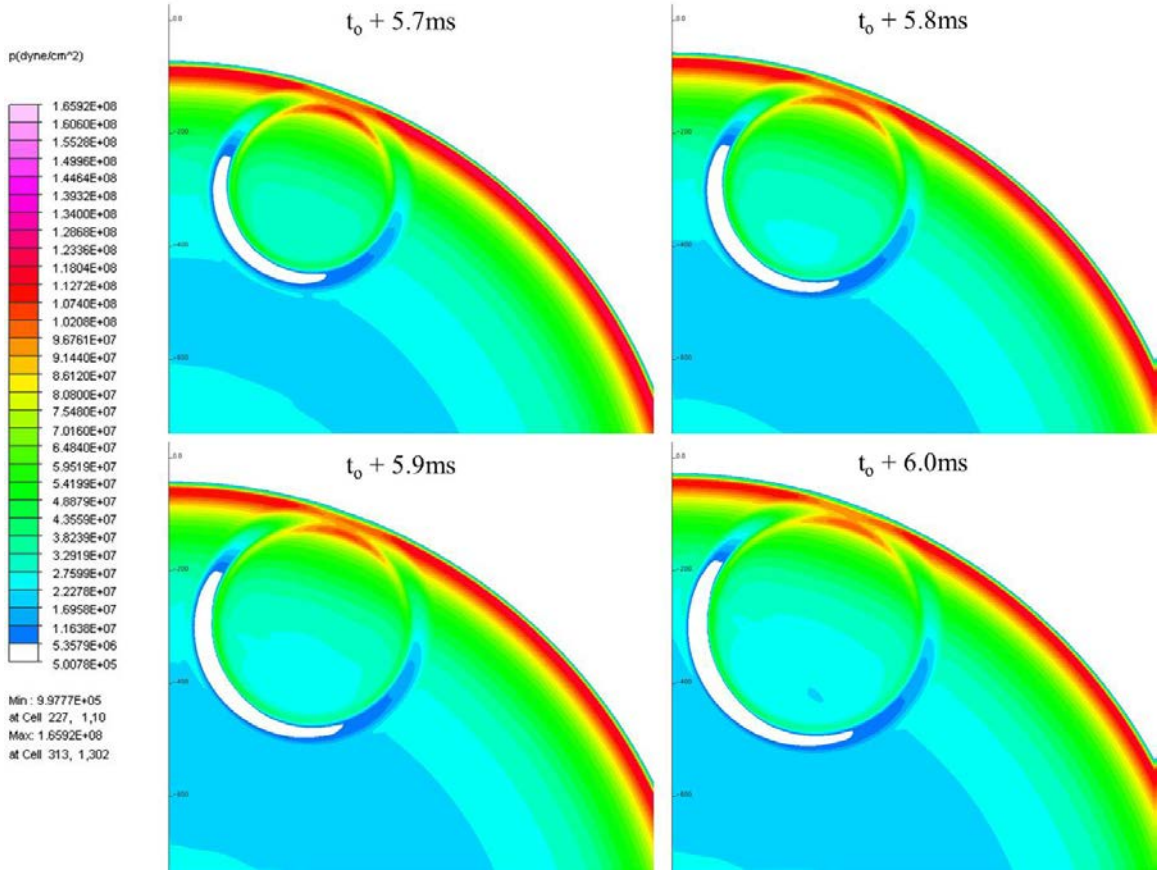

Figure 39. Interaction of Shockwave with a 4cm Diameter Air Bubble Region in a Refined Mesh from 5.7ms to 6.0ms following Detonation

Figure 40 shows the continued propagation of the shockwaves. At t_o+6.3ms, the initial shockwave interacts with the air-water interface and creates another cavitation area. This area is reminiscent of the typical cavitation zones created during a normal UNDEX event i.e., no air bubble layer. Throughout this series of images, the initial shock front continues to degrade in the region that interacted with the air bubble. After t_o+6.4ms, the visualization becomes irrelevant as the pressures decrease substantially and the surface cavitation zone encompasses the region of interest.

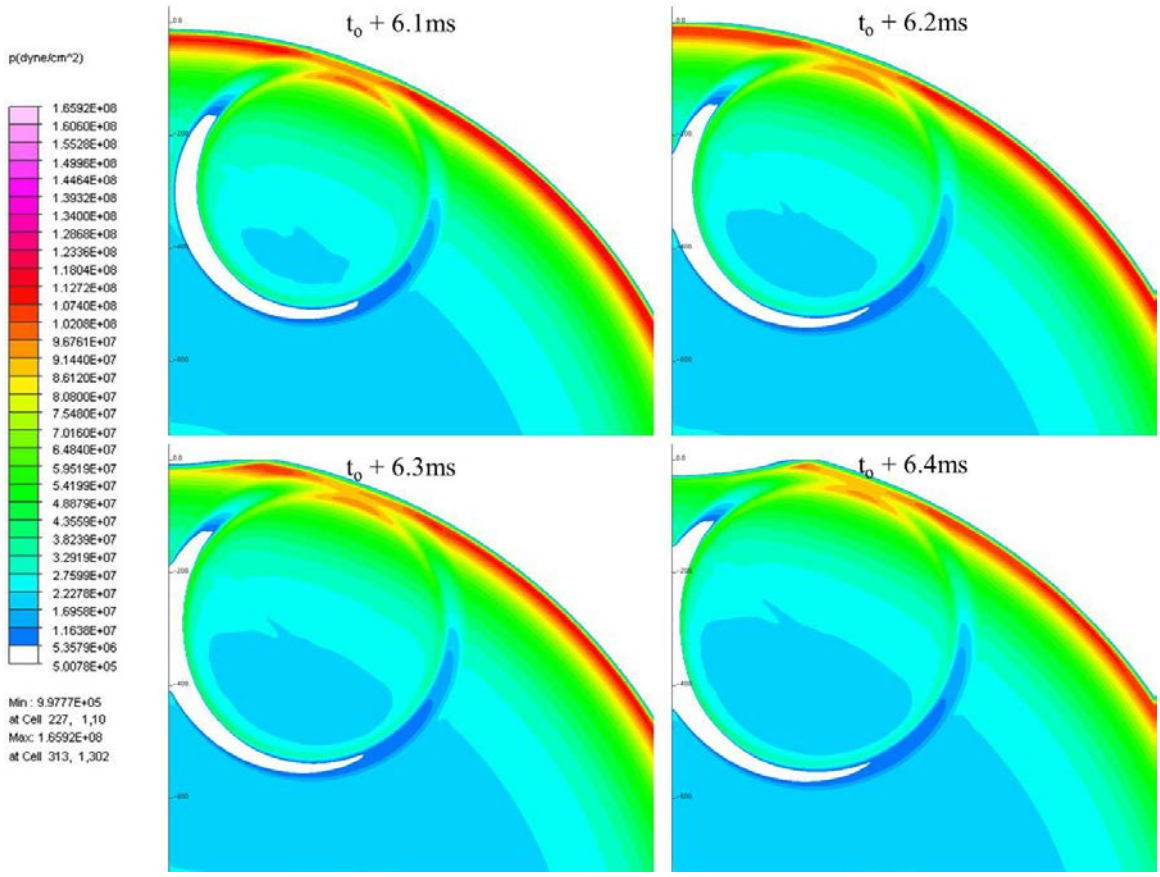

Figure 40. Interaction of Shockwave with a 4cm Diameter Air Bubble Region in a Refined Mesh from 6.1ms to 6.4ms following Detonation

4. Pressure-Time History Analysis

Due to the close proximity of the data collection locations, the pressure-time plots are essentially the same with some minor deviations. A better comparison of this data is compiled in Table 13. The table is arranged by the type of column from which the data was collected. The numbering increases from the bottom left corner towards the top right corner. See Figures 34 and 35 for a visual representation of these locations.

When examining the data, it is important to note the time at which the maximum pressure occurred. The majority of these pressures occur shortly after t_o+4.7ms. As seen previously in Figure 36, the shock front wrapped around the air bubble at approximately t_o+4.8ms and proceeded outward thereafter. These peak pressures all occur following the initial shock wave encounter which is at approximately t_o+4.5ms.

For the horizontal column data, cell (153,929) received the maximum pressure of 13.82E+08dyne/cm^2 which an extremely significant increase from the initial scenario without an air bubble. The increase in pressure is over 800%. This cell is considered to be the center of the bubble.

When looking at the vertical column data, cell (153,934) received the maximum pressure. It is the next cell vertically from the center of the bubble at a distance of 0.5cm. The pressure perceived at this location is 19.8952E+08dyne/cm^2 and is the maximum pressure of all the measured data cell locations. The increase in pressure at this location is over 1100%.

The diagonal data had the second highest pressure of 17.3422E+08dyne/cm^2 occur at cell (158,934). This cell is located diagonally up and to the right of the air bubble center. The distance from the center is 0.707cm.

The locations of the top five pressures are circled in red in Figure 41. It is important to note that they all occur near the center in the upper right quadrant of the air bubble.

The outlying data cells show sharp drops in pressure compared to the aforementioned pressure peaks. It is shown that although the pressure magnification is great in the adjoining locations, at locations further away the pressure drops off quickly. Cell (183,959) experiences the lowest pressure of all the cells located downstream of the shockwave and air bubble interaction. The pressure here is 3.3077E+08dyne/cm^2 which is still higher than the simulation with no air bubbles.

Table 13. Pressure Comparison of a 4cm Diameter Air Bubble in a Refined Mesh subjected to an UNDEX Event

	First Peak		Second Peak	
	Pressure ($dyne/cm^2$)	Time (ms)	Pressure ($dyne/cm^2$)	Time (ms)
HORIZONTAL COLUMN				
Cell (123,929)	1.2764E+08	4.542	3.1533E+08	4.810
Cell (133,929)	7.8621E+08	4.777	N/A	N/A
Cell (143,929)	9.8522E+08	4.771	N/A	N/A
Cell (148,929)	11.6822E+08	4.768	N/A	N/A
Cell (153,929)	13.8200E+08	4.766	N/A	N/A
Cell (158,929)	13.4661E+08	4.766	N/A	N/A
Cell (163,929)	11.3176E+08	4.769	N/A	N/A
Cell (173,929)	8.6605E+08	4.774	N/A	N/A
Cell (183,929)	0.7721E+08	4.564	3.9919E+08	4.800
VERTICAL COLUMN				
Cell (153,899)	1.3422E+08	4.524	3.5064E+08	4.804
Cell (153,909)	7.2024E+08	4.778	N/A	N/A
Cell (153,919)	8.9906E+08	4.772	N/A	N/A
Cell (153,924)	10.6853E+08	4.769	N/A	N/A
Cell (153,929)	13.8200E+08	4.766	N/A	N/A
Cell (153,934)	19.8952E+08	4.764	N/A	N/A
Cell (153,939)	15.3907E+08	4.766	N/A	N/A
Cell (153,949)	10.1809E+08	4.772	N/A	N/A
Cell (153,959)	3.5952E+08	4.806	N/A	N/A
DIAGONAL COLUMN				
Cell (123,899)	1.5135E+08	4.529	2.7866E+08	4.828
Cell (133,909)	6.4343E+08	4.786	N/A	N/A
Cell (143,919)*	8.2314E+08	4.775	N/A	N/A
Cell (148,924)	9.9510E+08	4.770	N/A	N/A
Cell (153,929)	13.8200E+08	4.766	N/A	N/A
Cell (158,934)	17.3422E+08	4.765	N/A	N/A
Cell (163,939)	11.9882E+08	4.769	N/A	N/A
Cell (173,949)	8.4626E+08	4.777	N/A	N/A
Cell (183,959)	3.3077E+08	4.820	N/A	N/A
Middle Cell (4cm Diameter, Unrefined)	2.9306E+08	4.798	N/A	N/A
Cell (143,919) (No Air Bubble, Refined)	1.5040E+08	4.582	N/A	N/A

*Equivalent cell for this location is the Middle Cell (4cm Diameter, Unrefined)

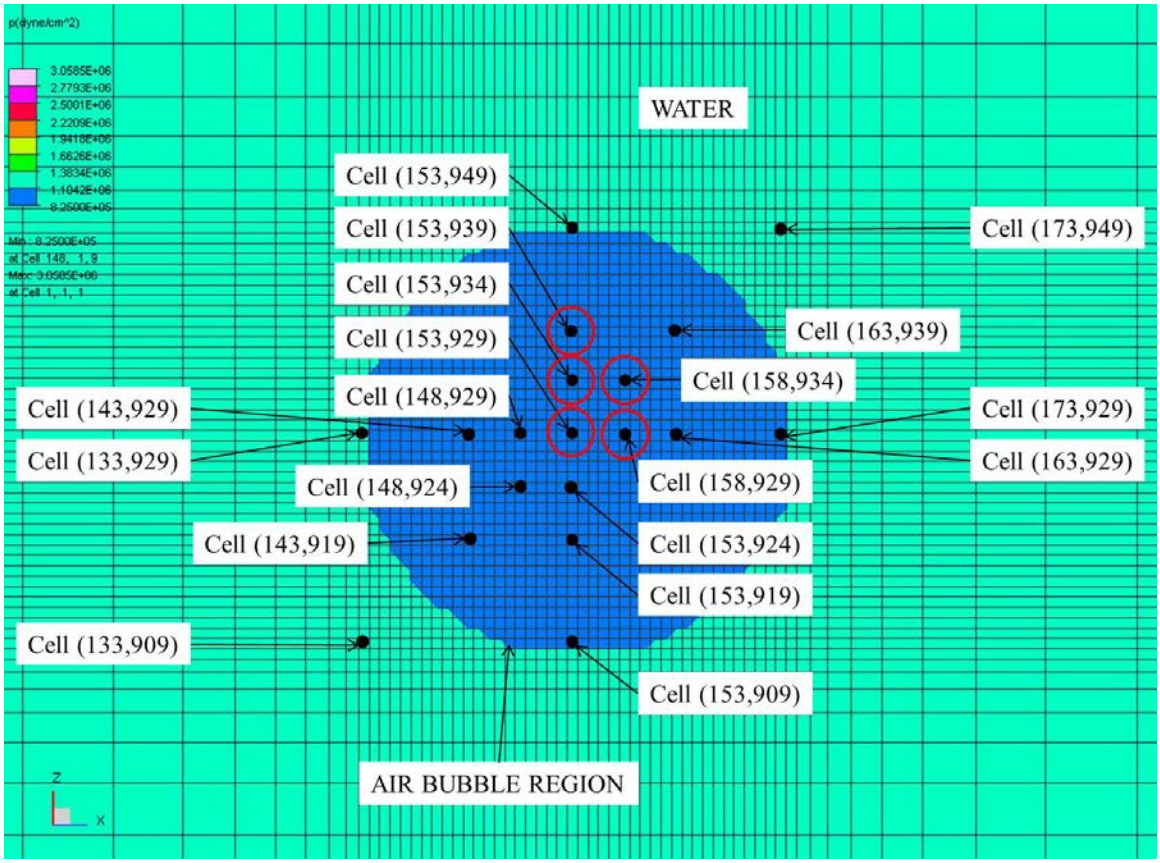

Figure 41. Maximum Pressure Locations for a 4cm Diameter Air Bubble

5. Discussion of Results

After comparing all the data, it is apparent that the pressure distribution for this simulation is not uniform. The pressures tend to peak along the vertical and diagonal columns in the immediate vicinity upward and right of the air bubble center. The reasoning for this new center of pressure is due to the buoyant effect of the air bubble and the outward movement incurred by the initial shockwave. However, as the distance is slightly increased from the air bubble center, the pressure drop becomes substantial.

Since the pressure increases in the immediate vicinity of the air bubble, it would be detrimental for a marine structure to be located in close proximity to it. Having a region of air bubbles surround the hull of a ship would not prove beneficial during an UNDEX event. However, if these bubbles were offset from the hull at a specified distance, then there would be some benefit in the form of buffering.

C. REFINED 1CM DIAMETER CIRCULAR AIR BUBBLE REGION

1. Justification

Following the refined 4cm diameter air bubble simulation, it was determined that the pressure increase due to the refinement of the mesh was substantial. An additional simulation was involving a 1cm diameter bubble was designed and evaluated. By reducing the diameter to 1cm, it better approximates an air bubble found in nature. The comparison of these two simulations ensured that the increase in pressure was not due to erroneous calculations during the mesh refinement process.

2. Grid Setup

The locations of the key components remained the same as shown in Figure 6. This simulation involved the refined mesh used previously in the 4cm diameter air bubble experiment, but with a smaller diameter air bubble of 1cm diameter. This permitted easy comparison of the data gathered at the various cell locations. These data locations are shown in Figure 42 and arranged in columns through the air bubble center. The outlying data collection locations remained the same as in Figure 34 and provided pressure data at greater distances.

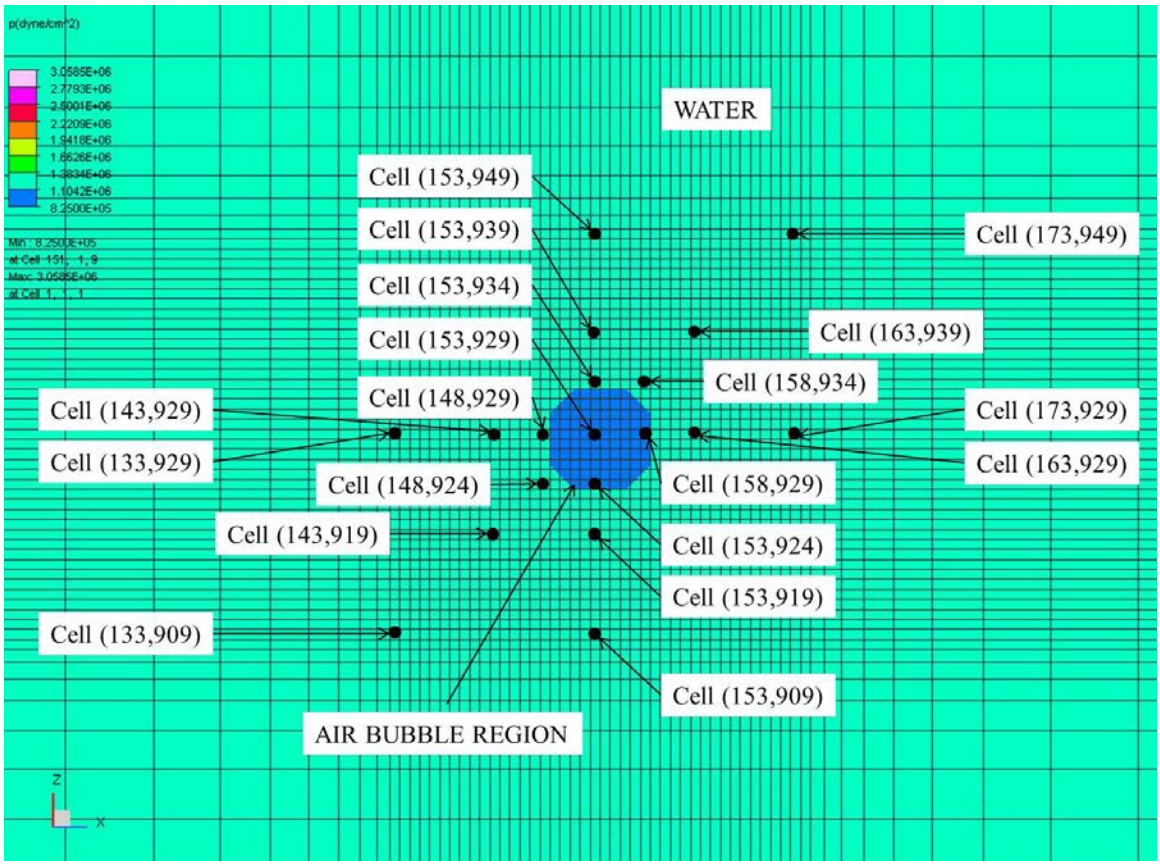

Figure 42. Inner Data Locations for a 1cm Diameter Circular Air Bubble Region in a Refined Mesh

3. Animated Results

During this simulation, the pressure wave propagates in similar fashion to the 2cm diameter air bubble. Figure 43 shows the pressure-time history from 4.5ms to 4.8ms after detonation time (t_o). The initial shockwave makes contact at t_o+4.6ms and produces an indentation in the shock front as the initial shockwave propagates around the air bubble. Due to its small size, the compression of the air bubble occurs rapidly and at t_o+4.7ms a reflection from the air bubble starts to propagate outward. At t_o+4.7ms, it is visually apparent that the top right portion of the reflected shockwave has a higher pressure, albeit briefly, than the surrounding initial shockwave. This higher pressure is referenced by the light pink color. In reality, the highest pressure occurs shortly before t_o+4.6ms, but it is not visible due to the image size. This will be reviewed during the pressure-time history analysis.

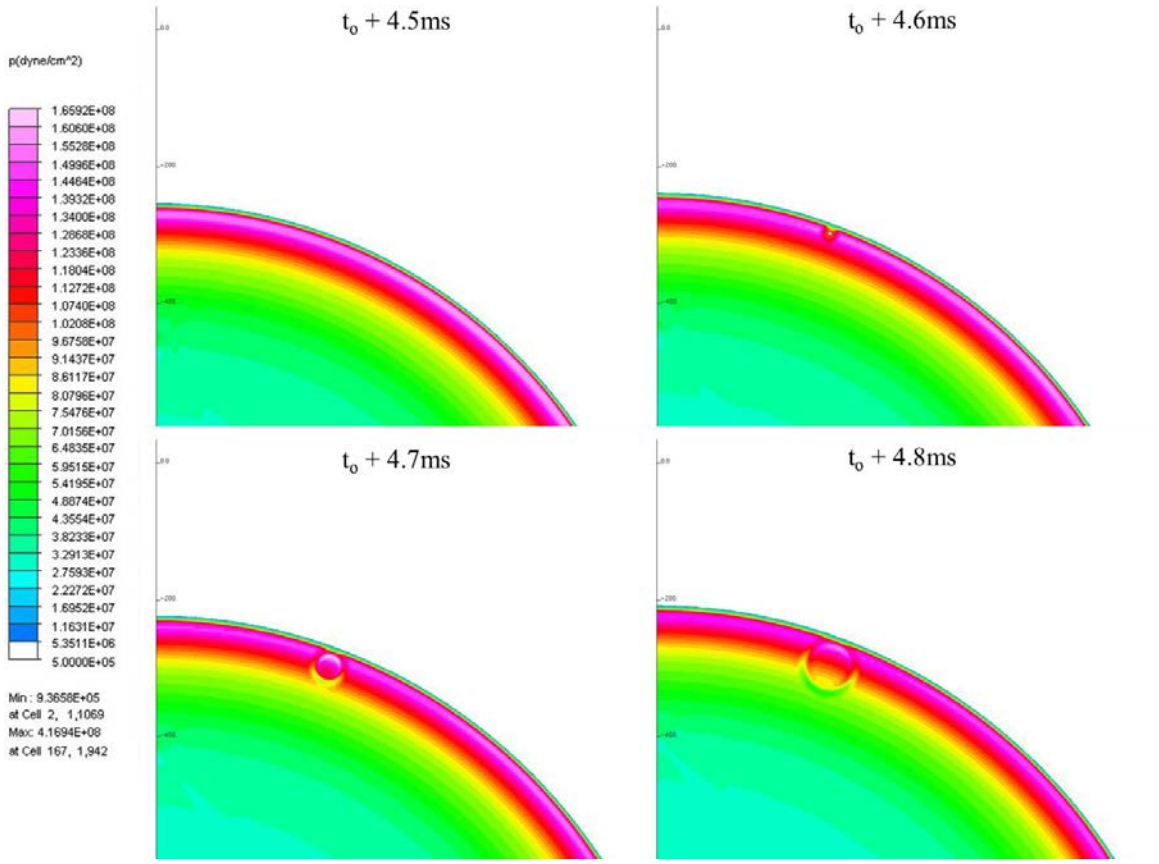

Figure 43. Interaction of Shockwave with a 1cm Diameter Air Bubble Region in a Refined Mesh from 4.5ms to 4.8ms following Detonation

The progression of the shockwave from t_o+5.0ms until t_o+5.6ms is shown in Figure 44. The reflected shockwave resembles a capillary wave, or ripple, generated by a drop of water colliding with the surface of a larger body of water. From t_o+5.0ms until t_o+5.4ms, the propagation of the reflected wave is easily visible. Due the interaction between the initial shockwave and the air bubble, there are some pressure irregularities at the shock front. A low pressure region, denoted by dark blue, is created at the lower left portion of the reflected shockwave at t_o+5.4ms and t_o+5.6ms. For larger diameter air bubbles, this low pressure region eventually formed an additional cavitation zone, but that was not the case in this simulation. A surface cavitation zone, due to the interaction with the air-water interface, occurred at a later time not shown in this set of images.

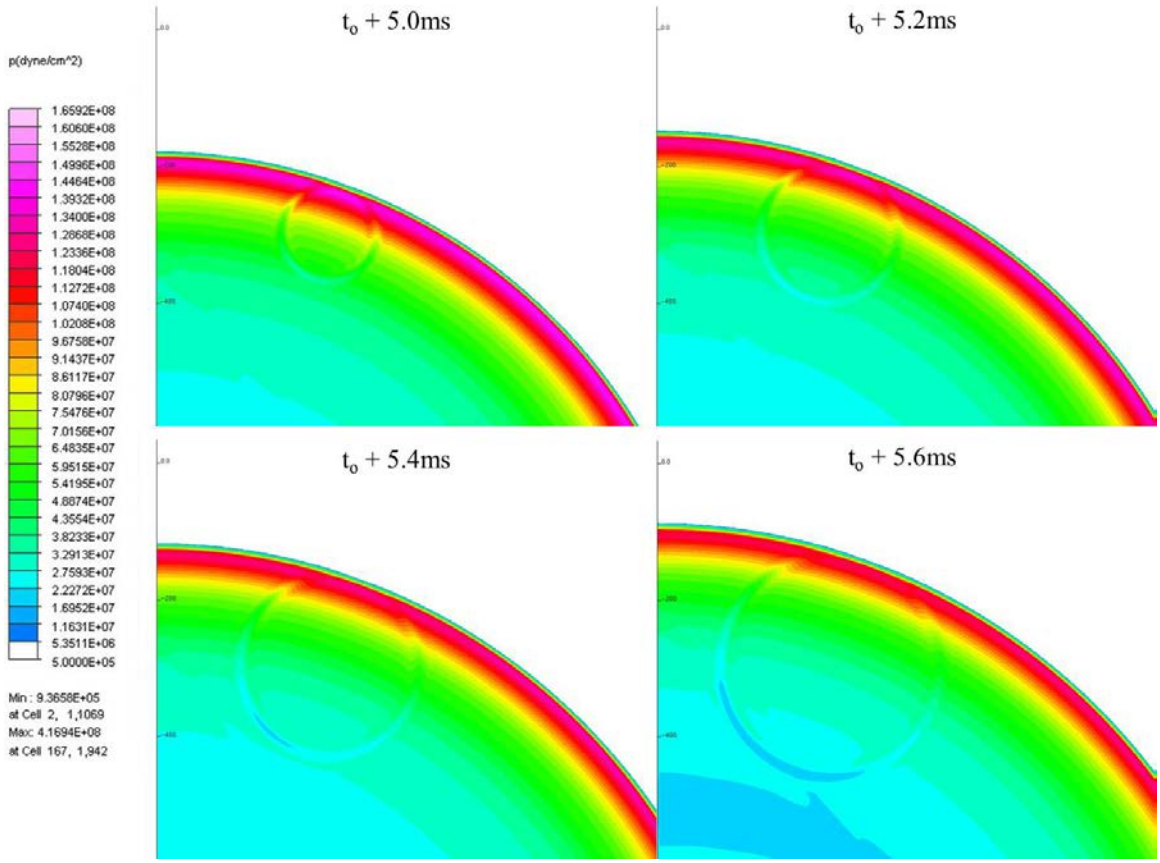

Figure 44. Interaction of Shockwave with a 1cm Diameter Air Bubble Region in a Refined Mesh from 5.0ms to 5.6ms following Detonation

4. Pressure-Time History Results

When comparing the pressure-time results, it is readily apparent that the pressures encountered from the addition of a 1cm diameter air bubble were substantially less than those encountered with a 4cm diameter bubble. Upon closer inspection, lower pressure readings were not the only difference discovered during this simulation.

The two pressure peaks which previously occurred at cell (183,929) were difficult to distinguish due to their closeness in time to each other. The output resembled one pressure peak which was recorded. The reason for the reduction in time between the two pressure peaks is due to the small size of the air bubble. As noted previously, large diameter air bubbles produce two well separated pressure peaks. The difference between these two peaks becomes minute when the air bubble size decreases.

The pressure-time profile of cells (153,959), (183,929), and (183,959) appear similar to the scenario without an air bubble. This is shown in Figure 45. The near-instantaneous pressure increase from the shockwave occurred at nearly the same time. The time difference is due to the varying data cell locations of these four pressure-time plots. All three locations experience a larger maximum pressure which is a result of the inclusion of the air bubble. However, after this pressure peak, the overall pressure drops in the same manner as the simulation with no air bubble.

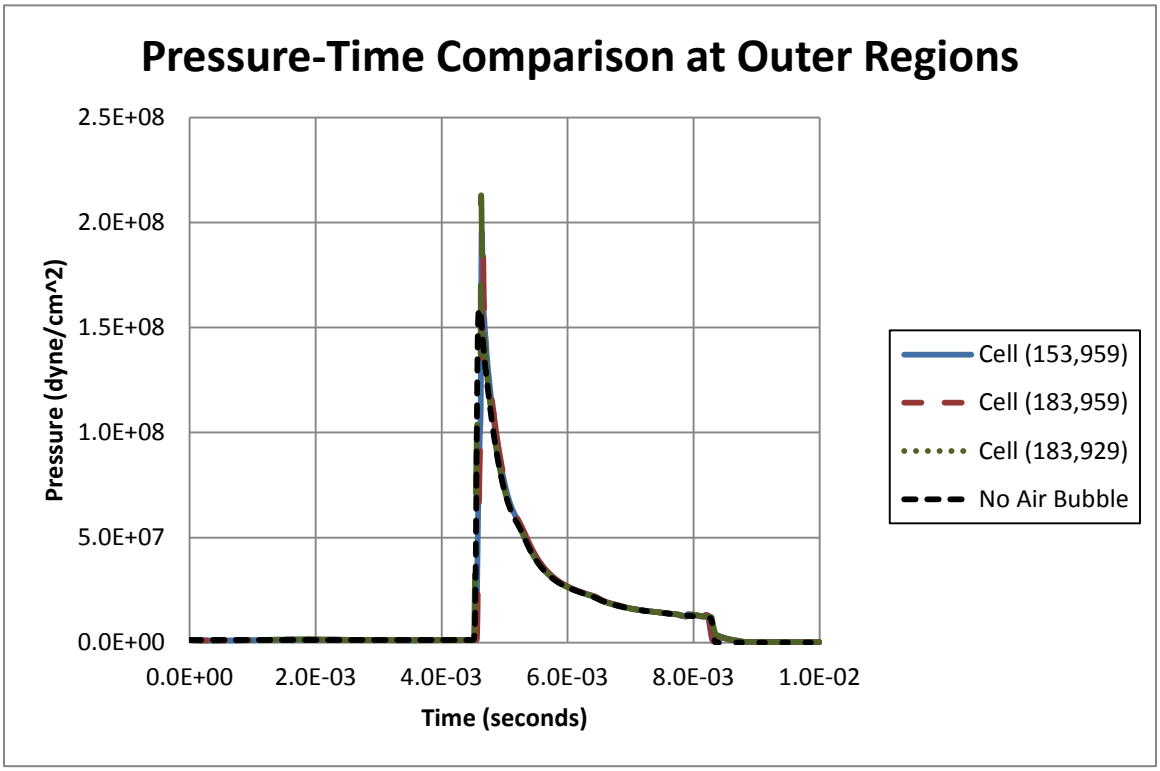

Figure 45. Pressure-Time Comparison of Outer Region Data Cells for a 1cm Diameter Air Bubble in a Refined Mesh

The peak pressure readings at all data cell locations are presented in Table 14. A peak pressure of 10.8409E+08dyne/cm^2 occurs in the approximated center of the air bubble, cell (153,929). This pressure is several times greater than the maximum pressure attained in the no air bubble simulation. This is due to the compression and expansion of the air bubble.

When reviewing the data, it is important to note the time that each maximum pressure occurred. One may think that the pressures in the lower left quadrant of the air bubble would receive a lesser amount of pressure incurred upon them. This is apparent at first glance of the animated results. However, the pressure peaks for cells in this region occur after the maximum pressure is attained at the center cell. This means that the air bubble compressed and expanded due to the initial shockwave. A product of this expansion is a reflected, or secondary, shockwave with a pressure magnitude greater than the initial shockwave. With the exception of the cells that experienced two pressure peaks, all the maximum pressures in Table 14 occur due to the reflected shockwave.

A visual representation of the maximum pressures attained due to the 1cm diameter air bubble is shown in Figure 46. Again these maximum pressures occur in the upper right quadrant of the air bubble with the exception of one.

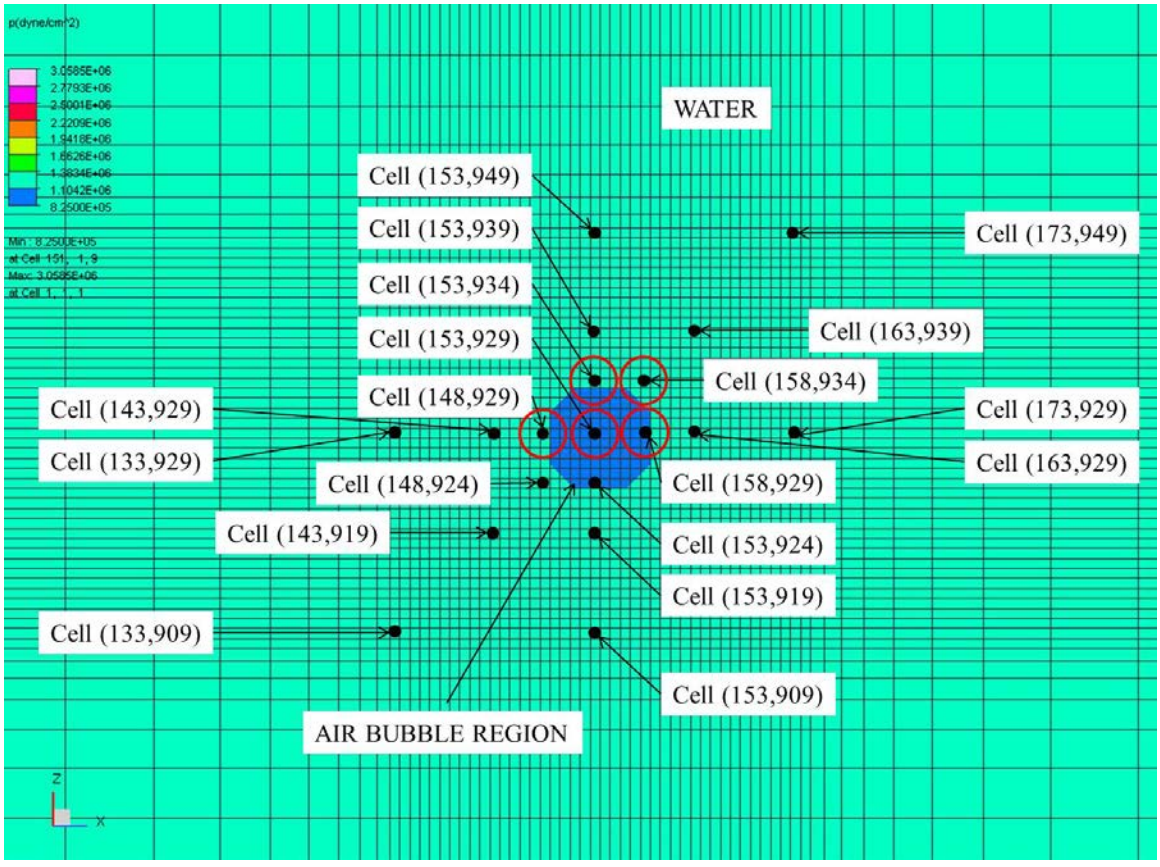

Figure 46. Maximum Pressure Locations for a 1cm Diameter Air Bubble

Table 14. Pressure Comparison of a 1cm Diameter Air Bubble in a Refined Mesh subjected to an UNDEX Event

	First Peak		Second Peak	
	Pressure ($dyne/cm^2$)	Time (ms)	Pressure ($dyne/cm^2$)	Time (ms)
HORIZONTAL COLUMN				
Cell (123,929)	1.4167E+08	4.550	1.8213E+08	4.637
Cell (133,929)	3.7210E+08	4.602	N/A	N/A
Cell (143,929)	4.6313E+08	4.595	N/A	N/A
Cell (148,929)	5.6854E+08	4.593	N/A	N/A
Cell (153,929)	10.8409E+08	4.589	N/A	N/A
Cell (158,929)	6.9666E+08	4.591	N/A	N/A
Cell (163,929)	5.2084E+08	4.594	N/A	N/A
Cell (173,929)	3.9508E+08	4.600	N/A	N/A
Cell (183,929)	2.1289E+08	4.628	N/A	N/A
VERTICAL COLUMN				
Cell (153,899)	1.4684E+08	4.534	1.9354E+08	4.629
Cell (153,909)	3.6778E+08	4.602	N/A	N/A
Cell (153,919)	4.5852E+08	4.595	N/A	N/A
Cell (153,924)	5.6416E+08	4.592	N/A	N/A
Cell (153,929)	10.8409E+08	4.589	N/A	N/A
Cell (153,934)	6.8965E+08	4.592	N/A	N/A
Cell (153,939)	5.1841E+08	4.594	N/A	N/A
Cell (153,949)	3.9786E+08	4.600	N/A	N/A
Cell (153,959)	1.9546E+08	4.636	N/A	N/A
DIAGONAL COLUMN				
Cell (123,899)	1.5195+08	4.537	1.6506E+08	4.653
Cell (133,909)	3.3032E+08	4.607	N/A	N/A
Cell (143,919)*	4.0762E+08	4.598	N/A	N/A
Cell (148,924)	5.0024E+08	4.594	N/A	N/A
Cell (153,929)	10.8409E+08	4.589	N/A	N/A
Cell (158,934)	6.2204E+08	4.593	N/A	N/A
Cell (163,939)	4.7145E+08	4.597	N/A	N/A
Cell (173,949)	3.6470E+08	4.606	N/A	N/A
Cell (183,959)	1.9354E+08	4.651	N/A	N/A
Middle Cell (No Air Bubble, Unrefined)	1.5964E+08	4.571	N/A	N/A
Cell (143,919) (No Air Bubble, Refined)	1.5040E+08	4.582	N/A	N/A

*Equivalent cell for this location is the Middle Cell (No Air Bubble, Unrefined)

5. Discussion of Results

Upon review of the animated results, the impact of a 1cm diameter air bubble appears insignificant. This is far from true. In order to get a better understanding of this event, the pressure-time data must be closely examined. The maximum pressures obtained at the majority of these locations exceed the values determined without any air bubbles. This amplification would prove disastrous for a marine structure in the immediate vicinity of this air bubble.

In order to avoid such a drastic increase in pressure, the problem may be solved by increasing the distance from the center. Consider cell (123,899) and cell (183,959) in Table 14. They are located approximately 8cm from the air bubble center. By increasing the distance by merely 8cm, the pressure incurred at this location is nearly the same as though there was no air bubble present. Had the distance from the air bubble been increased further, it is likely that the recorded pressure would decrease further. This would be indicative of the buffering effect which may occur at further distances from the air bubble center.

THIS PAGE INTENTIONALLY LEFT BLANK

IX. TWO DIMENSIONAL SIMULATION INVOLVING MULTIPLE AIR BUBBLE REGIONS USING A REFINED MESH

A. OVERVIEW

The final simulation analyzed the influence of a region of multiple small air bubbles. This region represented a real world situation where a large air bubble has broken down into several smaller ones. This is in contrast to previous simulations which involved larger homogeneous air bubble regions.

B. GRID SETUP

The overall dimensions remained the same as shown in Figure 6 with a couple exceptions. These exceptions were: (1) Region A contained an additional nine air bubbles and (2) the mesh was refined as annotated in Table 1. The data collection locations remained the same as previous simulations with a refined mesh. Their arrangement in relation to the multiple air bubble regions is shown in Figure 47.

A decision was made to ensure the total area of the nine bubbles equaled the total area of the 4cm diameter air bubble. This simulated the larger air bubble breaking down into several smaller air bubbles. The total area of the 4cm diameter bubble was 12.566cm^2. After division, the area of one small air bubble regions was 1.396cm^2. The resultant radius of this air bubble was determined to be 0.667cm. So the new diameter of each smaller air bubble is 1.334cm.

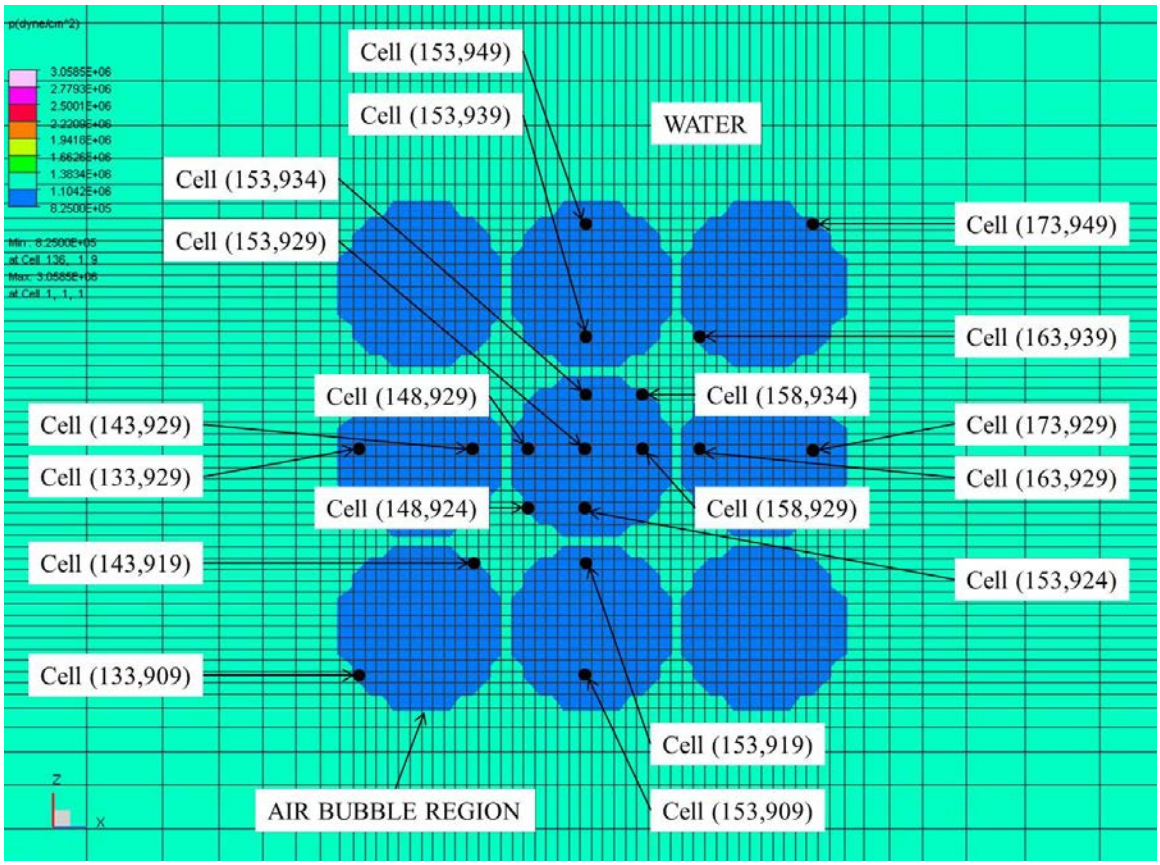

Figure 47. Inner Data Locations for a Multiple Circular Air Bubble Regions in a Refined Mesh

C. ANIMATED RESULTS

Due to the larger size of the overall air bubble region, the initial impact with the shockwave occurs slightly earlier at approximately 4.5ms after initial detonation (t_o). This can faintly be seen in Figure 48 at t_o+4.5ms. When comparing the initial stages of the reflected shockwave, it is apparent that this simulation closely resembles the previous simulation involving the 4cm diameter bubble, see Figure 36. The initial propagation of these reflected waves closely resemble each other. A minor difference is that the reflected shockwave for the multiple bubbles increases in diameter at a faster rate. This is likely due to the increased spacing required in between each small air bubble region creating a larger total affected area. The total affected area includes all nine air bubbles and the water in between them.

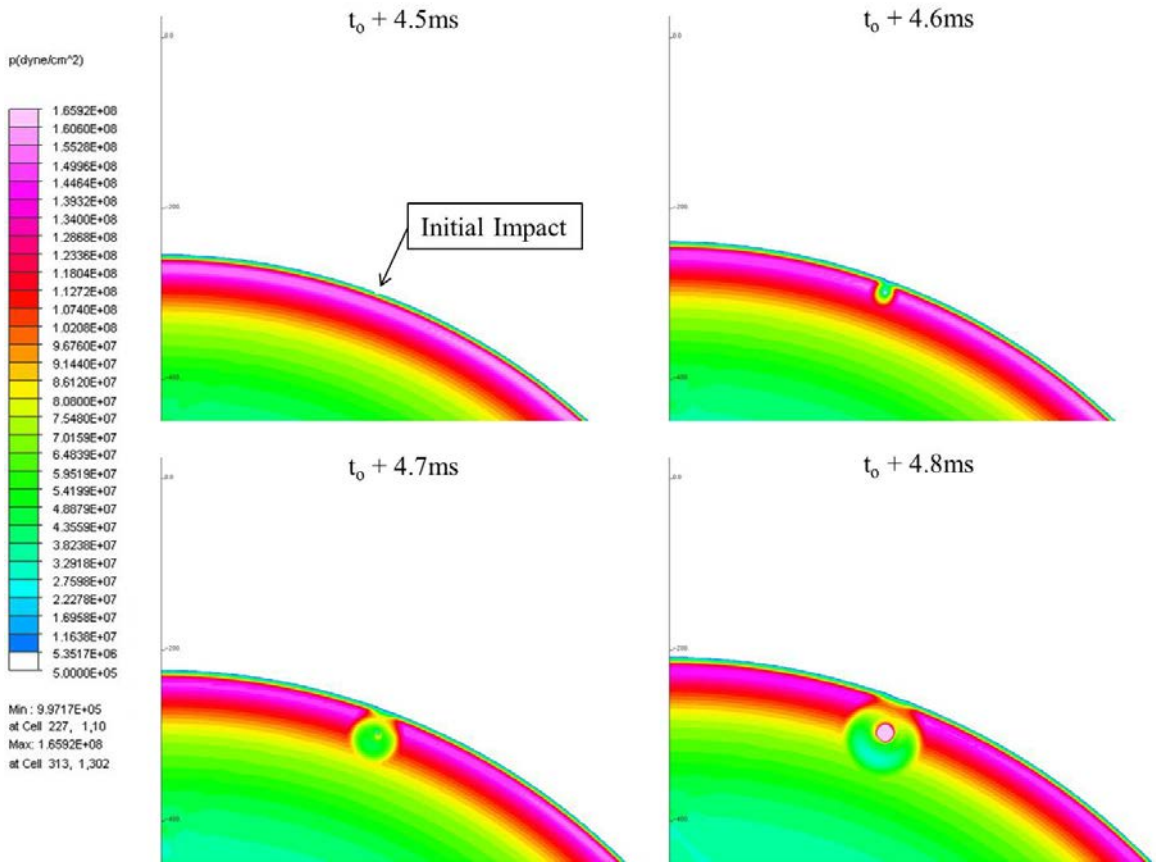

Figure 48. Interaction of Shockwave with Multiple Air Bubble Regions in a Refined Mesh from 4.5ms to 4.8ms following Detonation

Figure 49 shows the continuing progression of the initial and reflected shockwaves. Of note in this collection of images is the low pressure region that forms in the lower left quadrant of the reflected shockwave. The extreme low pressures for this simulation encompass a smaller area than the 4cm diameter air bubble shown in Figure 37. Eventually the pressures decrease to the low magnitude, but at a slower rate.

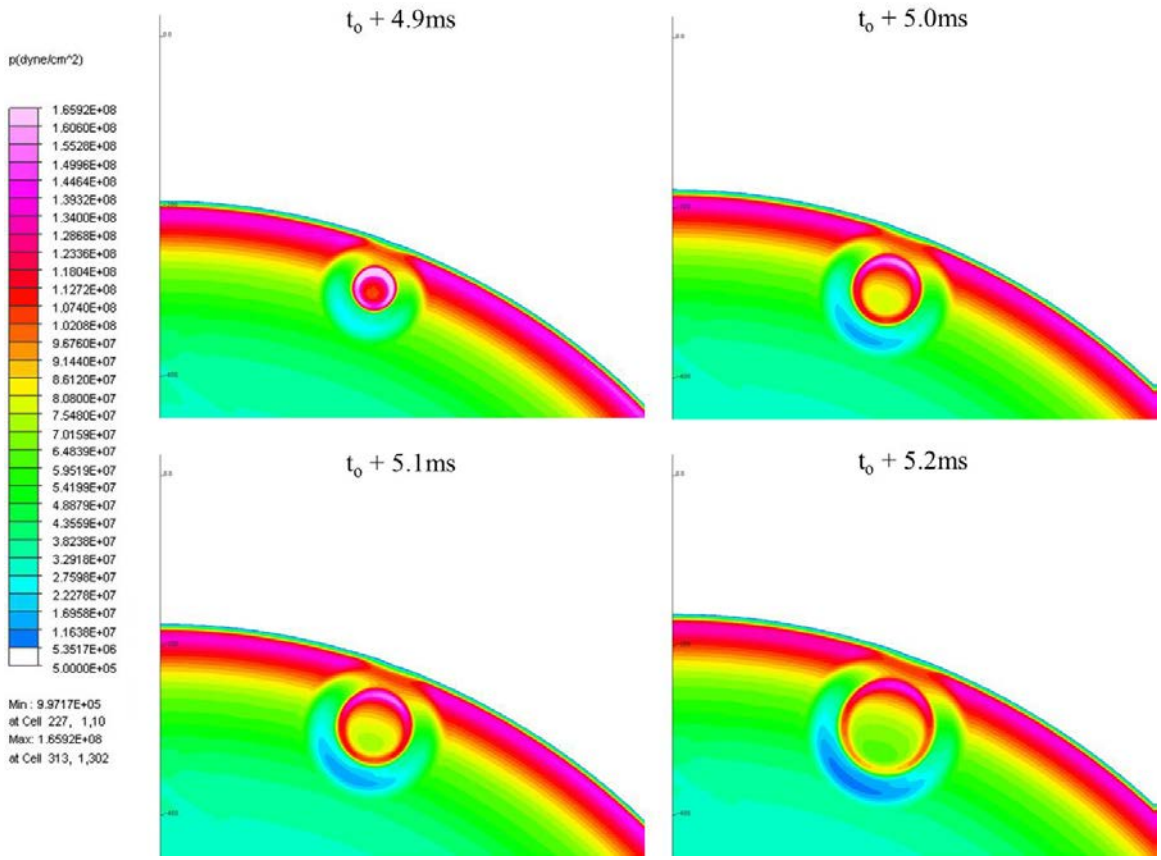

Figure 49. Interaction of Shockwave with Multiple Air Bubble Regions in a Refined Mesh from 4.9ms to 5.2ms following Detonation

The images in Figure 50 show the continued drop in pressure and formation of the cavitation zone in the lower left quadrant. The affected area by this zone appears slightly smaller to the zone formed at the equivalent time during the 4cm diameter air bubble.

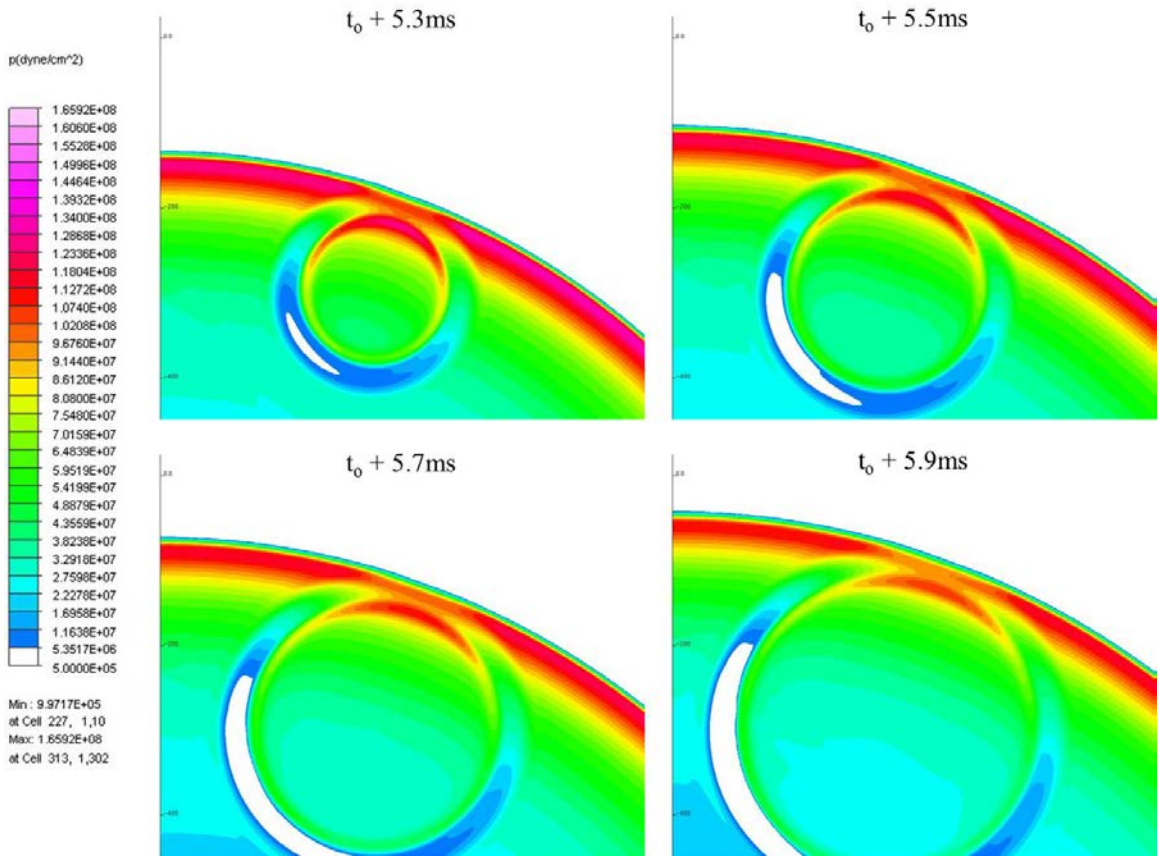

Figure 50. Interaction of Shockwave with Multiple Air Bubble Regions in a Refined Mesh from 5.3ms to 5.9ms following Detonation

D. PRESSURE-TIME HISTORY RESULTS

Upon review of the pressure-time history results, it is apparent that the pressures are not evenly distributed as is the case with the data compiled in Tables 12 and 13. This is due to the irregular shape of the total air bubble region. With individual air bubbles, there is a clearly defined contraction and expansion phase that occurs. However, when multiple air bubble regions are introduced, each air bubble undergoes a contraction and expansion phase which affects the neighboring air bubbles. This additional effect leads to irregular pressure readings annotated in Table 15.

The maximum pressures are no longer confined in one specific area, but are dispersed at random locations. This is shown in Figure 51.

Table 15. Pressure Comparison of Multiple Air Bubble Regions in a Refined Mesh subjected to an UNDEX Event

	First Peak		Second Peak	
	Pressure ($dyne/cm^2$)	Time (ms)	Pressure ($dyne/cm^2$)	Time (ms)
HORIZONTAL COLUMN				
Cell (123,929)	1.2149E+08	4.539	2.9002E+08	4.803
Cell (133,929)	8.5568E+08	4.767	N/A	N/A
Cell (143,929)	11.3387E+08	4.763	N/A	N/A
Cell (148,929)	9.9413E+08	4.763	N/A	N/A
Cell (153,929)	9.1774E+08	4.756	N/A	N/A
Cell (158,929)	10.4432E+08	4.757	N/A	N/A
Cell (163,929)	10.8315E+08	4.761	N/A	N/A
Cell (173,929)	8.6599E+08	4.765	N/A	N/A
Cell (183,929)	0.7062E+08	4.564	3.1664E+08	4.787
VERTICAL COLUMN				
Cell (153,899)	1.2762E+08	4.518	3.2515E+08	4.797
Cell (153,909)	6.5260E+08	4.774	N/A	N/A
Cell (153,919)	7.1976E+08	4.769	N/A	N/A
Cell (153,924)	7.7296E+08	4.753	N/A	N/A
Cell (153,929)	9.1774E+08	4.756	N/A	N/A
Cell (153,934)	8.9666E+08	4.755	N/A	N/A
Cell (153,939)	23.6528E+08	4.750	N/A	N/A
Cell (153,949)	8.2771E+08	4.755	N/A	N/A
Cell (153,959)	2.9506E+08	4.797	N/A	N/A
DIAGONAL COLUMN				
Cell (123,899)	1.5037E+08	4.524	2.6500E+08	4.819
Cell (133,909)	7.0101E+08	4.775	N/A	N/A
Cell (143,919)*	8.9481E+08	4.768	N/A	N/A
Cell (148,924)	9.5236E+08	4.765	N/A	N/A
Cell (153,929)	9.1774E+08	4.756	N/A	N/A
Cell (158,934)	13.3660E+08	4.757	N/A	N/A
Cell (163,939)	10.3108E+08	4.756	N/A	N/A
Cell (173,949)	6.3282E+08	4.762	N/A	N/A
Cell (183,959)	2.7346E+08	4.812	N/A	N/A
Middle Cell (No Air Bubble, Unrefined)	1.5964E+08	4.571	N/A	N/A
Cell (143,919) (No Air Bubble, Refined)	1.5040E+08	4.582	N/A	N/A

*Equivalent cell for this location is the Middle Cell (No Air Bubble)

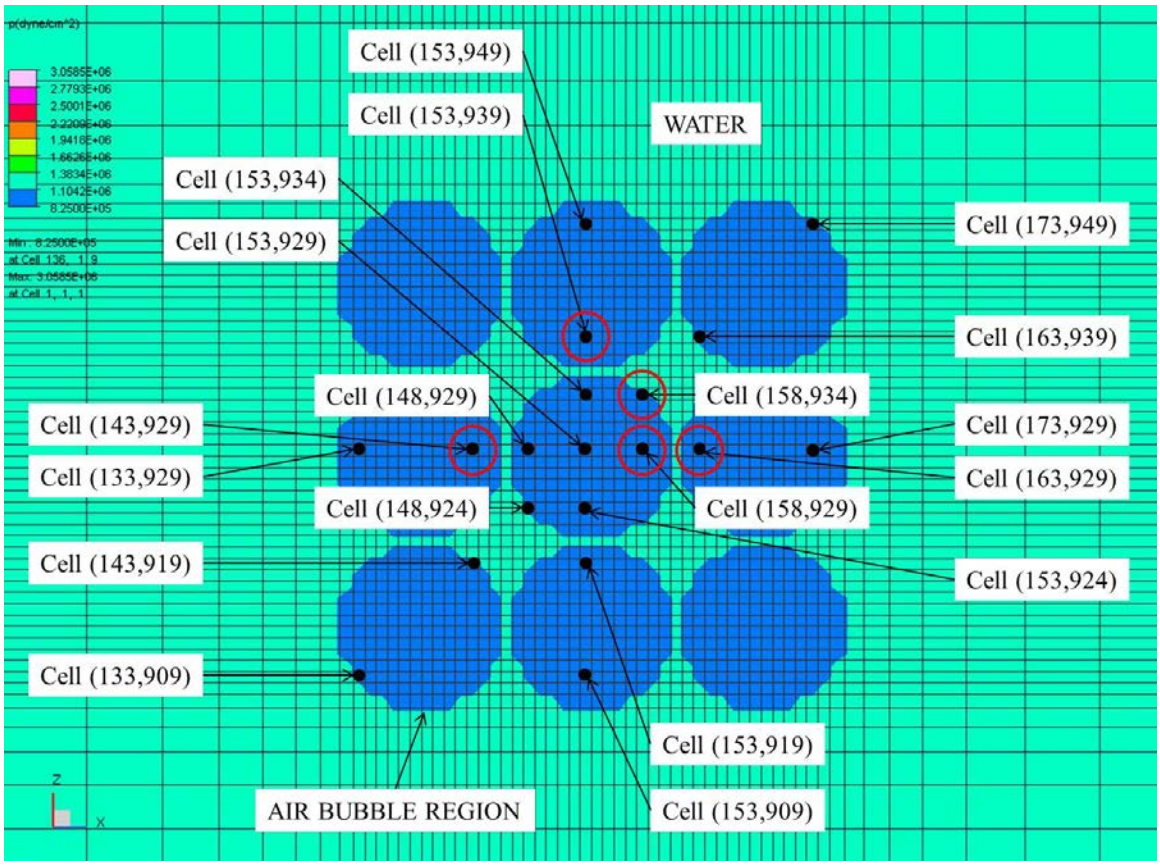

Figure 51. Maximum Pressure Locations

E. DISCUSSION OF RESULTS

Based on these results, it is apparent that multiple air bubbles in close proximity heavily influence each other. No longer are the maximum pressures uniformly distributed. Pressure peaks occur at seemingly random locations due to the individual bubble collapse and expansion. However, they are primarily restricted to upper right quadrant. The values of these peaks vary widely. The maximum pressure attained in this simulation was 23.6528E+08dyne/cm^2 while its neighboring cell was 8.9666E+08dyne/cm^2. This maximum pressure was the largest attained in this study.

When comparing pressures at greater distances, it was found that the distance from the center of the air bubble was an important factor when determining the extent of the secondary shockwave during UNDEX event. The further a cell was from the center of the charge, the pressure experience by this location was substantially lower than a cell

nearer to the center. This relationship is logical. For example, when comparing the pressure recorded at cell (183,959), it is apparent that the size and shape of the air bubble influenced the output pressure. This cell is located in the upper right quadrant of the bubble at approximately 8cm from its center for all the refined mesh simulations. Table 16 compares the pressures associated for this location during the various air bubble scenarios. The results show that there is a critical size of a single bubble which yields the maximum pressure. Furthermore, a single bubble produces a higher pressure than a collection of smaller size bubbles in the same area.

Table 16. Pressure Comparison of Cell (183,959) Located at a Short Distance from an Air Bubble during an UNDEX Event

	Pressure (dyne/cm^2)	Time (ms)
No Air Bubble	1.4869E+08	4.648
Single 4cm Diameter	3.3077E+08	4.820
Single 1cm Diameter	1.9354E+08	4.651
Multiple Small Bubbles	2.7346E+08	4.812

The multiple air bubble scenario depicts an arrangement of air bubbles that is likely to naturally occur around a naval vessel under normal operating conditions. During a real-world test, these bubbles would be at random locations, but for the most resemble the arrangement discussed in this study. The increased pressures due the interaction of these air bubbles on each other during an UNDEX event could produce detrimental effects on the ship hull.

X. FINAL REMARKS

A. CONCLUSIONS

The size and shape of an air bubble makes a tremendous impact on the pressures encountered during an UNDEX event. The pressure increase in the immediate vicinity of a shock-induced air bubble can be several times greater than the initial shockwave. This pressure change can adversely affect nearby marine structures. One possible scenario of concern is a U.S. Navy vessel operating its Prairie/Masker system that is subjected to an UNDEX event. While the Prairie/Masker is designed to mask the vessel's machinery noise from subsurface threats, the creation of air bubbles in close proximity to the hull will generate a substantial pressure region upon the ship hull.

This research shows that for long rectangular air bubble regions, a buffering effect is created. This would prove beneficial to any structures in the vicinity. However, it is not a realistic simulation since air bubbles do not naturally form long rectangular homogeneous shapes.

When the study shifted to the analysis of circular regions, the results became more realistic with greater similarity to naturally occurring air bubbles. For small regions (2cm diameter), the shockwave appeared to pass by largely uninhibited. Upon closer inspection of the pressure-time history analysis, it was discovered that a pressure rise occurred. This pressure increase was not nearly as substantial as the slightly larger region (4cm diameter). For these two small air bubble regions, the time to peak pressure lags slightly behind the time to peak pressure of the region with no air bubbles. This is due to the short time required for the shockwave to compress the region and its subsequent expansion.

In order to contrast these small bubble regions, a large bubble region was constructed using the principles of Hopkinson scaling. This large bubble (20cm diameter) produced an initial pressure peak of similar magnitude to the region without an air bubble. The time to peak pressure for this simulation was slightly shorter. This is due to the scaling and the data locations closer proximity to the charge. Figure 31 shows the

formation of a second pressure peak which has a magnitude slightly less than the first pressure peak. While this peak does not equal the initial peak, the pressure incurred is substantial and may lead to a second damaging effect on a marine structure. The delay in time to this pressure peak is due to additional energy required for compression and expansion of the air bubble. Also, when comparing the pressure-time histories, the history for the large diameter air bubble does not mirror any of the circular air bubble scenarios due to the presence of the second pressure peak.

Since the 4cm diameter air bubble produced the highest pressure output, it was studied in greater detail with a refined mesh. The refined mesh proved beneficial in generating more accurate results than with a coarse mesh. With an increased amount of data locations, a substantial amount of data was recorded. It was discovered that regions downstream of the air bubble, in relation to the detonated charge, received the largest increase in pressure, specifically regions in the vicinity of the upper right quadrant of the air bubble. Many of the pressures encountered in this region were nearly several times the maximum pressure perceived during the simulation with no air bubble. A handful of data locations experienced pressure increases in excess of ten times. While it was apparent that the pressure increase at locations near the center of the air bubble was significant, it was also shown that the pressure dropped off rapidly within a minimal distance from the center.

The refinement of the mesh had a significant impact on the measured results. As expected, unrefined simulations involving no air bubbles differed slightly from their refined counterparts. Their maximum pressures remained largely the same 1.5964E+08dyne/cm^2 (unrefined) versus 1.5040E+08dyne/cm^2 (refined). However, when comparing a simulation involving an air bubble, the difference became substantial. For the 4cm diameter air bubble, the pressure at cell (143,919) was 8.2314E+08dyne/cm^2. The equivalent unrefined location, cell (126,901), recorded a pressure of 2.9306E+08dyne/cm^2. The pressure encountered in the unrefined simulation was substantially lower than the refined simulation. This difference is due to the mesh refinement. Table 13 shows a comparison of the pressures recorded in the refined simulation.

The formation of air bubbles around a ship hull is a natural occurrence while the vessel is underway. The majority of these bubbles form in close proximity to the hull, but drift away due to the motion of the ship. However, the creation and loss of these bubbles is a continuous process as the ship proceeds through the water. Should this ship be subjected to an underwater explosion event, the subsequent collapse and expansion of these air bubbles will heavily increase the pressure in its immediate vicinity and possibly compromise hull integrity leading to loss of the vessel.

B. FURTHER RESEARCH

Additional research would include the determination of the optimum circular air bubble to generate the maximum amount of pressure. It was apparent in Figure 32 that the peak pressure increased as the bubble diameter increased. However, there is a point when the air bubble exceeds the size required to amplify the pressure and instead begins to reduce the incoming pressure. Finding this specific diameter would be of interest and require additional research and experimentation.

Since it is understood that the dramatic pressure increase occurs within the immediate vicinity of the air bubbles, it would be beneficial to determine the safe distance where the increased pressure effects are found to be negligible. This would vary by the bubble size and shape, but an additional study could explore these various sizes and shapes.

Another area of further research would be the inclusion of a ship model. This would allow the full effect of the air bubble and shockwave to be investigated on the ship structural model. Use of the refined mesh would prove beneficial to attain accurate results. However, the air bubble should be moved in close proximity to the model to simulate an air bubble near the ship hull. Discovering the impact this air bubble region has upon a marine structure would be of interest and require additional research and testing.

THIS PAGE INTENTIONALLY LEFT BLANK

APPENDIX

Sample PreGemini code used in this study.

```
format=00017

 <OPTIONS>
   Mode=start                        # PreGemini mode
(Start/Rezone/Overlay/Repartition)
   StartTime=0.                      # Set initial time (REAL/precalc;precalc)
   Gravity=-980.665                  # Gravity, positive upward (REAL/1g)
 <END OPTIONS>

 <GRID>
   Coordinates=cylindrical           # Coordinates: CARTESIAN, CYLINDRICAL, or
SPHERICAL
   xCells=591 dx=0. xDatum=0.
   yCells=1 dy=0. yDatum=0.
   zCells=1604 dz=0. zDatum=0.
   GridFile=./grid/grid.asc          # File name for grid file specify
(none/STRING)
 <END GRID>

 <SUBGRIDS>
   XSubGrids=2 XPartition=auto
   YSubGrids=1 YPartition=auto
   ZSubGrids=2 ZPartition=auto
 <END SUBGRIDS>

 <BOUNDARY CONDITIONS>
   xmin=wall xmax=free               # wall2/wall/freeng/free/REAL
   zmin=wall zmax=free               # wall2/wall/freeng/free/REAL
 <END BOUNDARY CONDITIONS>

 <MATERIALS>
   MaterialID=he_solid File=hbx_1solid.mtl
   MaterialID=he_gas File=hbx_1.mtl
   MaterialID=water File=tillwater.mtl
   MaterialID=air File=air.mtl
   MaterialID=gas_layer File=watervapor.mtl
 <END MATERIALS>

 <ADJUST EOS>
  Material=air EiMax=1.E+13
  Material=he_gas EiMax=1.E+13
  Material=gas_layer EiMax=1.E+13
 <END ADJUST EOS>

 <BURN>
   Unburned=he_solid  Burned=he_gas  Time=0. RefPt=(0., 0., -1000.)
  # unburned to burned    time      x0    y0    z0
 <END BURN>

 <HYDROSTATIC FIELD>
   pRef=1.0e+6 zRef=0. zMax=max     # Ref pressure, ref location, zMax
   Material=air  ei=eref zMin=0.
   Material=water  ei=eref zMin=min
  # matl name  matl zmin   matl int energy  (eos v1...vn)
```

```
 <END HYDROSTATIC FIELD>

 <INITIAL STATES>
   StateID=he_solid  Material=he_solid  Rho=rhoref ei=eref EOSvar=(0.)
   StateID=water  Material=water  Rho=rhoref ei=eref EOSvar=(0.)
   StateID=gas_layer  Material=gas_layer  Rho=rhoref ei=eref EOSvar=(0.)
  # state     matl      g    frac   rho         e        p   a0   u   v   w
 <END INITIAL STATES>

 <FLOWFIELD>
   Option=hydrostatic
   Option=ball state=he_solid mass=27215. RefPt=(0.,0.,-1000.)
#  First Column
   Option=ball state=gas_layer r=0.6667 RefPt=(250.5,0.,-296.5)
   Option=ball state=gas_layer r=0.6667 RefPt=(250.5,0.,-298)
   Option=ball state=gas_layer r=0.6667 RefPt=(250.5,0.,-299.5)
#  Second Column
   Option=ball state=gas_layer r=0.6667 RefPt=(252,0.,-296.5)
   Option=ball state=gas_layer r=0.6667 RefPt=(252,0.,-298)
   Option=ball state=gas_layer r=0.6667 RefPt=(252,0.,-299.5)
#  Third Column
   Option=ball state=gas_layer r=0.6667 RefPt=(253.5,0.,-296.5)
   Option=ball state=gas_layer r=0.6667 RefPt=(253.5,0.,-298)
   Option=ball state=gas_layer r=0.6667 RefPt=(253.5,0.,-299.5)


#   Option=block state=gas_layer xmin=50 xmax=100 zmin=-300. zmax=-296.
#stairstep=on
#   Option=block state=gas_layer xmin=150 xmax=200 zmin=-300. zmax=-296.
#stairstep=on
#   Option=block state=gas_layer xmin=250 xmax=300 zmin=-300. zmax=-296.
#stairstep=on
#   Option=block state=gas_layer xmin=350 xmax=400 zmin=-300. zmax=-296.
#stairstep=on
#   Option=block state=gas_layer xmin=450 xmax=500 zmin=-300. zmax=-296.
#stairstep=on
#   Option=block state=gas_layer xmin=550 xmax=600 zmin=-300. zmax=-296.
#stairstep=on
  # option       state
  # option       state           mass         center
 <END FLOWFIELD>

 <TEXT OUTPUT>
    imin=1  imax=1  jmin=1  jmax=1  kmin=1  kmax=1
 <END TEXT OUTPUT>
```

LIST OF REFERENCES

[1] Department of the Navy. “Shock Hardening of Surface Ships.” OPNAV Instruction 9072.2, Jan. 12, 1987.

[2] N. A. Schneider, “Ship Shock Trial Modeling and Simulation of USS Winston S. Churchill (DDG 81),” Naval Postgraduate School, Monterey, CA, Tech. Rep. NPS-ME-03-004, Sept 2003.

[3] A. Walters. "Investigation of an Explicitly Modeled Solid Ocean Floor on a Shallow Water UNDEX Event." M.S. thesis, Naval Postgraduate School, Monterey, California, United States, 2011.

[4] T. Moyer, “Full Ship Shock Test Modeling,” unpublished.

[5] Department of the Navy, Bureau of Ordnance. (1947, May 28). *OP1664: U.S. Explosive Ordnance (Vol. 1)* [Online]. Available: http://www.hnsa.org/doc/ordnance/index.htm#toc. [May 23, 2012].

[6] Bureau of Naval Weapons. “Explosive Compositions, HBX Type.” Military Specification MIL-E-22267A, May 31, 1963.

[7] H. G. Snay. “Hydrodynamics of underwater explosions,” in *Symposium on Naval Hydrodynamics*, 1957, pp. 325-327.

[8] R. H. Cole. *Underwater Explosions*. Arvonia, VA: SAVIAC, 2007.

[9] A. Wardlaw and R. Ilamni, “Simulation of Underwater Explosion Cavitation Phenomena,” NSWC Indian Head Division, Indian Head, MD, Final Rep. IHTR 2589, May 28, 2004.

[10] V. K. Kedrinskii, “Rarefaction Waves and Bubbly Cavitation in Real Liquid,” presented at the CAV 2001: Fourth International Symposium on Cavitation California Institute of Technology, Pasadena, CA, June 20-23, 2001.

[11] *Gemini: The DYSMAS Eulerian Solver - User’s Manual*, Gemini Version 6.1, NSWC Indian Head Division, Indian Head, MD, Oct. 4, 2011.

[12] *ME4525: Naval Ship Shock Design and Analysis*, Naval Postgraduate School, Monterey, CA, 2004.

[13] Federation of American Scientists. (March 8, 1999). *Prairie/Masker* [Online]. Available: http://www.fas.org/man/dod-101/sys/ship/weaps/prairie.htm. [May 25, 2012].

[14] The Engineering ToolBox. *Molecular Mass of Air* [Online]. Available: http://www.engineeringtoolbox.com/molecular-mass-air-d_679.html. [May 18, 2012].

[15] K. Markey. *Tell me why I can see my breath when it's cold* [Online]. Available: http://wondertime.go.com/learning/article/why-you-can-see-your-breath-in-winter.html. [May 30, 2012].

INITIAL DISTRIBUTION LIST

1. Defense Technical Information Center
   Ft. Belvoir, Virginia

2. Dudley Knox Library
   Naval Postgraduate School
   Monterey, California

3. Mechanical & Aerospace Engineering Department Chairman, Code MAE
   Naval Postgraduate School
   Monterey, California

4. Naval/Mechanical Engineering Curriculum Code 74
   Naval Postgraduate School
   Monterey, California

5. Distinguished Professor Young Kwon, Code MAE/Kw
   Department of Mechanical & Aerospace Engineering
   Naval Postgraduate School
   Monterey, California

6. Research Assistant Professor Jarema M. Didoszak, Code MAE/Di
   Department of Mechanical & Aerospace Engineering
   Naval Postgraduate School
   Monterey, California

7. Erica Hansen
   Program Executive Office Ships
   Washington Navy Yard
   Washington, DC

8. Gregory S. Harris
   Naval Surface Warfare Center, Indian Head Division
   Indian Head, Maryland

9. Roger Ilamni
   Naval Surface Warfare Center, Indian Head Division
   Indian Head, Maryland

10. Frederick A. Costanzo
    Underwater Explosion Research Department (UERD)
    Naval Surface Warfare Center, Carderock Division
    West Bethesda, Maryland

11. Steven Rutgerson
    Underwater Explosion Research Department (UERD)
    Naval Surface Warfare Center, Carderock Division
    West Bethesda, Maryland